UC Berkeley
UC Berkeley Electronic Theses and Dissertations

Title

Regulation of motility, the cell cycle, and magnetosome formation in Magnetospirillum magneticum AMB-1

Permalink

https://escholarship.org/uc/item/2bc762sw

Author

Greene, Shannon Elizabeth

Publication Date

2012

Peer reviewed|Thesis/dissertation

Regulation of motility, the cell cycle, and magnetosome formation in *Magnetospirillum magneticum* AMB-1

by

Shannon Elizabeth Greene

A dissertation submitted in partial satisfaction of the

requirements for the degree of

Doctor of Philosophy

in

Microbiology

in the

Graduate Division

of the

University of California, Berkeley

Committee in charge:

Professor Arash Komeili, Chair

Professor Kathleen Ryan

Professor Nicole King

Spring 2012

ABSTRACT

Regulation of motility, the cell cycle, and magnetosome formation in *Magnetospirillum magneticum* AMB-1

by

Shannon Elizabeth Greene

Doctor of Philosophy in Microbiology
University of California, Berkeley
Professor Arash Komeili, Chair

Despite their diminutive size and seemingly simple construction, bacteria lead remarkably complex lives. In order to fulfill their biological roles of growth and reproduction, they must integrate a wealth of information about their environment and, depending upon the suitability of the available conditions for survival, they can act to relocate themselves to more preferred locales. Doing so requires that bacteria be able to sense environmental stimuli and relay signals induced by those stimuli to various locomotive apparatuses. Once a cell has fulfilled its nutrient quota to support replication, cell division can occur. Cell division is also intricately timed and regulated in bacterial cells, which are now known to possess intracellular organization, cytoskeletal features, and, in some species, compartmentalization. Therefore, division of a bacterial cell must coordinate disassembly, reassortment, and segregation of these cell biological features. In this work, I investigate the connection between the cell cycle and bacterial organelle formation in the magnetotactic bacterium *Magnetospirillum magneticum* AMB-1. Magnetotactic bacteria, including AMB-1, are defined by their ability to synthesize chains of intracellular membrane-bounded magnetic minerals, which facilitate bacterial alignments with and responses to geomagnetic fields. To determine the role of the cell cycle in governing the production of these bacterial organelles, called magnetosomes, I disrupted homologs of regulatory factors known to control the progression of the cell cycle as well as polar organelle development in related Alphaproteobacteria. Surprisingly, mutants in the CtrA regulatory pathway were viable, indicating alternative mechanisms of cell cycle progression in AMB-1; in addition, magnetosome formation was also unaffected. Notably, motility was the only feature of AMB-1 disrupted by the CtrA pathway mutations. While subsequent studies to probe upstream regulators of motility in AMB-1 failed to yield additional insight, my results suggest a terminal role for CtrA in the transcription of flagellar biosynthesis genes. This role appears to be ancestral in the Alphaproteobacteria. Further, I have developed protocols which should enable future investigations of the cell cycle in AMB-1 and the temporal changes in gene expression which allow its progression. Preliminary studies indicate that genes involved in signal transduction and possibly magnetosome membrane formation vary their expression throughout the AMB-1 cell cycle. Continued investigation of the connections between the CtrA pathway, magnetosome gene expression, and the cell cycle may elucidate regulation of motility in magnetotactic bacteria and illustrate novel mechanisms of cell cycle progression in these unique organisms.

TABLE OF CONTENTS

CHAPTER ONE

Biogenesis and Subcellular Organization of the Magnetosome Organelles of Magnetotactic Bacteria

Shannon E Greene[1]
Arash Komeili[1*]

[1]Department of Plant and Microbial Biology
University of California, Berkeley
Berkeley, CA 94720

[*]corresponding author: komeili@berkeley.edu

INTRODUCTION

In 1884, Karl August Mobius first coined the term "organula" to describe the reproductive structures of protists (21). In the subsequent centuries, the distinction of organelle has expanded to include subcellular structures ranging from membrane-bounded compartments to molecular machines comprised of harmonious assemblages of proteins and other macromolecules. Such intracellular organization is primarily thought to be unique to the eukaryotic lineage, but research over the past two decades has identified complex subcellular compartments and cytoskeletal elements in bacteria (22, 40). The presence of these features in bacteria raises the question of whether principles governing eukaryotic organelle formation, including membrane shaping and protein targeting, also hold for bacterial organelles. If not, an understanding of bacterial compartments promises to reveal a number of unique cell biological mechanisms.

Magnetotactic bacteria (MTB), a phylogenetically diverse cohort of microorganisms characterized by their ability to orient in magnetic fields, provide one of the clearest examples of cytoplasmic compartmentalization in bacteria in the form of organelles called magnetosomes. Electron cryotomography (ECT) and other electron microscopy studies have shown that magnetosomes are lipid-bounded and derived from the inner cell membrane (7, 16) (**Fig 1**). In addition, magnetosomes have a specific protein content that allows for biomineralization of the crystalline magnetic minerals magnetite (Fe_3O_4) and/or greigite (Fe_3S_4). Finally, individual magnetosomes are aligned into chains by dynamic cytoskeletal filaments, whose ancestry and activities are reminiscent of eukaryotic actin systems (15). These characteristics have made magnetosomes a prime target for understanding the cell biology of bacterial organelles.

Biochemical analyses of magnetosome membrane protein content, genetic screens and comparative genomic studies of various MTB led to the identification of a conserved suite of magnetosome-associated genes organized in a large genomic island called the Magnetosome Island (MAI) (10, 11, 17, 27, 36). A subset of these genes, encoded by the *mamAB* gene cluster, has been identified as not only essential for magnetosome formation but also sufficient for this process (19, 23). Individual deletions of genes within this cluster produce strains arrested at various stages of magnetosome biogenesis and hint at a stepwise assembly of the organelle where membrane formation, protein sorting, biomineralization, and chain formation are distinct processes (23) (**Fig 2**). In this review we highlight some of the recent developments in understanding of the molecular pathways that govern the formation, organization and intracellular dynamics of magnetosomes.

MAGNETOSOME MEMBRANE FORMATION

A key step in the formation of a functional magnetosome chain is the invagination and shaping of the inner cell membrane. Among eukaryotes, key protein domains have been implicated in generating extensive membrane curvature (20, 44). Within MTB, however, homologs of these factors are not apparent. Thus far, four genes have been identified for their essential roles in magnetosome membrane formation; deletion of any four of these genes individuals results in AMB-1 cells completely devoid of inner membrane decoration (23). Two genes, *mamI* and *mamL*, encode small (~7-8 kDa), inner membrane proteins of no homology to any proteins beyond the magnetotactic bacteria and their role in magnetosome formation is unclear (23). It

has been hypothesized that the C-terminal tail of MamL, which is rich in positively charged amino acids, could potentially interact with or insert into the phosphate backbone of the inner membrane to induce local curvature (15). The magnetosome membrane protein MamQ is homologous to the LemA family of proteins, although no function is known for this group. Interestingly, it bears a potential resemblance to BAR domain proteins, known to be involved in bending membranes in eukaryotic cells (44). However, this similarity may be due to the presence of coiled-coil domains in MamQ and is not indicative of a specific function in altering membrane architecture.

Only MamB has homology to a family of proteins with a known function. MamB belongs to the cation diffusion facilitator (CDF) superfamily, which is known to transport divalent cation metals and includes a ferrous iron transport system (8). It has recently been shown that MamB interacts with a number of other magnetosome proteins (38). For example, MamB was shown to self-interact via its C-terminal domain. Additionally, it also appears to interact with, and in turn be stabilized by, a second CDF protein MamM (38).. Intriguingly, MamB potentially interacts with the PDZ_1 domain of MamE, a protein involved in the localization of various proteins to the magnetosome. Such an interaction could link the putative transporter to the network of magnetosome proteins managed by MamE (38). Thus, MamB may not be directly involved in magnetosome membrane biogenesis and may instead stabilize the membrane by acting as a hub for organization of other magnetosome proteins. Once a magnetosome compartment has been formed MamB might then act as a transporter of iron or other cations into the magnetosome.

Experiments thus far have been unable to establish sufficiency, however, for the four magnetosome membrane proteins MamI, MamL, MamQ, and MamB in establishing structures reminiscent of magnetosome membranes *in vivo* (23). Because no other individual gene deletions yield an absence of magnetosome membranes, additional functionally redundant factors are required. An additional player in shaping the magnetosome membrane may be MamY, an MAI-encoded protein exhibiting weak homology to BAR domain proteins. MamY is capable of inducing liposome tabulation *in vitro* and has been implicated in maintaining the size of cell membrane invaginations *in vivo* (34).

PROTEIN LOCALIZATION TO THE MAGNETOSOME

Once the magnetosome membrane invagination has been established, biomineralization can occur if environmental conditions are met. A number of proteins have been implicated in this process and several have been identified as integral or peripheral to the magnetosome membrane itself (1, 3, 10, 23, 25, 30, 36). How these proteins localize to the membrane is not well understood, and no evidence exists for a targeting or signal sequence that would uniquely direct proteins to the invagination. The most substantiated mechanism of protein localization to the magnetosome membrane appears to be mediated by protein-protein interactions. Interactions, described above between MamB, MamM, and MamE, have been suggested through *in vitro* work (38). Additionally, MamJ, MamA and Mms6 have all been implicated in the recruitment or stability of subsets of other magnetosome proteins (32, 35, 41, 43). Genetic analyses have shown that MamE, a DegP/HtrA serine protease with putative heme-binding motifs, is required for the localization of a number of proteins to the magnetosome. In its absence, empty magnetosome membranes are formed but a number of proteins such as MamJ, MamI and MamC

are mislocalized within the cell (25, 42). Interestingly, MamE appears to be a dual function protein. When its putative protease or heme-binding residues are mutated MamE is still capable of localizing proteins to the magnetosome (25). However, these mutants have a defect in biomineralization and cannot form mature magnetite crystals (25).

These results support a model where protein sorting depends on a specific network of protein-protein interactions that produce a functional magnetosome. An alternative possibility is that an affinity for established membrane curvature could drive a subset of proteins to the magnetosome; protein affinities for both positive and negative membrane curvature in bacteria have already been demonstrated (2, 18, 26). One could envision that both mechanisms could be at play in localizing magnetosome proteins to the invagination; negative curvature is highly accentuated at the neck of the magnetosome whereas the positive curvature of the magnetosome body could attract an alternate set of proteins.

MAGNETOSOME CHAIN FORMATION

To maximize their magnetic response, MTB align their magnetosomes into one or more chains along the long axis of the cell. Through ECT imaging of two magnetospirilla species, filaments have been observed running parallel to the magnetosome chain. These filaments are proposed to be comprised of MamK, a bacterial actin-like protein encoded by the MAI of all sequenced MTB (16, 28, 37). *mamK* deletions exhibit disorganized magnetosome chains, ectopic chain placement near cell poles, magnetosome clustering, and most tellingly – the absence of filaments near magnetosomes (13, 16). *In vitro* polymerization of MamK into bundles of long filaments further supports the hypothesis of MamK as the building block of the magnetosome cytoskeleton (37).
Recent evidence using fluorescence recovery after photobleaching (FRAP) indicates that MamK filaments, like most actin homologs, are dynamic within the cell (5). Bleached segments of MamK-GFP filaments were seen to recover fluorescence in a manner dependent on the putative ATPase activity of the protein (5). This pattern of recovery is often related to the exchange of unbleached monomers as a result of depolymerization and repolymerization events. However, recent evidence with other families of bacterial actins has shown that entire filaments are motile within the cell raising the possibility that MamK dynamics in the FRAP experiment may also be influenced by such movements (4, 6, 39).

MamK dynamics, however, are not an intrinsic property of the protein and are regulated by additional factors as MamK-GFP expressed in a MAI deletion strain fails to recover in FRAP experiments (5). A candidate MamK regulator is MamJ, a protein with an acidic repeat domain that is encoded by the *mamAB* gene cluster. When *mamJ* is deleted in *Magnetospirillum gryphiswaldense* MSR-1, magnetosomes cluster in clumps within the cell (31). Additionally, in some but not all cases, MamJ and MamK appear to interact in a bacterial two-hybrid assay (32). In *Magnetospirillum magneticum* AMB-1, MamJ and its paralog LimJ, are necessary for both chain organization and MamK dynamics in a redundant manner. In the absence of these two regulators, large gaps are apparent within the magnetosome chain and bundles of filaments, presumably composed of MamK, can be seen within these empty spaces. However, additional unknown factors encoded by the MAI are also necessary to regulate the dynamics of MamK *in*

vivo, as expression of either MamJ or LimJ in a ΔMAI strain is unable to rescue MamK filament dynamics (5).

Despite these advances in understanding the *in vivo* and *in vitro* properties of MamK, its specific function and the manner by which it contributes to chain organization are still unclear. MamK might act as a guide to establish the magnetosome chain by moving new magnetosomes into a preexisting chain. Such a model has been suggested for MSR-1, in which both MamK filaments and magnetic interactions between adjacent magnetosomes seem to be required for chain organization (14, 31). Alternatively, MamK may act to maintain the chain after it has already been formed. Finally, as discussed below, MamK may act during cell division to ensure the proper segregation of the magnetosome chain.

CELL CYCLE AND MAGNETOSOME FORMATION

Once the cell has formed its magnetosome membranes, properly sorted proteins to the compartment to promote biomineralization, and aligned the magnetosomes in a chain, it faces the additional challenge of cell division. In MTB, initial EM studies suggested that the magnetosome chain is divided evenly between the two daughter cells (24, 33). For the population to maintain its magnetic properties throughout multiple rounds of growth, each daughter cell must synthesize and incorporate new magnetosomes into the existing chain.

To determine how this process occurs requires investigation of both the timing of magnetosome formation and the mechanisms involved in magnetosome maturation. The time needed for a magnetosome to invaginate from the inner membrane and form a 50nm wide spherical compartment is currently unknown. Related to this issue is the outstanding question of the time frame during the division cycle in which new magnetosomes are formed and incorporated into the existing chain. Inner membrane invaginations could simply be synthesized continually throughout growth or there could be discrete portions of the cell cycle in which MTB are primed for magnetosome membrane synthesis.

The actual cell division event in MTB requires not only successful division plane formation in between two segregated chromosomes but also bisection of the magnetosome chain (**Fig 2**). Intriguingly, in MSR-1 cell division appears to proceed asymmetrically from one lateral edge of the cell which may provide the force necessary to segregate the magnetosome chain (12). Preferential localization of the chain spanning the future division site at midcell primes equal distribution of magnetosomes to the daughter cells. In MSR-1, chain halves rapidly relocalize from the poles to the new future division site in a process that is mediated by MamK filaments (12). In a broad sense this process is reminiscent of the segregation of the proteinaceous carbon-fixation microcompartments of cyanobacteria: carboxysomes. These organelles are linearly arranged in the cell and their alignment and equitable division to daughter cells is dependent upon with the action of ParA cytoskeletal filaments (29).

The coordination of the development of polar organelles such as flagella, stalks, and pili with the progression of the cell cycle has been extensively investigated in Alphaproteobacteria related to the magnetospirilla. These processes are controlled through the CtrA regulatory network, and it was hypothesized that the biogenesis of magnetosomes in the context of the cell cycle could be

similarly regulated by components of this pathway, most of which are conserved in MTB. While CtrA and other members of its pathway are essential for viability and cell cycle progression in some Alphaproteobacteria, they were recently shown to be dispensable in AMB-1 (9). Mutants lacking *ctrA* had no discernible cell cycle defects and produced functional magnetosome chains (9). Thus, the existence and identity of elements regulating the cell cycle in MTB and coordinating the formation of magnetosomes in its context remain elusive.

CONCLUSION

Over the last decade significant progress has been made in the discovery of magnetosome genes and the elucidation of a basic pathway for the assembly of this bacterial organelle. The next challenge is to understand the mechanisms by which these factors act and to define the coordination of these processes in the context of the cell cycle. Further investigations of bacterial organelles using magnetosomes and other compartments as model systems will continue to illuminate similarities and differences in how bacterial and eukaryotic cells solve the common problems associated with organelle biogenesis. As is the case for biological tasks across the entire tree of life, some solutions share an ancient derivation, whereas others may prove to have arisen independently and convergently. Regardless of their evolutionary histories, the mechanisms MTB have evolved to generate and organize intracellular compartments are proving to be elegant, intricate, and intriguing.

ACKNOWLEDGEMENTS

REFERENCES

1. **Amemiya, Y., A. Arakaki, S. S. Staniland, T. Tanaka, and T. Matsunaga.** 2007. Controlled formation of magnetite crystal by partial oxidation of ferrous hydroxide in the presence of recombinant magnetotactic bacterial protein Mms6. Biomaterials **28:**5381-5389.
2. **Antonny, B.** 2011. Mechanisms of Membrane Curvature Sensing. Ann. Rev. Biochem. **80:**101-123.
3. **Arakaki, A., J. Webb, and T. Matsunaga.** 2003. A novel protein tightly bound to bacterial magnetic particles in *Magnetospirillum magneticum* strain AMB-1. J. Biol. Chem. **278:**8745-8750.
4. **Dominguez-Escobar, J., A. Chastanet, A. H. Crevenna, V. Fromion, R. Wedlich-Soldner, and R. Carballido-Lopez.** 2011. Processive Movement of MreB-Associated Cell Wall Biosynthetic Complexes in Bacteria. Science **333:**225-228.
5. **Draper, O., M. E. Byrne, Z. Li, S. Keyhani, J. C. Barrozo, G. Jensen, and A. Komeili.** 2011. MamK, a bacterial actin, forms dynamic filaments in vivo that are regulated by the acidic proteins MamJ and LimJ. Mol. Microbiol. **82:**342-354.

6. **Garner, E. C., R. Bernard, W. Wang, X. Zhuang, D. Z. Rudner, and T. Mitchison.** 2011. Coupled, Circumferential Motions of the Cell Wall Synthesis Machinery and MreB Filaments in B. subtilis. Science **333:**222-225.

7. **Gorby, Y. A., T. J. Beveridge, and R. P. Blakemore.** 1988. Characterization of the bacterial magnetosome membrane. J. Bacteriol. **170:**834.

8. **Grass, G., M. Otto, B. Fricke, C. J. Haney, C. Rensing, D. H. Nies, and D. Munkelt.** 2005. FieF (YiiP) from *Escherichia coli* mediates decreased cellular accumulation of iron and relieves iron stress. Arch. Microbiol. **183:**9-18.

9. **Greene, S. E., M. Brilli, E. Biondi, and A. Komeili.** 2012. Analysis of the CtrA Pathway in Magnetospirillum Reveals an Ancestral Role in Motility in Alphaproteobacteria. J. Bacteriol.

10. **Grünberg, K., E. C. Muller, A. Otto, R. Reszka, D. Linder, M. Kube, R. Reinhardt, and D. Schüler.** 2004. Biochemical and Proteomic Analysis of the Magnetosome Membrane in *Magnetospirillum gryphiswaldense*. Appl. Environ. Microbiol. **70:**1040-1050.

11. **Grünberg, K., C. Wawer, B. M. Tebo, and D. Schuler.** 2001. A Large Gene Cluster Encoding Several Magnetosome Proteins Is Conserved in Different Species of Magnetotactic Bacteria. Appl. Environ. Microbiol. **67:**4573.

12. **Katzmann, E., F. D. Müller, C. Lang, M. Messerer, M. Winklhofer, J. M. Plitzko, and D. Schüler.** 2011. Magnetosome chains are recruited to cellular division sites and split by asymmetric septation. Mol. Microbiol. **82:**1316-1329.

13. **Katzmann, E., A. Scheffel, M. Gruska, J. M. Plitzko, and D. Schüler.** 2010. Loss of the actin-like protein MamK has pleiotropic effects on magnetosome formation and chain assembly in Magnetospirillum gryphiswaldense. Mol. Microbiol. **77:**208-224.

14. **Klumpp, S., and D. Faivre.** 2012. Interplay of Magnetic Interactions and Active Movements in the Formation of Magnetosome Chains. PLoS ONE **7:**e33562.

15. **Komeili, A.** 2011. Molecular mechanisms of compartmentalization and biomineralization in magnetotactic bacteria. FEMS Microbiol. Rev. **36:**232-255.

16. **Komeili, A., Z. Li, D. K. Newman, and G. J. Jensen.** 2006. Magnetosomes are cell membrane invaginations organized by the actin-like protein MamK. Science **311:**242-245.

17. **Komeili, A., H. Vali, T. J. Beveridge, and D. K. Newman.** 2004. Magnetosome vesicles are present before magnetite formation, and MamA is required for their activation. Proc. Natl Acad. Sci. USA **101:**3839-3844.

18. **Lenarcic, R., S. Halbedel, L. Visser, M. Shaw, and L. J. Wu.** 2009. Localisation of DivIVA by targeting to negatively curved membranes. EMBO J. **28:**2272.

19. **Lohbe, A., S. Ullrich, E. Katzmann, S. Borg, G. Wanner, M. Richter, B. Voigt, T. Schweder, and D. Schuler.** 2011. Functional Analysis of the Magnetosome Island in *Magnetospirillum gryphiswaldense*: The *mamAB* Operon Is Sufficient for Magnetite Biomineralization. PLoS ONE **6:**e25561.

20. **McMahon, H. T., and J. L. Gallop.** 2005. Membrane curvature and mechanisms of dynamic cell membrane remodelling. Nature **438:**590.

21. **Mobius, K. A.** 1884. Das Sterben der einzelligen und der vielzelligen Tiere. Vergleichend betrachtet. Biologisches Centralblatt **4:**389-392.

22. **Murat, D., M. Byrne, and A. Komeili.** 2010. Cell Biology of Prokaryotic Organelles. Cold Spring Harbor Perspectives in Biology **2**.

23. **Murat, D., A. Quinlan, H. Vali, and A. Komeili.** 2010. Comprehensive genetic dissection of the magnetosome gene island reveals the step-wise assembly of a prokaryotic organelle. Proc. Natl Acad. Sci. USA **107:**5593–5598.

24. **Posfai, M., T. Kasama, and R. Dunin-Borkowski.** 2006. Characterization of Bacterial Magnetic Nanostructures Using High-Resolution Transmission Electron Microscopy and Off-Axis Electron Holography. Microbiology Monograph**:**198-225.

25. **Quinlan, A., D. Murat, H. Vali, and A. Komeili.** 2011. The HtrA/DegP family protease MamE is a bifunctional protein with roles in magnetosome protein localization and magnetite biomineralization. Mol. Microbiol. **80:**1075-1087.

26. **Ramamurthi, K. S., S. Lecuyer, H. A. Stone, and R. Losick.** 2009. Geometric cue for protein localization in a bacterium. Science **323:**1354.

27. **Richter, M., M. Kube, D. A. Bazylinski, T. Lombardot, F. O. Glockner, R. Reinhardt, and D. Schüler.** 2007. Comparative Genome Analysis of Four Magnetotactic Bacteria Reveals a Complex Set of Group-Specific Genes Implicated in Magnetosome Biomineralization and Function. J. Bacteriol. **189:**4899-4910.

28. **Rioux, J.-B., N. Philippe, S. Pereira, D. Pignol, L.-F. Wu, and N. Ginet.** 2010. A Second Actin-Like MamK Protein in *Magnetospirillum magneticum* AMB-1 Encoded Outside the Genomic Magnetosome Island. PLoS ONE **5:**e9151.

29. **Savage, D. F., B. Afonso, A. H. Chen, and P. A. Silver.** 2010. Spatially Ordered Dynamics of the Bacterial Carbon Fixation Machinery. Science **327:**1258-1261.

30. **Scheffel, A., A. Gardes, K. Grunberg, G. Wanner, and D. Schüler.** 2008. The major magnetosome proteins MamGFDC are not essential for magnetite biomineralization in magnetospirillum gryphiswaldense but regulate the size of magnetosome crystals. J. Bacteriol. **190:**377-386.

31. **Scheffel, A., M. Gruska, D. Faivre, A. Linaroudis, J. M. Plitzko, and D. Schüler.** 2006. An acidic protein aligns magnetosomes along a filamentous structure in magnetotactic bacteria. Nature **440:**110-114.

32. **Scheffel, A., and D. Schüler.** 2007. The acidic repetitive domain of the Magnetospirillum gryphiswaldense MamJ protein displays hypervariability but is not required for magnetosome chain assembly. J. Bacteriol. **189:**6437-6446.

33. **Staniland, S. S., C. Moisescu, and L. G. Benning.** 2010. Cell division in magnetotactic bacteria splits magnetosome chain in half. Journal of Basic Microbiology **50:**392-396.

34. **Tanaka, M., A. Arakaki, and T. Matsunaga.** 2010. Identification and functional characterization of liposome tubulation protein from magnetotactic bacteria. Mol. Microbiol. **76:**480-488.

35. **Tanaka, M., E. Mazuyama, A. Arakaki, and T. Matsunaga.** 2011. Mms6 Protein Regulates Crystal Morphology during Nano-sized Magnetite Biomineralization in Vivo. J. Biol. Chem. **286:**6386-6392.

36. **Tanaka, M., Y. Okamura, A. Arakaki, T. Tanaka, H. Takeyama, and T. Matsunaga.** 2006. Origin of magnetosome membrane: Proteomic analysis of magnetosome membrane and comparison with cytoplasmic membrane. Proteomics **6:**5234-5247.

37. **Taoka, A., R. Asada, L.-F. Wu, and Y. Fukumori.** 2007. Polymerization of the actin-like protein MamK, which is associated with magnetosomes. J. Bacteriol. **189:**8737-8740.

38. **Uebe, R., K. Junge, V. Henn, G. Poxleitner, E. Katzmann, J. M. Plitzko, R. Zarivach, T. Kasama, G. Wanner, M. Pósfai, L. Böttger, B. Matzanke, and D.**

Schüler. 2011. The cation diffusion facilitator proteins MamB and MamM of *Magnetospirillum gryphiswaldense* have distinct and complex functions, and are involved in magnetite biomineralization and magnetosome membrane assembly. Mol. Microbiol. **82:**818-835.

39. **van Teeffelen, S., S. Wang, L. Furchtgott, K. C. Huang, N. S. Wingreen, J. W. Shaevitz, and Z. Gitai.** 2011. The bacterial actin MreB rotates, and rotation depends on cell-wall assembly. Proceedings of the National Academy of Sciences.

40. **Vats, P., J. Yu, and L. Rothfield.** 2009. The dynamic nature of the bacterial cytoskeleton. Cellular and Molecular Life Sciences **66:**3353-3362.

41. **Yamamoto, D., A. Taoka, T. Uchihashi, H. Sasaki, H. Watanabe, T. Ando, and Y. Fukumori.** 2010. Visualization and structural analysis of the bacterial magnetic organelle magnetosome using atomic force microscopy. Proc. Natl Acad. Sci. USA **107:**9382-9387.

42. **Yang, W., R. Li, T. Peng, Y. Zhang, W. Jiang, Y. Li, and J. Li.** 2010. *mamO* and *mamE* genes are essential for magnetosome crystal biomineralization in *Magnetospirillum gryphiswaldense* MSR-1. Res. Microbiol. **161:**701-705.

43. **Zeytuni, N., E. Ozyamak, K. Ben-Harush, G. Davidov, M. Levin, Y. Gat, T. Moyal, A. Brik, A. Komeili, and R. Zarivach.** 2011. Self-recognition mechanism of MamA, a magnetosome-associated TPR-containing protein, promotes complex assembly. Proc. Natl Acad. Sci. USA **108:**E480-E487.

44. **Zimmerberg, J., and M. M. Kozlov.** 2006. How proteins produce cellular membrane curvature. Nat Rev Mol Cell Biol **7:**9-19.
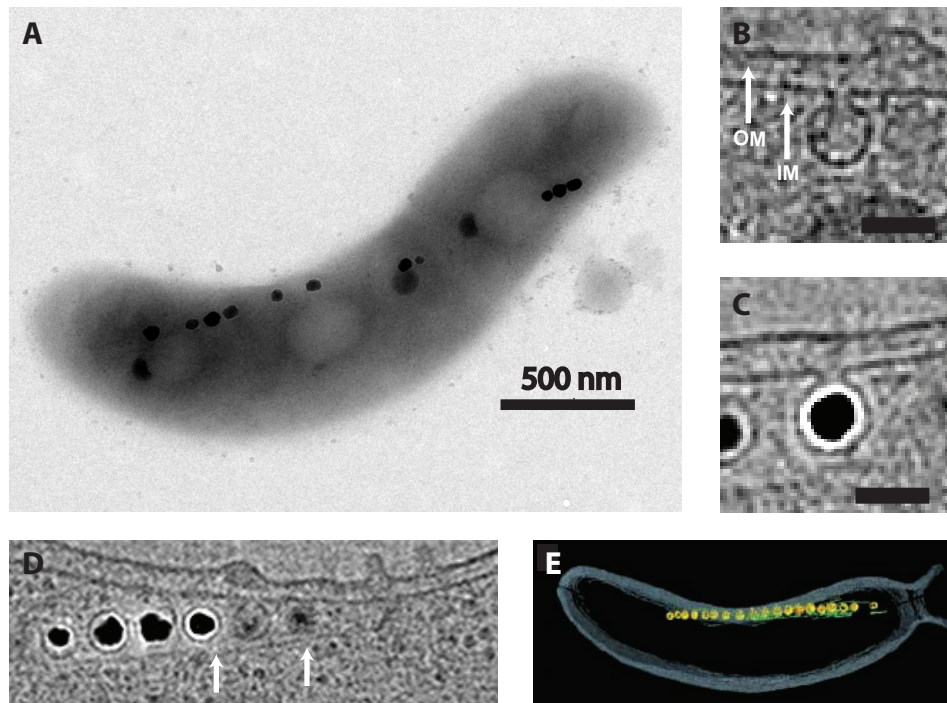
Figure 1: Cell biological features of magnetotactic bacteria. (A) Transmission electron micrograph (TEM) of *Magnetospirillum magneticum* AMB-1 reveals a linear chain of electron-dense magnetite crystals. (B) Single section of an electron cryotomographic (ECT) image of AMB-1 shows that magnetosome membranes invaginate from the inner membrane prior to biomineralization. (C) Inner membrane invaginations remain even when filled with a mature magnetite crystal. (D) ECT images also reveal cytoskeletal filaments flanking the magnetosome chain. (E) Magnetosome membranes (yellow), magnetite crystals (orange) and filaments (green) are highlighted in a 3D reconstruction of AMB-1 from an ECT image.
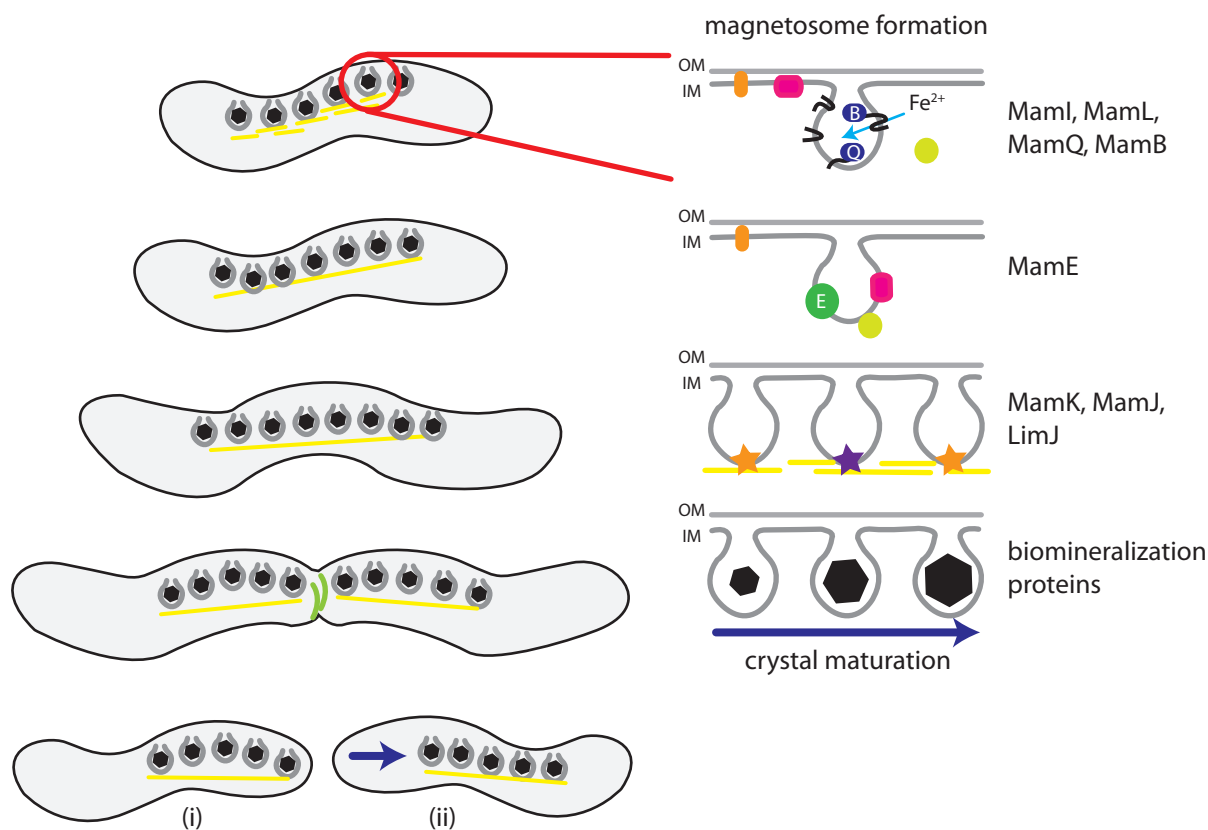
Figure 2: Magnetosome formation during cell cycle progression. (A) Magnetotactic bacteria increase the number of magnetosomes per cell throughout growth, with the chains centrally located. As the septum forms at the midcell, facilitated by constricting FtsZ rings (green), cytoskeletal filaments flanking the magnetosome chains (yellow) must be separated or stimulated to disassemble. Following cell division, polarly-localized magnetosome chains (i) quickly relocalize to the new midcell (ii). (B) The formation of an individual magnetosome is a step-wise process. Magnetosome membrane invagination from the inner cell membrane occurs via the combined actions of MamI, -L, -Q, and –B and other factors. The serine protease MamE is required to properly localize other magnetosome membrane (pink) and soluble (olive) proteins to the compartment. MamK, comprising the cytoskeletal filaments, functions with MamJ (orange star), and in some cases LimJ (purple star), to coordinate chain organization of the magnetosomes. Several factors participate in the regulation of crystal number, size, and shape.

CHAPTER TWO

Analysis of the CtrA Pathway in *Magnetospirillum* Reveals an Ancestral Role in Motility in Alphaproteobacteria

Shannon E Greene[1]
Matteo Brilli[2]
Emanuele Biondi[3]
Arash Komeili[1*]

[1]Plant and Microbial Biology
University of California, Berkeley
Berkeley, CA 94720

[2]INRIA - Rhone-Alpes et
Laboratorie de Biométrie et Biologie Evolutive
 UMR CNRS 5558
 Université Lyon 1
 43, bvd du 11 novembre
 69622 Villeurbanne Cedex, France

[3]Department: Interdisciplinary Research Institute
Institution: CNRS-Univ. Lille1-Lille2
50 Avenue de Halley
Villeneuve d'Ascq, France

[*]corresponding author: komeili@berkeley.edu

Developmental events across the prokaryotic life cycle are highly regulated at the transcriptional and post-translational levels. Key elements of a few regulatory networks are conserved among phylogenetic groups of bacteria, although the features controlled by these conserved systems are as diverse as the organisms encoding them. In this work, we probe the role of the CtrA regulatory network, conserved throughout the Alphaproteobacteria, in the magnetotactic bacterium, *Magnetospirillum magneticum* strain AMB-1, which possesses unique intracellular organization and compartmentalization. While we show that CtrA in AMB-1 is not essential for viability, it is required for motility, and its putative phosphorylation state dictates the ability of CtrA to activate the flagella biosynthesis gene cascade. Gene expression analysis of strains expressing active and inactive CtrA alleles point to the composition of the extended CtrA regulon, including both direct and indirect targets. These results, combined with a bioinformatic study of the AMB-1 genome, enabled the prediction of an AMB-1 specific CtrA binding site. Further, phylogenetic studies comparing CtrA sequences from Alphaproteobacteria in which the role of CtrA has been experimentally examined reveals an ancestral role of CtrA in the regulation of motility and suggests that its essential functions in other Alphaproteobacteria were acquired subsequently.

INTRODUCTION

The past decades have proved exciting for bacterial cell biology, as the mechanisms underlying subcellular organization and developmental processes in microorganisms have been increasingly uncovered. Developmental processes include flagella, pili, and secretion system biogenesis while subcellular organization is exemplified by cytoskeletal elements which coordinate chromosome replication, cell wall synthesis, and even the organization of intracellular organelles (17, 35, 54). The temporal and spatial regulation of developmental events across the bacterial cell cycle has been most thoroughly investigated in the Alphaproteobacterium *Caulobacter crescentus*. The proper execution of *C. crescentus* asymmetric cell division requires timed coordination of gene expression, protein activation, and assembly of polar organelles, as well as physically partitioning in different parts of the cell proteins which regulate these processes (18). Coordination of these events involves a regulatory network of proteins that activate or repress one another through gene expression, post-translational modification, and protein stability (9). At the core of this network is the response regulator and transcription factor CtrA.

In *C. crescentus*, *ctrA* is an essential gene, whose product is tightly regulated at the level of gene expression, protein activation, and proteolysis (9). CtrA represses initiation of DNA replication by directly binding several sites flanking the origin of replication (39). Additionally, CtrA acts as a transcription factor to directly control the expression of a quarter of cell-cycle regulated genes in *C. crescentus*, including genes involved in DNA methylation, cell division, signal transduction, and motility (29, 30, 51). CtrA activity depends on the phosphorylation state of a conserved aspartate residue; phosphorylation of CtrA through the histidine kinase-response regulator CckA and the histidine phosphotransferase ChpT enables CtrA to bind and inhibit the origin of replication, as well as activate or repress gene promoters, including its own, at specific recognition sites (3, 11, 48). Phosphate flow to CtrA via CckA is inhibited by the essential response regulator DivK, whose transcription is also under CtrA control (3, 7)).

In addition to its essential role in the progression of the *C. crescentus* cell cycle, CtrA homologs in *Sinorhizobium meliloti*, *Agrobacterium tumefaciens* and *Brucella abortus* have been shown, or have been suggested, to be essential for viability (1, 2, 23, 40). In contrast, in *Rhodobacter capsulatus*, *Rhodospirillum centenum* and *Silicibacter* sp. TM1040, *ctrA* can be disrupted with

no adverse effects on the division cycle or cell survival, but is essential for regulating motility in these organisms (4, 27, 33, 34, 47). The disparate roles of CtrA in various members of the Alphaproteobacteria raises questions about the flexibility of regulatory networks, in which certain components are conserved, and yet play vastly different roles in the cell (6). What role might the response regulator CtrA play in an organism, for example, which possesses sub-cellular compartmentalization? If CtrA functions to direct polar organelle biogenesis and cell division in some Alphaproteobacteria, perhaps it may direct the fates of bacterial organelles in others. Here, we explore the regulatory network controlled by CtrA in the magnetotactic Alphaproteobacterium *Magnetospirillum magneticum* sp. AMB-1 (AMB-1), an organism capable of forming intracellular organelles.

Magnetotactic bacteria (MB) are a diverse group of prokaryotes which biomineralize chains of magnetosomes, membrane-enclosed magnetic crystals, within their cells, allowing these bacteria to align with the geomagnetic field and locate microaerobic environments more efficiently in a process termed magnetoaerotaxis. Biochemical and genetic analyses of magnetotactic species, such as *Magnetospirillum magneticum* AMB-1, have identified a number of proteins that participate in magnetic mineral biomineralization, magnetosome "activation," and magnetosome alignment (25, 26, 36, 46). Genes encoding most of the known magnetosome proteins are found in a genomic region conserved across magnetotactic bacteria; this 98 kb genomic region is essential for magnetosome formation in AMB-1 and is termed the Magnetosome Island (MAI) (15, 36, 53). While progress has been made in uncovering genes specific to steps of magnetosome formation, the integration of these processes within the global regulatory circuits of the organism is poorly understood. In this study, we took a targeted approach to investigate the global regulation of CtrA in the context of a microorganism possessing intracellular organelles by generating deletions of homologs of known cell cycle control genes: *ctrA* and *divK*. Interestingly, while *ctrA* and *divK* are not essential for viability or cell cycle progression in AMB-1, the deletion strains have motility defects indicating conservation of the CtrA phosphorylation pathway in flagella biosynthesis. A *ctrA* deletion in a hyper-motile Magnetosome Island deletion strain abolishes motility, while a deletion of CtrA's negative regulator *divK* induces motility in a previously non-motile wild-type genetic background. Global gene expression analysis of *ctrA* and *divK* deletion strains, as well as *ctrA* deletions complemented with active and inactive *ctrA* alleles, has revealed a novel CtrA regulon in AMB-1.

MATERIALS AND METHODS

Growth conditions *Magnetospirillum magneticum* strain AMB-1 was grown in Magnetospirillum Growth media (MG) under microaerobic conditions, as previously described (36). AMB-1 was grown in conical tubes filled with MG medium and incubated at 30°C. On plates, AMB-1 was grown on MG containing 0.7% agar, and media was supplemented with antibiotics as follows: kanamycin on solid media at 15μg/mL, kanamycin in liquid media at 7μg/mL, and carbenicillin in liquid media at 20μg/mL. For growth curves, AMB-1 was grown in 10mL MG medium in 20mL culture tubes and incubated at 30°C in a microaerobic chamber in which the oxygen concentration was kept below 10%. After two days of growth, cultures were diluted to OD_{400} 0.02 in fresh MG medium and returned to the microaerobic growth chamber. OD_{400} and Coefficient of magnetism (Cmag) measurements (performed as described previously),

14

were assayed every 90 minutes (26). Briefly, optical density of cultures are assessed with a bar magnet placed parallel or perpendicular to the light path in the spectrophotometer. Cmag values are expressed as a ratio of parallel to perpendicular OD_{400} values; thus a Cmag of 1 indicates a non-magnetic culture.

Strain construction and complementation All clonings were performed in *Escherichia coli* DH5αλpir grown in LB media. The antibiotic kanamycin was used at 50μg/mL. Gene deletions in *M. magneticum* AMB-1 via a two-step recombination method as described previously (36). A region (approximately 1000bp) upstream of each target gene was PCR amplified with BglII and BamHI restriction sites at the 5' and 3' ends, respectively. Similarly, a region (approximately 1000bp) downstream of the target gene was PCR amplified with BamHI and SpeI restriction sites at the 5' and 3' ends, respectively. These fragments were cloned in two steps into the BamHI and SpeI restriction sites of pAK0, a suicide plasmid carrying a kanamycin resistance cassette and the *sacB* gene, to yield vectors for deleting *ctrA* (*amb0629*) and *divK* (*amb3750*), respectively (**Table 2**). The plasmids were transferred to AMB-1 using conjugation via *E. coli* WM3064, and the transconjugants were selected for on MG plates containing kanamycin. Transconjugants were grown in liquid MG media and deletion mutants selected for on MG plates containing 2% sucrose. The sucrose resistant colonies were screened for the desired deletion and the absence of the kanamycin resistance cassette and *sacB* gene by PCR (36).

ctrA deletion strains were complemented by expressing WT, CtrA D51E, or D51A alleles from the *tac* promoter. The wild-type *ctrA* was PCR amplified and cloned into the expression vector pAK22 (25) using the EcoRI and SpeI restriction sites downstream of the *tac* promoter. The D51E and D51A alleles were generated following the Stratagene QuikChange PCR protocol. The gene conferring ampicillin resistance (*bla*), expressed downstream of a second *tac* promoter, was subsequently cloned using the SpeI restriction site, as increased complementation had been found to result when selecting on carbenicillin rather than kanamycin in AMB-1 (36) An empty vector negative control was constructed by mutating the EcoRI restriction site upstream of *ctrA* in the complementation vector to a SpeI site; *ctrA* was then excised by SpeI digestion followed by self-ligation.
All primers are listed in **Table S1**.

Synchronization of AMB-1 Exponentially growing cells were passaged in 4 x 50mL conical tubes until mid-exponential phase (OD_{400} 0.07-0.09). Continuous Percoll gradients were established in 15mL conical tubes by centrifuging 10mL 50% Percoll/MG solution (100% Percoll represents 90% Percoll diluted by 10% 10x MG salts) at 10,000x*g* for 30 minutes. AMB-1 cells were harvested by pelleting at 8000x*g* for 10 minutes, pooling the pellets in a single 1.5mL eppendorf. Cells were further concentrated by centrifugation at 16,000x*g* for 2 minutes. Cells were resuspended in 100μL and loaded on the top of the gradient. Gradients were centrifuged in a swing rotor at 800x*g* for 20 minutes. The top 500μL containing few cells were removed, and the next 200μL fraction was used to inoculate a 10mL MG culture which was grown in the microaerobic chamber. To verify synchronization of the culture, 100μL were removed every 40 minutes for triplicate cell counts using a haematocytometer.

RNA extraction and cDNA synthesis Exponentially growing cells were passaged in 50mL conical tubes until exponential phase (OD_{400} 0.04-0.08). Cells were vacuum-filtered using a

side-arm flask apparatus onto sterile Whatman Nucleopore Track-Etch Membrane filters. Filters were removed with sterilized forceps and deposited in sterile microcentrifuge tubes, which were immediately plunge frozen in liquid nitrogen and stored thereafter at -80°C. RNA was extracted directly off of the filters by applying 1mL Trizol reagent to each microcentrifuge tube. Samples were mixed by vortexing and left to incubate for five minutes. Supernatants were then transferred to 2mL Heavy Phase Lock tubes, to which 200µL chloroform were added and mixed. Phase Lock tubes were spun at 4°C at 12,000xg for 15 minutes, after which the supernatants were decanted into fresh microcentrifuge tubes. 500µL isopropanol were added, and the tubes were tilted gently for 10 minutes at room temperature before a second spin at 4°C of 12,000xg for 15 minutes. The supernatant was removed and the pellet washed with 1mL cold 75% ethanol and vortexed. Tubes were spun at 4°C at 7500xg for 5 minutes and the supernatants again removed. Pellets were air-dried for 10 minutes, then resuspended in 100µL RNase-free water. RNA quantity and quality were assessed using a NanoDrop (Thermo Scientific). Samples were treated with DNaseI (Invitrogen) and purified using the Qiagen RNeasy kit. Removal of genomic DNA was verified via PCR against two target genes. 1µg RNA was reverse transcribed using the Invitrogen SuperScript RT III kit as directed. Resulting cDNA was treated with RNaseA (NEB) and RNaseH (Invitrogen) to remove residual RNA, and was purified using the Qiagen PCR Clean up-kit, and eluted in 10% EB. cDNA quantity and quality was assessed using a NanoDrop.

Microarray sample preparation and array design 0.5µg cDNA was fluorescently-labeled with Cy3 using the Nimblegen One Color DNA Labeling kit as directed. Labeling reactions were incubated at 37°C overnight in the dark. Labeling reactions were stopped as directed, and samples were resuspended in 25µL nuclease-free water. 2µg Cy3-labeled cDNA was dried in a SpeedVac at 30°C in the dark. Microarray sample hybridization and scanning were conducted at the Fred Hutchinson Cancer Research Center, Seattle WA.

Our microarray consists of full coverage of the AMB-1 genome (GenBank Accession NC_007626), with each gene covered by 7 60nt probes. The entire genomic probe-set was duplicated on the array, and in addition, contained probe sets designed for 22 unannotated ORFs in the Magnetosome Island (genomic coordinates 977403-1097027), with 7 60nt probes per potential ORF. Potential ORFs in this genomic region were identified using NCBI ORF Finder and are listed in **Table 3**. The microarray design also included tiling of the Magnetosome Island, from genomic coordinates 977403-1097027. This region was covered by 8038 probes, 50 nt in length. However, results from these probes were not evaluated in this work.

Microarray data analysis Scanned microarray images were processed using ArrayScan software (Nimblegen). .pair files were generated for all arrays in the dataset, which were then normalized together using quantile normalization as described (5); gene calls were generated using the Robust Multichip Average (RMA) algorithm (20, 21). Gene expression changes between strains were considered significant if an average change across three biological replicates was greater than 1.5-fold above or below the average of three biological replicates of the comparison strain. Select targets of interest were chosen from among the list of significantly up-regulated genes for confirmation with quantitative RT-PCR.

Taqman RT-PCR Primer and probe sets for each target gene and endogenous gyrase control were designed using Primer Express (Applied Biosystems). Primer pair concentrations (900nM, 300nM, 100nM) were tested with a standard probe concentration (250nM) for optimal dilution curves against genomic DNA. Optimized primer/target-FAM probe sets were tested in multiplex reactions against the gyrase-VIC internal controls in 50 µL reactions. Multiplex Taqman reactions contained 2x Gene Expression Master Mix (Applied Biosystems), 250nM of both target and endogenous probes, 900nM gyrase forward and reverse primers, either 900 or 300nM target primers (**Table S2**), and were amended with nuclease-free water to 40µL. 10µL cDNA (0.4ng/mL) or nuclease water was added. The PCR protocol was executed as follows: 50°C for 2 min, 98°C for 10 min, followed by 40 cycles of 95°C for 15 sec and 60°C for 1 min on an Applied Biosystems Sequence Detection System 7300.

CtrA regulon prediction CtrA regulons were predicted by using a position weight matrix (PWM) modeling the position-specific variability of CtrA binding motifs. The PWM was learned on experimentally defined CtrA targets in *C. crescentus* as described (6). Although the use of a heterologous model can be justified by the conservation of the binding motif in phylogenetically diverse Alphaproteobacteria, we here decided to obtain a model trained on *M. magneticum* AMB-1, which could improve the predictions by taking into account the specific variability of DNA in this organism. Indeed, the 16mer corresponding to the CtrA binding motif comprises 9 positions that are well conserved and that give specificity to the matrix, but there are also 7 very variable positions, which in fact seem to model the background DNA, and thus it is specific of a given genome. To obtain the matrix we used MDscan, an algorithm designed for enriched sequence motifs identification (31). As input we used the sequence from 500 nt upstream of the ATG to 100 nt within the coding sequence of genes with significant change of expression in the *ctrA* mutant, and the full complement of intergenic sequences that is used by MDscan to derive a background model of DNA to weight the motifs occurrences using a Markov model of the appropriate order. We obtained a sequence motif closely resembling the one known in *C. crescentus*, which was subsequently used to characterize the presence of CtrA binding motifs in the whole genome. The PWM was used to scan the *M. magneticum* AMB-1 genome looking for occurrences of the CtrA binding motif in the region from 400 nucleotides upstream of the translation start site of a gene to 100 nucleotides within the coding sequence. Occurrences of the motif were scored using the following formula:

$$S = \frac{1}{L} \sum_{j=1}^{L} 2 \log_2 f_{ij}$$

where L is the length of the binding motif (in this case 16), and f_{ji} stands for the value located in the jth row i^{th} column of the PWM, and the column is determined by the nucleotide found at the jth position of the motif. This score is related to information theory, and indeed represents the information content of the motif given the PWM. When scanning an entire genome and assigning a score to every overlapping L-mer, the distribution of scores follow a normal distribution (6), so that the scores can be transformed in Z-scores to collect only those significant at a given threshold.

Enrichment analysis of CtrA regulon Once a threshold was established for assigning a gene to the CtrA regulon on the basis of the Z-score of the binding motif it owns upstream, we calculated if there is some bias in the functional categories belonging to the regulon. We measured the enrichment of the regulon by means of 10000 random sampling simulations in the genome. These results should be taken with caution, since this analysis simply reveals if the positive samples contain more genes of a given category than the average random samples, which is different from the effect of the regulator on the functional category, since indirect regulations can amplify the scope of a regulator with respect to its direct targets.

Transmission Electron Microscopy For TEM characterization, strains were grown in microaerobic conditions to OD_{400} ~0.2 and 1mL of cells were centrifuged and resuspended in ~10µL of MG medium. The cells were adsorbed onto 400-meshcopper grids (Ted Pella Inc) and the grids were analyzed as described previously (36).

Phylogenetic Analysis Orthologous sequences were retrieved using the bidirectional best hit criterion whereby orthology relationships were established between proteins occurring reciprocal first blast hits. Orthologous sets for the universal proteins were further refined on the basis of a preliminary phylogenetic analysis to remove deviant proteins placed in unexpected phylogenetic positions with respect to known taxonomic relationships between organisms in the dataset. Evolutionary analyses were performed using tools in Mega 5 (52) and all alignments were obtained with Muscle (12).

To build the tree of universal sequences (**Figure S5**), which we use as a proxy for the species tree, we used the Neighbor-Joining method (42) and a multi-alignment containing eight concatenated universal proteins. The proteins used were FusA, IleS, LepA, LeuS, PyrG, RecA, RecG and RplB, and were identified as useful molecular markers (43). The optimal universal tree based on CtrA sequences (**Figure S6**) has a sum of branch length of 8.065 (7.256). The percentage of replicate trees in which the associated taxa clustered together in the bootstrap test (50 replicates) are shown next to the branches, whose lengths correspond to evolutionary distances between sequences computed using the JTT matrix-based method (22). The units expressed are the number of amino acid substitutions per site. The rate variation among sites was taken into account with a discrete Gamma distribution (shape parameter = 1.3, 4 categories of rates). The analysis involved 48 amino acid sequences for the universal tree, comprising the same 47 present in the CtrA tree in addition to the *E. coli* concatamer that was used as an outgroup to place the root of the Alphaproteobacterial lineage in the tree. All positions containing gaps and missing data were eliminated giving a total of 2188 positions for the universal and 182 for the CtrA the final datasets.

A smaller CtrA tree in **Figure 5** was built by including only those species of Alphaproteobacteria in which the role of CtrA had been experimentally investigated, and it maintains the relative position of those species with respect to the complete tree. The bootstrap consensus tree inferred from 50 replicates (13) is taken to represent the evolutionary history of the taxa analyzed (13). Branches corresponding to partitions reproduced in less than 50% bootstrap replicates are collapsed. The percentage of replicate trees in which the associated taxa clustered together in the bootstrap test (50 replicates) are shown next to the branches (13). Initial tree(s) for the heuristic search were obtained automatically as follows. When the number of common sites was < 100 or

less than one fourth of the total number of sites, the maximum parsimony method was used; otherwise BIONJ method with MCL distance matrix was used. A discrete Gamma distribution was used to model evolutionary rate differences among sites (3 categories (+G, parameter = 0.9031)). The rate variation model allowed for some sites to be evolutionarily invariable ([+I], 12.9413% sites). The tree is drawn to scale, with branch lengths measured in the number of substitutions per site. The analysis involved 9 amino acid sequences, with a total of 231 positions in the final dataset.

Microarray data accession number. Microarray results obtained in this work are available in the NCBI GEO database under the accession number GSE35625.

RESULTS

CtrA is not essential for viability or progression of the AMB-1 cell cycle. Components of the CtrA signal transduction pathway, essential for cell viability and progression of the *Caulobacter crescentus* cell cycle, are conserved throughout the Alphaproteobacteria (6). A search of the AMB-1 genome revealed the presence of homologs not only of *ctrA* (*amb0629*), but also its negative regulator *divK* (*amb3750*) and its histidine-kinase partner *cckA* (*amb0620*). We generated non-polar deletions of the AMB-1 homologs of *ctrA* and *divK* and found that deletion strains were viable. Triplicate wild-type and Δ*ctrA* mutant strains were assayed for overall growth, as well as ability to align in an external magnetic field, as determined through a spectrophotometric assay represented by the coefficient of magnetism (Cmag). In all stages of growth, Δ*ctrA* behaved identically to wild-type, both in growth characteristics and acquisition of magnetism (**Figure 1A**). The slight decrease in Cmag in both wild-type and Δ*ctrA* strains around 15 hours could be attributed to cell division and thus segregation of existing magnetosome chains to daughter cells prior to the synthesis of new magnetosomes which follows the depletion of oxygen in the culture tubes.

To determine whether any aspect of the cell division cycle was affected by the loss of CtrA, we synchronized populations of AMB-1, released cells into fresh growth medium, and visually monitored cell cycle progression. Previous studies investigating the role of the cell cycle in magnetosome formation in AMB-1 have relied on lengthy repeated cold treatments to synchronize cells (45, 56); in this work, density gradient centrifugation was used as a potentially less disruptive method to rapidly obtain synchronous populations of both wild-type and Δ*ctrA* strains. Briefly, exponential phase cells are harvested and layered upon a pre-formed density gradient of 50% Percoll in conical tubes. Upon subsequent centrifugation, AMB-1 cells are separated according to size as confirmed by light microscopy. Small, newly-divided cells, concentrated at the top of the gradient, are harvested by pipette and used to inoculate fresh cultures of AMB-1. Synchronization of resulting cultures was assessed through visual cell counts. Wild-type cultures maintain relatively constant cell numbers throughout the four-hour growth period, after which point the population doubles in size. AMB-1 cultures remain synchronized throughout two doubling periods. In triplicate synchronization experiments, the Δ*ctrA* strain also exhibited synchronous growth with a four-hour doubling period when subjected to the same treatment as wild-type AMB-1 (**Figure 1B, Figure S1**). The timing offset of the initial cell doublings between wild-type and Δ*ctrA* strains reflects variation between experiments in the accuracy of harvesting the most newly-divided cells from the uppermost Percoll layer

19

rather than a growth rate difference, supported by the results in **Figure 1A**.These results suggest that CtrA is not essential for AMB-1 viability, nor does it play a prominent role in the progression of the cell cycle.

CtrA and DivK regulate motility in AMB-1. During mutant characterization, it was observed that 30% of Δ*divK* mutant cells exhibited constitutive motility. This is unlike the motility behavior of wild-type AMB-1, which upon isolation and under standard laboratory conditions is non-motile (less than 1% of exponential phase cells swim) (32). In contrast to the minimal wild-type swimming activity, a spontaneous loss of the Magnetosome Island (MAI) renders the cells not only incapable of producing magnetosomes, but also motile such that 100% of the cells are swimming in liquid culture. Further, wild-type AMB-1 rarely produces flagella, while MAI cells are consistently flagellated (**Figure S2**). Potentially, the MAI encodes a negative regulator of motility, which, when lost, renders the cells incapable of regulating their swimming behavior. While a *divK* deletion does not phenocopy a deletion of the MAI, the phenotype was intriguing, as *ctrA* has been well-characterized as a class I flagellar biosynthesis gene for its regulation of flagellar gene expression in *C. crescentus* and a regulator of motility in a number of other Alphaproteobacteria (6, 29, 38).

To determine whether CtrA could indeed act as an upstream regulator of flagellar biosynthesis in AMB-1, and its relation to factors controlling motility in the MAI, we generated a deletion of *ctrA* in the hyper-motile ΔMAI background. The double mutant was completely non-motile, suggesting a role for the CtrA pathway in motility in AMB-1, and furthermore suggesting that its regulation of motility is downstream of factors in the MAI (**Figure 2A**). Expression of CtrA from a plasmid was sufficient to restore motility to the double mutant strain.

Putative phosphorylation of CtrA is essential for motility. CtrA belongs to the OmpR subfamily of response regulators, and is characterized by an additional C-terminal DNA binding domain (38). Members of this family possess a conserved aspartate residue inside the receiver domain, phosphorylation of which alters activity. In *C. crescentus*, phosphorylation of CtrA occurs exclusively at position D51 and is essential for cell viability (38). As such, phosphorylation is tightly regulated, with negative regulation of CtrA stemming from the response regulator DivK (3). Replacing the conserved aspartate residue in CtrA with a glutamate prohibits actual phosphorylation of the protein yet mimics the active, phosphorylated state and provides essential cell activities (10, 48). This critical aspartate residue is conserved in the AMB-1 homolog of CtrA (**Figure 2B**). The motility phenotype of the *divK* deletion, ostensibly removing a negative regulator of CtrA in the signal transduction pathway, suggests that CtrA's activity in AMB-1 is controlled in a manner similar to that in *C. crescentus*.

To determine whether potential phosphorylation of CtrA is involved in regulation of motility in AMB-1, we complemented the Δ*ctrA* and Δ*ctrA*ΔMAI strains with alleles mimicking the phosphorylated and active (D51E), and unphosphorylatable and inactive (D51A) versions of CtrA. Mutating the conserved aspartate residue to glutamate (CtrA D51E) yielded an increase in motile cells above the levels achieved with wild-type CtrA in the Δ*ctrA* background (50% against 33%, respectively) (**Figure 2A**). CtrA D51E expressed in Δ*ctrA*ΔMAI did not increase the level of swimming beyond that of wild-type CtrA (50% against 57%, respectively), possibly indicating that although the CtrA D51E allele is sufficient to overcome the negative regulation of motility

from the MAI, expression of wild-type CtrA is better able to complement the Δ*ctrA*ΔMAI strain. In both complementation experiments, expression from the vector and plasmid maintenance may explain the lack of fully restored motility in these strains.

In contrast to complementation experiments with wild-type CtrA and CtrA D51E alleles, no motile cells were ever observed when expressing CtrA D51A from the identical construct. These results suggest that the phosphorylation state of CtrA is essential for motility in AMB-1, and that swimming behavior observed in the *divK* deletion strain potentially stems from an increased population of phosphorylated and active CtrA.

CtrA regulon in AMB-1 is distinct from that of *Caulobacter*. In Alphaproteobacterial species where CtrA is not essential for viability such as *R. capsulatus, R. centenum* and *Silicibacter* sp. TM1040 (4, 27, 34, 47), CtrA still appears to regulate flagellar motility. In AMB-1, CtrA is also not essential, does not appear to play a role in the formation of magnetosome organelles, and seems to be involved in the regulation of motility. To ascertain the role of CtrA more specifically in motility, and to learn about its regulon in a bacterium in which it is not essential for viability, we used microarrays to probe global gene expression patterns when different alleles of CtrA were expressed.

Microarrays were designed using the published AMB-1 genome (GenBank AP007255). Each array contained duplicated genomic probe sets, with seven probes per gene. Additional probe sets were designed detecting the expression of unannotated ORFs in the Magnetosome Island; these 22 ORFs were predicted by ORF finder (**Table 3**). To identify the CtrA regulon in AMB-1, we analyzed cDNA reverse-transcribed from RNA extracted from triplicate biological replicates of wild-type AMB-1, Δ*ctrA*, Δ*divK*, and Δ*ctrA* complemented with CtrA D51E, CtrA D51A or an empty expression vector. Because the *ctrA* deletion behaves phenotypically like wild-type AMB-1 in the conditions tested, we relied on the expression of mutant CtrA alleles to identify genes regulated, positively and negatively, by CtrA. Genes whose expression increased at least 1.5-fold in both Δ*ctrA* +CtrA D51E relative to Δ*ctrA* + CtrA D51A and Δ*ctrA* + empty vector were considered in this study to be up-regulated by CtrA (**Figure 3A**). This positive CtrA regulon contains 283 genes, with 103 genes having at least 2-fold increases in gene expression.

Of the 283 genes comprising the potential CtrA regulon in AMB-1, 14 were identified with roles in flagellum biosynthesis, 7 of which are in a putative operon (*amb0498* to *amb0506*) (**Figure 3B**). These genes encode proteins which comprise the motor-switch and hook and basal body components of the flagella. Eleven of those fourteen flagella biosynthesis genes were similarly up-regulated in the *divK* deletion strain. Flagellin-like genes *amb1999* and *amb0684* were expressed at high and moderate levels, respectively, in all genetic backgrounds and thus do not appear to account for the lack of motility in wild-type AMB-1. Rather, the production of the basal aspects of the flagella appears to be the limiting factor in determining the ability of AMB-1 to swim. The increased expression of flagella biosynthesis genes in Δ*divK* and cells expressing the active-mimic allele CtrA D51E suggests that phosphorylated CtrA is necessary for the transcription of these genes, either directly or indirectly, and supports the observed motility phenotypes. Microarray gene expression results for two genes, *amb2833* and *amb0504*, which encode a hypothetical protein and the flagellar hook protein FlgE, respectively, were confirmed by quantitative RT-PCR **(Figure S3).**

Other members of the potential CtrA regulon which could contribute to the regulation of swimming behavior of AMB-1 include four transcriptional regulators (*amb0659, amb1405, amb2069,* and *amb2080*), two histidine kinases (*amb1336* and *amb2644*), and five additional response regulators (*amb0348, amb0848, amb2829, amb3405,* and *amb4301*). While up-regulation of several flagella biosynthetic gene clusters was observed, it is possible that this gene expression pattern is due to a downstream effect of the CtrA D51E allele, and not to direct transcriptional control by CtrA itself. Bioinformatic prediction of CtrA binding sites in AMB-1, discussed subsequently, supports the hypothesis that the CtrA regulon as identified by microarray contains several indirect targets, possibly a result of downstream regulatory and transcription factors.

Beyond genes with putative motility and regulatory functions, genes encoding metabolic and transport factors were highly enriched in the identified CtrA regulon (**Figure 4A**). This class of genes includes several ABC-type transporters, electron transfer flavoproteins, NADH oxidoreductases, and factors involved in nitrogen metabolism. In sum, these genes constitute 57 of the 283 genes in the potential CtrA regulon. Under standard laboratory conditions, no growth advantage or disadvantage has been detected for cells expressing CtrA D51E (data not shown), nor does the growth of Δ*ctrA* deviate from wild-type (**Figure 1**). However, these results do not preclude the possibility of growth effects under different growth conditions.

As compared to the positive CtrA regulon, fewer genes (169 in sum) were down-regulated more than 1.5-fold in Δ*ctrA* + CtrA D51E relative to both Δ*ctrA* + CtrA D51A, and the empty vector control (**Figure S4**), 31 of which were down-regulated more than 2-fold. The majority of these genes encode hypothetical proteins, although among them are additional metabolic and redox proteins and 18 putative regulatory proteins. Again, the only deviation in phenotype observed under standard laboratory conditions between Δ*ctrA* + CtrA D51E and Δ*ctrA* was increased motility, so the effects of down-regulating these 169 genes are unknown. Given the number of regulatory genes affected both positively and negatively by the expression of CtrA D51E, it is likely that many of the components of the putative regulon are not direct targets of CtrA.

In *C. crescentus*, CtrA has been shown to regulate genes cotranscribed in operons or divergently transcribed from a shared promoter region (29). A search in AMB-1 revealed that 81 genes up-regulated by the expression of CtrA D51E are potentially transcribed in operons, and 4 are potentially divergently transcribed from a shared regulatory region. These gene clusters include genes encoding for flagella biosynthesis, cytochrome synthesis, nitrogen fixation, and sulfite reduction functions. Similarly, repressed expression of 30 genes is potentially due to transcription from 14 shared promoters, while an additional 9 genes are potentially divergently expressed from 4 shared regulatory regions.

Of particular note is the paucity of cell cycle control genes found to be regulated by the expression of CtrA D51E. In *C. crescentus*, the CtrA regulon is known to directly control the transcription of such factors as *ftsZ, ftsW, dnaA* and *ccrM* (24, 29, 30). Of these factors, only the AMB-1 homolog of the essential *C. crescentus* methyltransferase CcrM (*amb3988*) was up-regulated by expression of CtrA D51E, but as a *ctrA* deletion mutant was viable, *ccrM* is also unlikely to be essential in AMB-1. Additionally, our microarray data suggests that *ccrM* is

expressed in Δ*ctrA* but that its expression increases upon the introduction of the CtrA D51E allele. Because homologs of other critical cell cycle genes were not identified in our data set, the progression of the cell cycle is potentially decoupled from CtrA, suggested by our viability and synchronization data. The regulation of these factors and the progression of the AMB-1 cell cycle remain elusive.

CtrA regulon in AMB-1 is enriched in potential CtrA binding sites. Because the putative CtrA regulon as predicted by microarray results contained several genes encoding regulatory proteins, it is possible that some gene expression changes are due to indirect effects of CtrA D51E expression. To more precisely determine the potential CtrA regulon in AMB-1, we modeled the AMB-1 CtrA binding motif as a probability matrix as explained in Materials and Methods. Genes identified as part of the putative CtrA regulon by microarray analysis were scanned across a -500 to +100 window relative to the start site and assigned Z-scores according to the probability that their upstream sequence contains occurrences of CtrA binding, with respect to the background DNA. The consensus AMB-1 CtrA binding motif was determined as TTAA(CGNANNT)TAA[T/A]C. This motif was then used to scan the entire AMB-1 genome for putative CtrA binding sites.

Using a threshold of 4 for the Z-score per CtrA motif occurrence, the CtrA regulon as defined by the gene expression results is enriched in the potential CtrA binding sites relative to the rest of the AMB-1 genome (p-value 0.0018). Genes possessing a significant CtrA binding motif include *amb0614* and *amb0506*, which encode flagellar basal body and hook-length regulatory proteins, respectively (**Figure 3A**). While there remains a significant proportion of the proposed CtrA regulon which does not contain detectable CtrA binding sites by homology to the *C. crescentus* motif, these genes could be under indirect CtrA control, as several proteins of putative regulatory function were identified as being both up-regulated by CtrA D51E and possessing a possible upstream CtrA binding motif (*amb2014*, *amb0659*, *amb2080*, *amb2069*, *amb3405*, *amb2829*, *amb3261*, *amb2643*, *amb0848*). False negatives are also present in the predictions, because (i) we applied a necessary, but arbitrary threshold to include a motif occurrence, and (ii) transcription factor binding motifs are intrinsically variable, which is at the basis of the difficulties in reconstructing gene regulatory networks from sequence alone. Auto-regulation of CtrA is a feature well-characterized in *C. crescentus* (11), and has also been suggested for *S. meliloti* CtrA based on the presence of five CtrA-binding motifs identified in its own promoter (1). A low score motif was detected upstream of CtrA itself in AMB-1, which indicates possible auto-regulation as well (data not shown).

Random sampling of the AMB-1 genome for genes carrying the CtrA motif, and a subsequent comparison of the representation of Cluster of Orthologous Gene (COG) categories in this group of genes against the genomic COG distribution (6) reveals that targets of CtrA are enriched in genes with no assigned function, inorganic ion transport and metabolism, and to a lesser extent, signal transduction mechanisms and transcription (**Figure 4B**). The modest enrichment in genes with putative roles in transcription could suggest that the effect of CtrA is mediated by specific regulators. It should be noticed that enrichment analyses in general provide a biased estimate of the importance of CtrA for regulating a given functional category. Indeed, it has been shown that CtrA is crucial for motility in AMB-1, while the category is not enriched. For motility, this depends on the functional role of the targets and their position in a hierarchical network of

events. One of the targets we obtained, *amb0614* (*flgB*) has been classified in *C. crescentus* as a class II flagellar gene, demonstrating that, despite the little number of genes directly regulated by CtrA, the influence of the regulator is important.

While the predictions made regarding the identity and role of the CtrA binding motifs in AMB-1 has not yet been confirmed by *in vitro* or *in vivo* DNA binding assays, the detected motif is quite similar to that characterized in *C. crescentus* and its enrichment upstream of genes in the CtrA regulon is suggestive of direct CtrA control.

Regulation of Magnetosome Island genes by CtrA. Based on gene expression and computational data sets, genes in the MAI are among the CtrA regulon in AMB-1. Three genes in particular were highly-upregulated by the expression of CtrA D51E with respect to CtrA D51A and empty vector control strains. These genes are *amb0934*, *amb0935* and *amb0970*, whose expression levels increased 3.2-fold, 4.5-fold, and 2.5-fold, respectively, between CtrA D51E-expressing and CtrA D51A-expressing strains. None of these genes has an upstream predicted CtrA binding site, and no phenotype was detected in a deletion of a region of the MAI encompassing both *amb0934* and *amb0935* (36). However, a deletion of *amb0970*, which encodes the magnetosome membrane protein MamP, results in the biomineralization of only one or two very large magnetite crystals per cell (36). Because no biomineralization defect was detected in Δ*ctrA* complemented with CtrA D51E as compared to wild-type, this suggests that the degree of overexpression of *mamP* in the microarray experiments does not adversely affect magnetosome formation (data not shown). Additional MAI genes were up-regulated by the expression of CtrA D51E; these include three potentially unannotated open reading frames. As mentioned above, our microarray contains seven 60mer probes designed against open reading frames not present in the annotated AMB-1 genome, but which are predicted by ORF Finder. Two of these genes are predicted hypothetical ORFs in Region 2 of the MAI (R2-1, R2-2), and a third is a predicted hypothetical ORF in Region 8 of the MAI (R8-1). Of further note was the slight over-expression of *amb0994*, a predicted methyl-accepting chemotaxis protein, which was recently shown to form polar clusters in AMB-1 and to interact with MamK, an actin-like protein involved in the chain organization of magnetosomes (37). Although *amb0994* was not as significantly overexpressed relative to other genes in the CtrA regulon (1.74-fold), its promoter region does possess strong homology to a CtrA binding site suggesting direct CtrA control. Altogether, these results indicate that CtrA-dependent changes in the expression level of some MAI genes do not lead to discernible disruptions in magnetosome formation or magnetotaxis.

Phylogenetic analysis of CtrA homologs in Alphaproteobacteria Phylogenetic trees constructed from concatenated sequences of universal proteins and from CtrA sequences retrieved across the Alphaproteobacteria are mostly congruous, indicating a lack of horizontal transfer of CtrA homologs within the group (**Figure S5 and S6**). Integrating a condensed phylogenetic tree of CtrA sequences, which highlights only those species of Alphaproteobacteria in which the biological roles of CtrA have been experimentally investigated, with the associated experimental results allows us to place a divergence event, denoted by a star, beyond which point one CtrA lineage acquired an essential role in its hosts (**Figure 5**). Mapping observed functions of CtrA onto this condensed tree further suggests an ancestral role in motility for CtrA in the Alphaproteobacteria.

DISCUSSION

Regulation of motility in AMB-1 In this study, we have shown that CtrA in AMB-1 is not essential for cell viability, nor does its loss induce observable cell division defects. Further, we have shown that the Δ*ctrA* mutant is indistinguishable from wild-type AMB-1 in its ability to align in a magnetic field throughout its growth. A comparison of wild-type AMB-1 with Δ*ctrA* mutants provides only a faint hint at the role of CtrA, as the occasionally swimming wild-type cells are never observed in Δ*ctrA*. However, as a deletion of *ctrA* in the hypermotile ΔMAI genetic background is non-motile, this work suggests a terminal role for CtrA in the regulation of motility in AMB-1. The inability of the Δ*ctrA*ΔMAI strain to swim suggests that CtrA itself is genetically downstream of factors regulating motility encoded in the MAI. In addition, complementing a *ctrA* deletion with CtrA D51E renders half of the cells motile, thus overcoming inhibition from the MAI. The motility of the *divK* deletion strain further supports the model that phosphorylated CtrA is necessary for expression of flagella biosynthesis genes and the swimming behavior of AMB-1 (**Figure 6**).

However, the *divK* deletion achieved only 30% motility compared to the cells of the ΔMAI strain, 100% of which are motile. Thus, other regulatory factors are certain to play roles in the phosphorylation or stability of CtrA in AMB-1. These regulatory agents could be linked to the MAI or could be independent. The C-terminus of CtrA in AMB-1 is highly divergent from that of CtrA in *C. crescentus*, and does not possess an *ssrA*-like degradation tag, however, so regulation by ClpXP proteolysis seems unlikely (10, 41).

Magnetoaerotaxis The ability to swim proves beneficial for aquatic microorganisms, as they can propel themselves through liquid media to seek out environments most suited to their metabolic capabilities. Combining flagellar motility with chemotactic sensory and regulatory systems further enables bacteria to sample their current environment and either maintain or alter their trajectory based upon the chemicals sensed. Magnetotactic bacteria, such as *Magnetospirillum magneticum* sp. AMB-1, possess an additional directional sense, in that they can use their internal magnetosome chains to passively align with external magnetic fields. It has been proposed that such an alignment limits a three-dimensional search for optimal aquatic environments to one-dimension, thus increasing the efficiency with which these organisms find microaerobic or anaerobic environments (49). This behavior is termed magnetoaerotaxis when alignment with magnetic fields is combined with an aerotactic search for low oxygen concentrations (14).

Interestingly, the model organism in this study was isolated and characterized as a primarily non-motile magnetotactic species (32). This is in stark contrast to other species of MB, most of which constitutively swim. Given the current hypothesis explaining the evolutionary benefits of magnetosome chain formation, this observation is indeed surprising. Wild-type AMB-1 fails to swim even when challenged with increased or decreased iron or oxygen concentrations (unpublished results). Potentially the isolation and current growth conditions are sufficient to satisfy the nutritional and energetic requirements of AMB-1, thus negating any reason to devote cellular energies towards building and rotating flagella. Still, the dramatic swimming behavior of the Δ*MAI* strain and the motility induced upon expression of CtrA D51E shows that AMB-1 is indeed capable of swimming, but that this behavior is repressed in wild-type cells. Given that

magnetoaerotaxis is a defining characteristic of AMB-1, of which motility is a critical part, a means to regulate that motility could be evolutionarily advantageous. Understanding the mechanism by which factors in the MAI influence motility through the CtrA pathway will be fruitful progress in the field. Thus far, a genetic dissection of the MAI has not yielded mutants with increased motility like that seen in ΔMAI mutants, hinting at genetic redundancy or multiple layers of regulation within the MAI (36). It is also important to note that MB are commonly isolated using a magnetically guided swimming-based procedure termed the "racetrack assay" (55). Thus, it is possible that the isolation of these organisms has been biased towards specific species or genetic-variants that are constitutive swimmers.

Role of CtrA in AMB-1 Beyond the motility phenotypes observed in the Δ*divK* and the Δ*ctrA*ΔMAI strains, no additional phenotypic variations from wild-type were observed. CtrA does not appear to play an essential role in the viability or the cell division cycle of AMB-1. One of our initial questions was whether the CtrA pathway might play a role in the development or segregation of bacterial organelles, as it serves to direct flagella and stalk biogenesis in *C. crescentus*, as well as the production of Gene Transfer Agent particles in *R. capsulatus* (27, 28). Again, we could detect no defect in magnetosome formation in the *ctrA* deletion or complemented strains either by the Cmag assay or by TEM. Interestingly, some MAI genes are constituents of the proposed CtrA regulon, as detected by microarray analysis of Δ*ctrA* complemented with CtrA alleles mimicking either active or inactive forms of the protein. One such gene, *amb0970* or *mamP*, was significantly up-regulated when D51E was expressed relative to D51A or empty vector controls; it was shown previously that the loss of *mamP* has severe consequences for crystal number and size (36). Potentially the transcriptional increases of *mamP* beyond wild-type levels are not sufficient for altering magnetite biomineralization.

Essential features of CtrA in *C. crescentus*, such as the regulation of DNA replication and cell division, fall outside the sphere of influence of CtrA in AMB-1. The coordination of these events with the segregation and division of the magnetosome chain remains elusive.

Divergent roles of CtrA in Alphaproteobacteria The common feature of the CtrA pathways in many Alphaproteobacteria appears to be its role in motility, and more specifically in flagellar biosynthesis. Genetic, gene expression and promoter analyses in *C. crescentus*, *Rhodobacter capsulatus*, *Rhodospirillum centenum*, *Silicibacter* sp. TM1040, and now *M. magneticum* AMB-1 have shown the involvement of CtrA in the regulation of motility. In particular, phosphorylation of CtrA appears to be essential for this role. Expression of CtrA D51A in *R. centenum* is not sufficient to restore wild-type swarm behavior in a Δ*ctrA* mutant (4). While dependence on phosphorylation state has not been established for CtrA in *R. capsulatus*, gene expression analysis of a *ctrA* disruption mutant revealed that CtrA is primarily a positive regulator of genes in this organism and is required for expression of flagellar biosynthesis and chemotaxis genes (33). Despite the commonality of motility regulation by the CtrA regulatory pathway in these species, CtrA also takes on alternative, and sometimes essential, roles in each organism which carries the gene.

Analysis of the phylogenetic relationships among CtrA alleles from organisms in which its biological role has been investigated suggests that regulation of motility by CtrA is an ancestral trait (**Figure 5**). A divergence event, noted with a star, demarks a boundary between organisms

in which CtrA has acquired an essential role from those in which CtrA retains control of motility and other, non-essential functions unique to its host. In *C. crescentus*, the essential role of CtrA in viability, as well as its role in flagellar biosynthesis has been well-characterized. While a direct link between CtrA and motility has not been established in *A. tumefaciens*, motility and flagellin gene expression vary across the cell cycle, progression of which is hypothesized to rely on CtrA (23). *B. abortus*, while itself a non-motile species, encodes some elements of the flagella biosynthesis pathway (19). *S. meliloti* has hierarchical assembly of flagella, expression of which is essential for establishment of nitrogen-fixing nodules on roots of legumes (50); regulation by CtrA is unknown, although predicted based on potential CtrA binding sites (6).

The recently sequenced genomes of two deeply branching alphaproteobacteria, *Odyssella thessalonicensis* and *Midichloria mitochondrii*, pose intriguing questions regarding the origin of motility in the *Alphaproteobacteria* and the transition to intracellular lifestyles. *M. mitochondrii* diverged ancestrally to the *Rickettsiales*, and while it adopts an intracellular lifestyle, it retains a full complement of flagellar biosynthesis genes, some of which are possibly expressed inside host tissues (44). This organism, however, does not encode a definitive CtrA homolog; on the other hand, *O. thessalonicensis*, which by 16S phylogeny is placed between the *Rickettsiales* and the rest of the *Alphaproteobacteria*, does possess a CtrA homolog in addition to some flagellar biosynthesis genes (16).

In light of these new findings, we can posit that the ancestral alphaproteobacterium was motile and during its evolutionary journey acquired regulation of motility by the response regulator CtrA. In the *Rickettsiales* and protomitochondrial lineages, the necessity for motility was removed upon the transition to intracellular lifestyles, and the flagellar biosynthesis genes were lost.

Amino acid sequence across the C-terminal domains of CtrA in Alphaproteobacteria is highly conserved (**Figure 2B**), and identified CtrA binding sites are quite similar among species in which where they have been determined. Therefore, it appears likely that the divergent cellular functions adopted by CtrA across the phyla are due not to divergent properties of CtrA itself, but rather the promoter sequences of the genes on which it exerts transcriptional control. Regulation of CtrA's activity, no doubt, will also vary between species due to differences in the upstream phosphorelay signals that it receives, but the output will be chiefly determined by the presence or absence of a CtrA binding motif in the promoter region of target genes (6). In AMB-1, these targets are primarily genes with motility, metabolic, or unknown functions and bear little overlap with regulons of species in which CtrA plays direct roles in DNA replication and cell division. In species where CtrA is essential for those processes, the regulation of CtrA's activity is more intricately controlled through checks and balances of protein levels, localization, and phosphorylation state than is predicted for species in which CtrA plays a more accessory role in the organism's lifestyle (6). AMB-1 potentially occupies an intermediary evolutionary niche, as gene expression results and bioinformatic predictions suggest control of DNA methylation through CcrM, although CtrA is likely not the only regulator of this process, as CcrM expression remained even in the absence of CtrA.

The results of the study presented here are the most comprehensive experimental examination of a putative CtrA regulon in an organism in which the protein is not essential. As such it has

provided a glimpse into the evolution and divergent specialization of this important regulator and provides the basis for future detailed mechanistic studies into its function in AMB-1.

ACKNOWLEDGEMENTS

REFERENCES

1. **Barnett, M. J., D. Y. Hung, A. Reisenauer, L. Shapiro, and S. R. Long.** 2001. A homolog of the CtrA cell cycle regulator is present and essential in *Sinorhizobium meliloti*. J. Bacteriol. **183:**3204-3210.
2. **Bellefontaine, A. F., C. E. Pierreux, P. Mertens, J. Vandenhaute, J. J. Letesson, and X. D. Bolle.** 2002. Plasticity of a transcriptional regulation network among alpha-proteobacteria is supported by the identification of CtrA targets in *Brucella abortus*. Mol. Microbiol. **43:**945-960.
3. **Biondi, E. G., S. J. Reisinger, J. M. Skerker, M. Arif, B. S. Perchuk, K. R. Ryan, and M. T. Laub.** 2006. Regulation of the bacterial cell cycle by an integrated genetic circuit. Nature **444:**899-904.
4. **Bird, T., and A. MacKrell.** 2011. A CtrA homolog affects swarming motility and encystment in *Rhodospirillum centenum*. Arch. of Microbiol. **193:**451-459.
5. **Bolstad, B. M., R. A. Irizarry, M. Ã…strand, and T. P. Speed.** 2003. A comparison of normalization methods for high density oligonucleotide array data based on variance and bias. Bioinformatics **19:**185-193.
6. **Brilli, M., M. Fondi, R. Fani, A. Mengoni, L. Ferri, M. Bazzicalupo, and E. Biondi.** 2010. The diversity and evolution of cell cycle regulation in alpha-proteobacteria: a comparative genomic analysis. BMC Sys. Bio. **4:**52.
7. **Chen, Y. E., C. Tropini, K. Jonas, C. G. Tsokos, K. C. Huang, and M. T. Laub.** 2011. Spatial gradient of protein phosphorylation underlies replicative asymmetry in a bacterium. Proc. Natl. Acad. Sci. USA **108:**1052-1057.
8. **Cheng, Z., K. Miura, V. L. Popov, Y. Kumagai, and Y. Rikihisa.** 2011. Insights into the CtrA regulon in development of stress resistance in obligatory intracellular pathogen *Ehrlichia chaffeensis*. Mol. Microbiol. **82:**1217-1234.
9. **Curtis, P. D., and Y. V. Brun.** 2010. Getting in the loop: regulation of development in *Caulobacter crescentus*. Microbiol. Mol. Biol. Rev. **74:**13-41.
10. **Domian, I. J., K. C. Quon, and L. Shapiro.** 1997. Cell type-specific phosphorylation and proteolysis of a transcriptional regulator controls the G1-to-S transition in a bacterial cell cycle. Cell **90:**415-424.
11. **Domian, I. J., A. Reisenauer, and L. Shapiro.** 1999. Feedback control of a master bacterial cell-cycle regulator. Proc. Natl Acad. Sci. USA **96:**6648-6653.

12. **Edgar, R. C.** 2004. MUSCLE: multiple sequence alignment with high accuracy and high throughput. Nucl. Acids Res. **32:**1792-1797.

13. **Felsenstein, J.** 1985. Confidence limits on phylogenies: An approach using the bootstrap. Evolution **39:**783-791.

14. **Frankel, R. B., D. A. Bazylinski, and D. Schüler.** 1998. Biomineralization of magnetic iron minerals in bacteria. Supramolecular Science **5:**383-390.

15. **Fukuda, Y., Y. Okamura, H. Takeyama, and T. Matsunaga.** 2006. Dynamic analysis of a genomic island in *Magnetospirillum* sp. strain AMB-1 reveals how magnetosome synthesis developed. FEBS letters **580:**801-12.

16. **Georgiades, K., M.-A. Madoui, P. Le, C. Robert, and D. Raoult.** 2011. Phylogenomic Analysis of *Odyssella thessalonicensis* Fortifies the Common Origin of *Rickettsiales*, *Pelagibacter ubique* and *Reclimonas americana* Mitochondrion. PLoS ONE **6:**e24857.

17. **Gitai, Z., N. A. Dye, A. Reisenauer, M. Wachi, and L. Shapiro.** 2005. MreB actin-mediated segregation of a specific region of a bacterial chromosome. Cell **120:**329.

18. **Hallez, R., A.-F. Bellefontaine, J.-J. Letesson, and X. De Bolle.** 2004. Morphological and functional asymmetry in α-Proteobacteria. Trends Microbiol. **12:**361-365.

19. **Halling, S. M.** 1998. On the presence and organization of open reading frames of the nonmotile pathogen *Brucella abortus* similar to Class II, III, and IV flagellar genes and to LcrD virulence superfamily. Microb. Comp. Genomics **3:**21-29.

20. **Irizarry, R. A., B. M. Bolstad, F. Collin, L. M. Cope, B. Hobbs, and T. P. Speed.** 2003. Summaries of Affymetrix GeneChip probe level data. Nucleic Acids Res **31:**e15.

21. **Irizarry, R. A., B. Hobbs, F. Collin, Y. D. Beazer€ Barclay, K. J. Antonellis, U. Scherf, and T. P. Speed.** 2003. Exploration, normalization, and summaries of high density oligonucleotide array probe level data. Biostatistics **4:**249-264.

22. **Jones, D. T., W. R. Taylor, and J. M. Thornton.** 1992. The rapid generation of mutation data matrices from protein sequences. Computer applications in the biosciences : CABIOS **8:**275-282.

23. **Kahng, L. S., and L. Shapiro.** 2001. The CcrM DNA methyltransferase of *Agrobacterium tumefaciens* Is essential, and its activity is cell cycle regulated. J. Bacteriol. **183:**3065-3075.

24. **Kelly, A. J., M. J. Sackett, N. Din, E. Quardokus, and Y. V. Brun.** 1998. Cell cycle-dependent transcriptional and proteolytic regulation of FtsZ in Caulobacter. Genes Dev. **12:**880-893.

25. **Komeili, A., Z. Li, D. K. Newman, and G. J. Jensen.** 2006. Magnetosomes are cell membrane invaginations organized by the actin-like protein MamK. Science **311:**242.

26. **Komeili, A., H. Vali, T. J. Beveridge, and D. K. Newman.** 2004. Magnetosome vesicles are present before magnetite formation, and MamA is required for their activation. Proc. Natl Acad. Sci. USA **101:**3839-3844.

27. **Lang, A. S., and J. T. Beatty.** 2002. A bacterial signal transduction system controls genetic exchange and motility. J. Bacteriol. **184:**913-918.

28. **Lang, A. S., and J. T. Beatty.** 2000. Genetic analysis of a bacterial genetic exchange element: The gene transfer agent of Rhodobacter capsulatus. Proc. Natl Acad. Sci. USA **97:**859-864.

29. **Laub, M. T., S. L. Chen, L. Shapiro, and H. H. McAdams.** 2002. Genes directly controlled by CtrA, a master regulator of the Caulobacter cell cycle. Proc. Natl Acad. Sci. USA **99:**4632-4637.

30. **Laub, M. T., H. H. McAdams, T. Feldblyum, C. M. Fraser, and L. Shapiro.** 2000. Global analysis of the genetic network controlling a bacterial cell cycle. Science **290:**2144-2148.

31. **Liu, X. S., D. L. Brutlag, and J. S. Liu.** 2002. An algorithm for finding protein-DNA binding sites with applications to chromatin-immunoprecipitation microarray experiments. Nat Biotech **20:**835-839.

32. **Matsunaga, T., T. Sakaguchi, and F. Tadokoro.** 1991. Magnetite formation by a magnetic bacterium capable of growing aerobically. Appl. Environ. Microbiol. **35:**651-655.

33. **Mercer, R. G., S. J. Callister, M. S. Lipton, L. Pasa-Tolic, H. Strnad, V. Paces, J. T. Beatty, and A. S. Lang.** 2010. Loss of the response regulator CtrA causes pleiotropic effects on gene expression but does not affect growth phase regulation in *Rhodobacter capsulatus*. J. Bacteriol. **192:**2701-2710.

34. **Miller, T. R., and R. Belas.** 2006. Motility is involved in *Silicibacter* sp. TM1040 interaction with dinoflagellates. Environ. Microbiol. **8:**1648-1659.

35. **Murat, D., M. Byrne, and A. Komeili.** 2010. Cell Biology of Prokaryotic Organelles. Cold Spring Harbor Perspectives in Biology **2**.

36. **Murat, D., A. Quinlan, H. Vali, and A. Komeili.** 2010. Comprehensive genetic dissection of the magnetosome gene island reveals the step-wise assembly of a prokaryotic organelle. Proc. Natl Acad. Sci. USA **107:**5593–5598.

37. **Philippe, N., and L.-F. Wu.** 2010. An MCP-like protein interacts with the MamK cytoskeleton and is involved in magnetotaxis in *Magnetospirillum magneticum* AMB-1. J. Mol. Biol. **400:**309-322.

38. **Quon, K. C., G. T. Marczynski, and L. Shapiro.** 1996. Cell cycle control by an essential bacterial two-component signal transduction protein. Cell **84:**83-93.

39. **Quon, K. C., B. Yang, I. J. Domian, L. Shapiro, and G. T. Marczynski.** 1998. Negative control of bacterial DNA replication by a cell cycle regulatory protein that binds at the chromosome origin. Proc. Natl Acad. Sci. USA **95:**120-125.

40. **Robertson, G. T., A. Reisenauer, R. Wright, R. B. Jensen, A. Jensen, L. Shapiro, and R. M. Roop, II.** 2000. The *Brucella abortus* CcrM DNA methyltransferase is essential for viability, and its overexpression attenuates intracellular replication in murine macrophages. J. Bacteriol. **182:**3482-3489.

41. **Ryan, K. R., S. Huntwork, and L. Shapiro.** 2004. Recruitment of a cytoplasmic response regulator to the cell pole is linked to its cell cycle-regulated proteolysis. Proc. Natl Acad. Sci. USA **101:**7415-7420.

42. **Saitou, N., and M. Nei.** 1987. The neighbor-joining method: a new method for reconstructing phylogenetic trees. Mol. Biol. Evol. **4:**406-425.

43. **Santos, S. R., and H. Ochman.** 2004. Identification and phylogenetic sorting of bacterial lineages with universally conserved genes and proteins. Environ. Microbiol. **6:**754-759.

44. **Sassera, D., N. Lo, S. Epis, G. D'Auria, M. Montagna, F. Comandatore, D. Horner, J. PeretÃ³, A. M. Luciano, F. Franciosi, E. Ferri, E. Crotti, C. Bazzocchi, D. Daffonchio, L. Sacchi, A. Moya, A. Latorre, and C. Bandi.** 2011. Phylogenomic Evidence for the Presence of a Flagellum and cbb3 Oxidase in the Free-Living Mitochondrial Ancestor. Mol. Biol. Evol. **28:**3285-3296.

45. **Sato, R., T. Miyagi, S. Kamiya, T. Sakaguchi, R. Thornhill, and T. Matsunaga.** 1995. Synchronous culture of *Magnetospirillum* sp. AMB-1 by repeated cold treatment. FEMS Microbiol. Lett. **128:**15-19.

46. **Scheffel, A., A. Gardes, K. Grunberg, G. Wanner, and D. Schüler.** 2008. The major magnetosome proteins MamGFDC are not essential for magnetite biomineralization in magnetospirillum gryphiswaldense but regulate the size of magnetosome crystals. J. Bacteriol. **190:**377-386.

47. **Shelswell, K. J., T. A. Taylor, and J. T. Beatty.** 2005. Photoresponsive flagellum-independent motility of the purple phototrophic bacterium *Rhodobacter capsulatus*. J. Bacteriol. **187:**5040-5043.

48. **Siam, R., and G. T. Marczynski.** 2003. Glutamate at the phosphorylation site of response regulator CtrA provides essential activities without increasing DNA binding. Nucl. Acids Res. **31:**1775-1779.

49. **Smith, M. J., P. E. Sheehan, L. L. Perry, K. O Connor, L. N. Csonka, B. M. Applegate, and L. J. Whitman.** 2006. Quantifying the magnetic advantage in magnetotaxis. Biophys. J. **91:**1098-1107.

50. **Sourjik, V., P. Muschler, B. Scharf, and R. d. Schmitt.** 2000. VisN and VisR are global regulators of chemotaxis, flagellar, and motility genes in *Sinorhizobium* (*Rhizobium*) *meliloti*. J. Bacteriol. **182:**782-788.

51. **Stephens, C. M., G. Zweiger, and L. Shapiro.** 1995. Coordinate cell cycle control of a *Caulobacter* DNA methyltransferase and the flagellar genetic hierarchy. J. Bacteriol. **177:**1662-1669.

52. **Tamura, K., D. Peterson, N. Peterson, G. Stecher, M. Nei, and S. Kumar.** 2011. MEGA5: Molecular evolutionary genetics analysis using maximum likelihood, evolutionary distance, and maximum parsimony methods. Mol. Biol. Evol. **28:**2731-2739.

53. **Ullrich, S., M. Kube, S. Schübbe, R. Reinhardt, and D. Schüler.** 2005. A hypervariable 130-kilobase genomic region of *Magnetospirillum gryphiswaldense* comprises a magnetosome island which undergoes frequent rearrangements during stationary growth. J. Bacteriol. **187:**7176-7184.

54. **White, C. L., A. Kitich, and J. W. Gober.** 2010. Positioning cell wall synthetic complexes by the bacterial morphogenetic proteins MreB and MreD. Mol. Microbiol. **76:**616-633.

55. **Wolfe, R. S., R. K. Thauer, and N. Pfennig.** 1987. A "capillary racetrack" method for isolation of magnetotactic bacteria. FEMS Microbiol. Lett. **45:**31-35.

56. **Yang, C.-D., H. Takeyama, T. Tanaka, A. Hasegawa, and T. Matsunaga.** 2001. Synthesis of bacterial magnetic particles during cell cycle of *Magnetospirillum magneticum* AMB-1. Appl. Biochem. Biotechnol. **91:**155-160.

Table 1: Strains of AMB-1 used in this work

Strain number	Name and Description
AK30	AMB-1 wild-type
AK31	ΔMAI spontaneous magnetosome island deletion
AK115	Δ*ctrA*
AK116	Δ*divK*
AK117	Δ*ctrA* ΔMAI

Table 2: Plasmids generated in this work

Plasmid name	Plasmid of origin	Experiment	Antibiotic
pAK607	pAK0-derived	deletion of *ctrA* (*amb0629*)	kan
pAK614	pAK0-derived	deletion of divK (*amb3570*)	kan
pAK611	pAK22-derived	complementation of Δ*ctrA,* WT allele	kan, amp
pAK612	pAK22-derived	complementation of Δ*ctrA,* D51A allele	kan, amp
pAK613	pAK22-derived	complementation of Δ*ctrA,* D51E allele	kan, amp
pAK617	pAK22-derived	complementation of Δ*ctrA,* empty	kan, amp

Table 3: Genomic coordinates of unannotated ORFs in the Magnetosome Island

ORF ID	genomic start site	genomic termination site	predicted function
R1-1	999169	999474	conserved hypothetical in *M. gryphiswaldense MSR-1*
R1-2	1000521	1000664	PAS domain
R1-3	1000624	1001148	Amb0942; transposase/integrase
R2-1	1012739	1013047	hypothetical
R2-3	1012526	1012876	hypothetical
R6-1	1040560	1039265	CheY-like receiver
R6-2	1047290	1049650	histidine kinase with PAS domain
R7-1	1050077	1060490	transcriptional regulator
R7-2	1051136	1051576	hemerythrin-like
R7-3	1053698	1052136	hemerythrin-like plus receiver domain
R7-4	1054569	1053712	hemerythrin-like plus receiver domain
R7-5	1054581	1055096	hemerythrin-like
R8-1	1055440	1056360	hypothetical
R8-2	1056558	1056959	hypothetical
R8-3	1061118	1061810	hypothetical
R8-4	1062536	1062712	Mms7
R8-5	1062783	1063055	weak homology to peptidase sortase, TadE
R8-6	1063419	1063667	weak homology to lipoprotein, thioredoxin
R10-1	1070046	1070339	potential hydrogenase, ferric iron uptake regulator
R11-1	1075142	1075708	hypothetical
R13-1	1092108	1092449	hypothetical
R13-2	1091305	1090352	hypothetical

Table S1: Primers used to generate deletion and complementation vectors

Name	Sequence	Experiment	In plasmid
bglII 629a F	gacAGATCTgaggtaattcggcgaaga	Δ*ctrA*	pAK607
629b R bamHI	gacGGATCCatacgggtgtattctgac	Δ*ctrA*	pAK607
bamHI 629c F	gacGGATTCaatcaaagggaggtttgg	Δ*ctrA*	pAK607
629d R spe1	ACTAGTttctattccgccttcgacgaca	Δ*ctrA*	pAK607
bglII 3570a F	gacAGATCTtggtaacccgcaccaatc	Δ*divK*	pAK614
3570b R bamHI	gacGGATCCtcgcggacaaagaaaag	Δ*divK*	pAK614
bamHI 2570c F	gacGGATCCgtcatcaaacttattccac	Δ*divK*	pAK614
3570d R spe1	ACTAGTaataggagggcggcatggg	Δ*divK*	pAK614
amb0629 EcoRI F	gggGAATTCatgcgagtcttggtggtc	pCtrA WT	pAK611
amb0629 Spe1 R	gggACTAGTaatgaatcactccgccgc	pCtrA WT	pAK611
amb0629 d51e F	atcatcctgctgGAGctgatgctg	pCtrA D51E	pAK613
amb0629 d51e R	cagcatcagCTCcagcaggatgat	pCtrA D51E	pAK613
amb0629 d51a F	atcatcctgctgGCCctgatgctg	pCtrA D51A	pAK612
amb0629 d51a R	cagcatcagGCCcagcaggatgat	pCtrA D51A	pAK612
amb3570 EcoRI F	gggGAATTCatggctaagtctgtgctg	pDivK WT	pAK615
amb3570 SpeI R	gggACTAGTctattccaggaagcgcgc	pDivK WT	pAK615

Table S2: Primers and probes used for Taqman qRT-PCR

Name	Sequence	Target	Tag
RT Taq amb2833 1F	atgcggatgaccttcgactt	*amb2833*	primer (300nM)
RT Taq amb2833 1R	gggccatgtgggaaaagc	*amb2833*	primer (300nM)
amb28331Fam1BHQ	[6-FAM]accccggactggatggatt[BHQ1a]	*amb2833*	probe-FAM
RT Taq amb0504 1F	gactacatcaaggtcagcaacag	*amb0504*	primer (300nM)
RT Taq amb0504 1R	ggcgggcgtcaggtaca	*amb0504*	primer (300nM)
FAM-amb0504-BHQ	[6-FAM]aggtctccagcaagactgc[BHQ1a]	*amb0504*	probe-FAM
RT Taq gyrase 1F	caacaacgtgccgcagaa	*amb0639*	primer (900nM)
RT Taq gyrase 1R	aatcattggcataggcgttga	*amb0639*	primer (900nM)
Gyrase1VICMGB	VIC-ggccggctttcgcgcc-MGBNFQ	*amb0639*	probe-VIC

Table S3: Abbreviations of species names used in phylogenetic trees of Alphaproteobacteria

Organism	Abbreviation
Acidiphilium cryptum JF-5	ACIcryp
Agrobacterium tumefaciens str. C58	AGRtume
Anaplasma marginale str. St. Maries	ANAmarg
Bartonella henselae str. Houston-1	BARhens
Bartonella quintana str. Toulouse	BARquin
Bradyrhizobium japonicum USDA 110	BRAjapo
Bradyrhizobium sp. ORS278	BRAsp.
Brucella abortus biovar 1 str. 9-941	BRUabor
Brucella melitensis 16M	BRUmeli
Caulobacter crescentus CB15	CREcres
Ehrlichia canis str. Jake	EHRcani
Ehrlichia chaffeensis str. Arkansas	EHRchaf
Ehrlichia ruminantium str. Gardel	EHRrumi
Erythrobacter litoralis HTCC2594	ERYlit
Gluconobacter oxydans 621H	GLUoxy
Hyphomonas neptunium ATCC 15444	HYPnept
Jannaschia sp. CCS1	JANsp.
Magnetospirillum magneticum AMB-1	MAGmagn
Maricaulis maris MCS10	MARmari
Mesorhizobium loti MAFF303099	MESloti
Neorickettsia sennetsu str. Miyayama	NEOsenn
Nitrobacter hamburgensis X14	NIThamb
Nitrobacter winogradskyi Nb-255	NITwino
Novosphingobium aromaticivorans DSM 12444	NOVarom
Ochrobactrum anthropi ATCC 49188	OCHanth
Orientia tsutsugamushi Boryong	ORItsut
Paracoccus denitrificans PD1222	PARdeni
Parvibaculum lavamentivorans DS-1	PARlava
Rhizobium etli CFN 42	RHIetli
Rhizobium leguminosarum bv. viciae 3841	RHIlegu
Rhodobacter capsulatus sb 1003	RHOcaps
Rhodobacter sphaeroides 2.4.1	RHOspha
Rhodopseudomonas palustris CGA009	RHOpalu
Rhodospirillum centenum SW	RHOcent
Rhodospirillum rubrum ATCC 11170	RHOrubr
Rickettsia conorii str. Malish 7	RICcono
Rickettsia prowazekii str. Madrid E	RICprow
Rickettsia typhi str. Wilmington	RICtyph
Roseobacter denitrificans OCh 114	ROSdeni

Organism	Abbreviation
Silicibacter pomeroyi DSS-3	SILpome
Sinorhizobium medicae WSM419	SINmedi
Sinorhizobium meliloti 1021	SINmeli
Sphingomonas wittichii RW1	SPHwitt
Wolbachia endosymbiont of Drosophila melanogaster	WOLendo
Xanthobacter autotrophicus Py2	XANauto
Zymomonas mobilis subsp. mobilis ZM4	ZYMmob
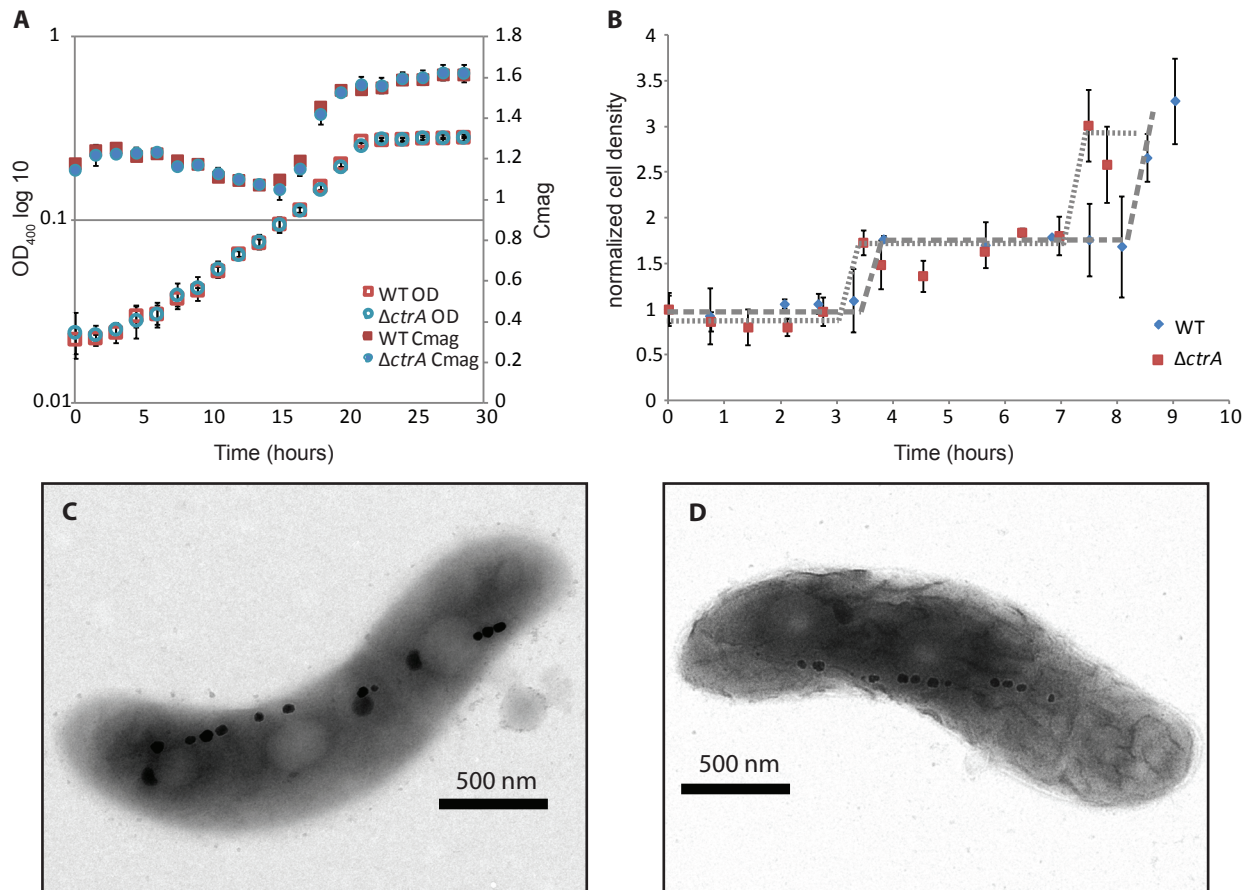
Figure 1: CtrA is conserved but not essential for viability or growth in AMB-1. (A) Growth (OD_{400}) and magnetism (Cmag) of wild-type and *ctrA* deletion strains. Ability to turn in a magnetic field was assessed spectrophotometrically as described previously (26). A Cmag of 1 indicates a non-magnetic culture. (B) Synchronization of wild-type and Δ*ctrA* AMB-1 via density gradient centrifugation was assessed through visual cell counts of cells released in fresh MG medium. Shown are representative data from single synchronies of each strain. Triplicate biological replicates were performed and data from these experiments are included in **Figure S1**. Error bars reflect error in cell counting from triplicate cell counts at each time point. (C and D) Transmission electron micrograph of a representative wild-type (C) or Δ*ctrA* (D) strain, highlighting the presence of magnetosome chains containing cubo-octahedral crystals.
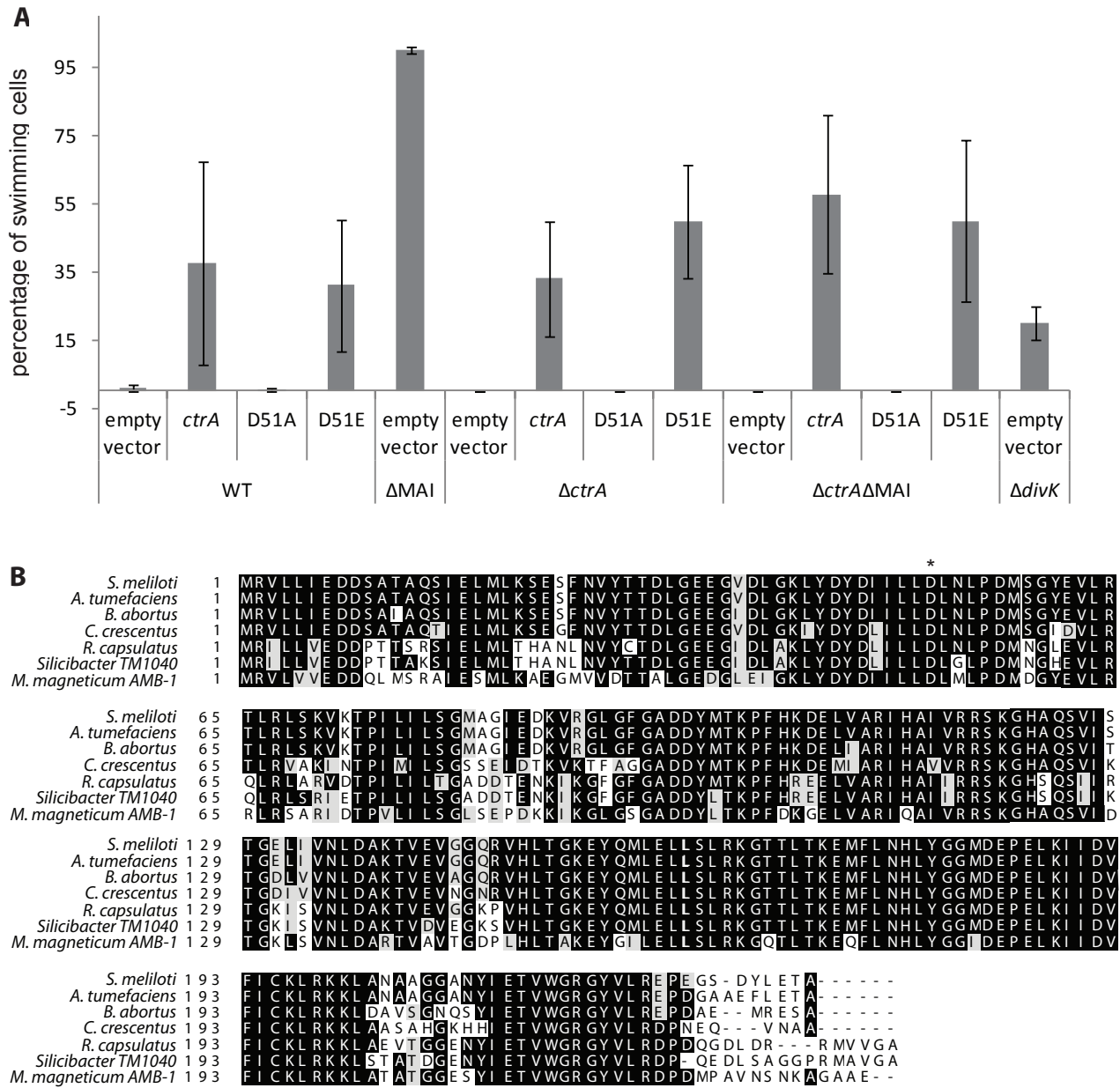
Figure 2: (A) Percentage of motile cells in wild-type and mutant strains of AMB-1 as assessed visually using light microscopy. Error bars represent standard error from at least 10 biological replicates for each strain, grown in separate experiments. (B) Multiple sequence alignment of CtrA homologs from Alphaproteobacteria in which the role of CtrA has been investigated (ClustalW). The phosphorylation site, position D51 in *C. crescentus*, is conserved in all species.

A

Table columns: putative CtrA binding site | fold change in ctrA + ctrA D51E vs ctrA + ctrA D51A | fold change in ctrA + ctrA D51E vs ctrA + empty vector | fold change in ctrA + ctrA D51A vs ctrA empty vector | gene name

putative CtrA binding site	D51E vs D51A	D51E vs empty	D51A vs empty	gene name
	3.08	3.25	1.06	amb0034
	1.63	1.95	1.20	amb0035
	1.58	1.54	0.98	amb0048
	2.28	2.50	1.10	amb0051
4.09	3.03	3.10	1.03	amb0125
	1.65	1.97	1.20	amb0133
	2.48	2.91	1.17	amb0158
3.71	1.78	1.86	1.04	amb0229
	1.53	1.73	1.13	amb0345
	1.52	1.67	1.10	amb0348
	1.90	1.94	1.02	amb0353
	1.96	2.11	1.08	amb0354
	1.51	1.51	1.00	amb0376
	1.91	2.22	1.16	amb0388
3.72	3.88	4.39	1.13	amb0389
	1.62	1.84	1.13	amb0390
4.18	1.94	1.80	0.92	amb0399
4.35	2.34	2.52	1.08	amb0412
	1.82	1.74	0.96	amb0415
	2.20	2.54	1.15	amb0424
	1.82	1.96	1.08	amb0426
3.89	1.91	1.70	0.89	amb0436
	1.65	1.80	1.09	amb0479
3.89	1.59	1.60	1.00	amb0483
4.02	2.52	2.50	0.99	amb0485
	2.11	2.23	1.06	amb0496
3.64	1.57	1.83	1.16	amb0498
	2.39	2.50	1.05	amb0500
	2.42	2.91	1.20	amb0502
	1.86	1.88	1.02	amb0503
	6.25	5.65	0.90	amb0504
	2.94	2.96	1.01	amb0505
4.63	2.00	2.46	1.23	amb0506
	2.43	2.84	1.17	amb0529
5.93	2.01	1.83	0.91	amb0609
5.53	1.84	1.79	0.97	amb0614
	2.27	2.24	0.99	amb0615
	1.71	1.68	0.98	amb0618
3.68	2.47	2.48	1.00	amb0641
4.62	1.78	1.69	0.95	amb0643
3.55	1.68	1.60	0.95	amb0653
4.01	4.54	4.25	0.93	amb0659
	3.17	3.13	0.99	amb0660
3.71	1.50	1.51	1.01	amb0677
	2.01	1.78	0.89	amb0681
	1.96	2.03	1.03	amb0700
	1.54	1.51	0.98	amb0741
	1.93	1.93	1.00	amb0765
	1.71	1.73	1.01	amb0779
	2.57	2.52	0.98	amb0792
	1.81	2.08	1.15	amb0797
	1.90	2.38	1.25	amb0833
	1.81	1.91	1.05	amb0848
3.72	1.79	1.54	0.86	amb0853
3.61	1.59	1.80	1.13	amb0858
4.92	1.75	1.76	1.00	amb0870
4.45	1.96	1.77	0.91	amb0899
3.55	3.24	3.88	1.20	amb0934
4.80	4.53	4.26	0.94	amb0935
3.40	2.24	1.95	0.87	amb0947
4.31	2.06	1.77	0.86	amb0950
	2.51	2.56	1.02	amb0970
	1.90	1.92	1.01	amb0971
	1.79	1.80	1.00	amb0994
	2.38	2.21	0.93	amb1039
	4.06	3.58	0.88	amb1063
	1.58	1.58	1.00	amb1084
	2.91	2.67	0.92	amb1095
	2.39	2.08	0.87	amb1096
	2.31	2.18	0.94	amb1099
3.67	1.72	1.73	1.01	amb1154
	1.75	1.88	1.07	amb1185
	2.91	3.08	1.06	amb1186
	1.54	1.52	0.99	amb1219
	1.60	1.56	0.97	amb1285
	2.14	2.54	1.19	amb1302
	1.56	1.71	1.10	amb1313
	3.37	3.08	0.91	amb1336
3.40	1.84	1.91	1.03	amb1338
3.58	2.08	2.03	0.98	amb1346
	1.83	1.92	1.05	amb1352
	2.03	2.47	1.22	amb1365
3.64	1.58	2.05	1.29	amb1377
3.82	2.62	3.16	1.21	amb1395
3.84	1.79	1.99	1.11	amb1398
	1.63	2.00	1.23	amb1399
3.72	1.69	1.59	0.94	amb1400
	2.13	2.69	1.26	amb1401
	1.65	1.79	1.09	amb1405
4.59	1.70	1.82	1.07	amb1450
	1.50	1.54	1.03	amb1451
	2.68	3.01	1.12	amb1453
	1.66	1.54	0.93	amb1456
	1.88	2.10	1.11	amb1461

putative CtrA binding site	D51E vs D51A	D51E vs empty	D51A vs empty	gene name
	2.28	2.06	0.90	amb1530
	2.74	3.20	1.17	amb1563
	2.85	3.08	1.08	amb1564
	3.68	4.35	1.18	amb1565
	2.64	2.90	1.10	amb1566
	1.69	1.76	1.04	amb1567
	4.60	5.81	1.26	amb1572
	7.47	9.56	1.28	amb1573
3.69	4.15	5.11	1.23	amb1574
	4.02	4.24	1.05	amb1579
	3.00	3.35	1.12	amb1580
	3.58	4.09	1.14	amb1581
	3.18	3.71	1.17	amb1582
	3.70	3.94	1.07	amb1587
	2.45	2.50	1.02	amb1589
	1.80	1.69	0.94	amb1614
	2.32	2.43	1.05	amb1637
	2.11	2.18	1.03	amb1638
	1.66	2.12	1.28	amb1689
4.17	1.69	1.76	1.04	amb1694
	1.54	1.53	0.99	amb1702
	2.22	2.18	0.98	amb1705
	1.64	1.57	0.95	amb1712
	1.56	1.57	1.00	amb1713
	2.31	2.37	1.03	amb1715
4.44	1.69	1.56	0.93	amb1719
	1.74	1.54	0.88	amb1728
	1.78	2.16	1.22	amb1785
	2.01	2.65	1.32	amb1815
	1.85	3.05	1.65	amb1816
4.07	1.57	2.25	1.44	amb1817
	1.69	1.63	0.97	amb1843
3.74	1.92	1.98	1.03	amb1887
	2.52	2.80	1.11	amb1893
	1.84	1.64	0.89	amb1895
3.61	2.05	2.06	1.01	amb1957
	1.52	1.61	1.06	amb1960
3.97	1.79	2.38	1.33	amb1969
	2.25	1.55	0.69	amb2011
4.31	1.64	1.67	1.02	amb2014
	1.97	1.79	0.91	amb2032
4.14	1.73	1.59	0.92	amb2046
	2.82	2.70	0.96	amb2057
	2.33	2.99	1.28	amb2058
3.69	1.84	1.73	0.94	amb2069
	2.23	2.31	1.04	amb2073
3.93	1.59	1.57	0.99	amb2080
	1.50	1.53	1.02	amb2082
4.45	2.84	3.17	1.12	amb2127
	1.70	1.73	1.02	amb2159
3.62	2.18	1.84	0.84	amb2182
4.12	2.45	2.58	1.05	amb2183
	2.03	1.84	0.91	amb2196
	2.10	2.14	1.02	amb2200
4.73	1.76	1.63	0.93	amb2208
	1.90	1.99	1.05	amb2220
	1.93	2.22	1.15	amb2226
	2.15	1.93	0.90	amb2236
	1.50	1.56	1.04	amb2253
	1.60	1.60	1.00	amb2285
	1.88	2.18	1.16	amb2289
4.00	1.54	1.68	1.09	amb2306
	1.90	2.01	1.06	amb2387
4.27	2.58	2.78	1.08	amb2395
	1.84	1.91	1.04	amb2399
	2.92	3.13	1.07	amb2400
	1.50	1.87	1.24	amb2402
	1.68	1.53	0.91	amb2421
4.04	1.51	1.50	1.00	amb2490
4.68	1.98	1.94	0.98	amb2495
	1.57	1.95	1.24	amb2541
	1.56	1.65	1.05	amb2572
	1.58	1.66	1.05	amb2583
	2.59	2.98	1.15	amb2613
	2.31	2.71	1.17	amb2616
	1.91	1.98	1.04	amb2617
	1.63	1.76	1.08	amb2620
	1.74	2.02	1.16	amb2633
	1.81	1.69	0.93	amb2640
	1.93	1.93	1.00	amb2643
	1.54	1.58	1.03	amb2644
	1.72	1.96	1.14	amb2686
3.60	5.81	6.76	1.16	amb2687
	1.81	1.68	0.93	amb2695
	1.60	1.78	1.11	amb2724
	1.81	1.94	1.07	amb2785
3.61	1.59	1.67	1.05	amb2829
	8.55	9.10	1.06	amb2833
	4.26	4.60	1.08	amb2834
	1.91	2.17	1.14	amb2891
	2.36	2.75	1.17	amb2892
	1.95	1.81	0.93	amb2908
	1.58	1.77	1.12	amb2973
	1.53	1.60	1.04	amb3020

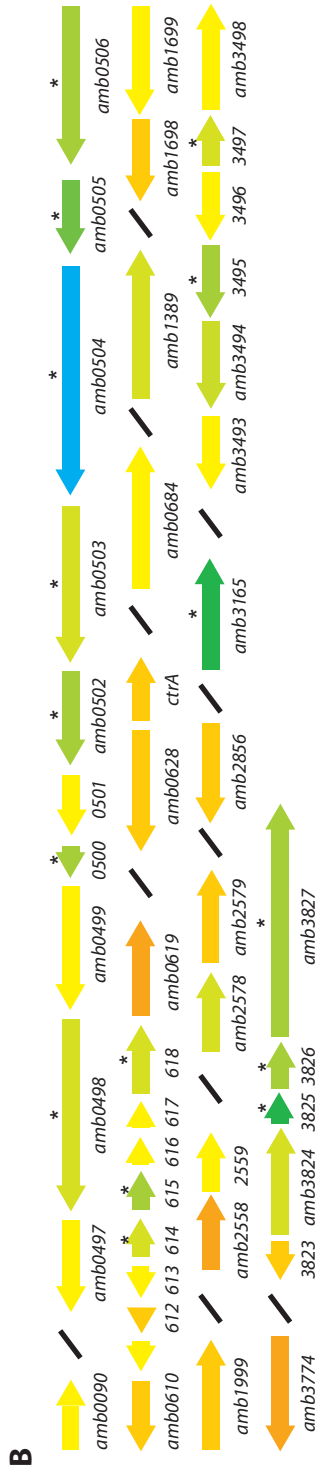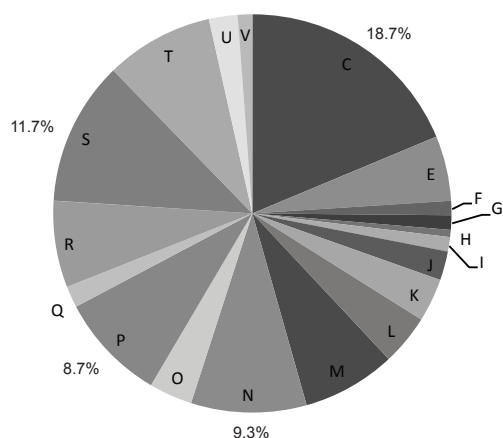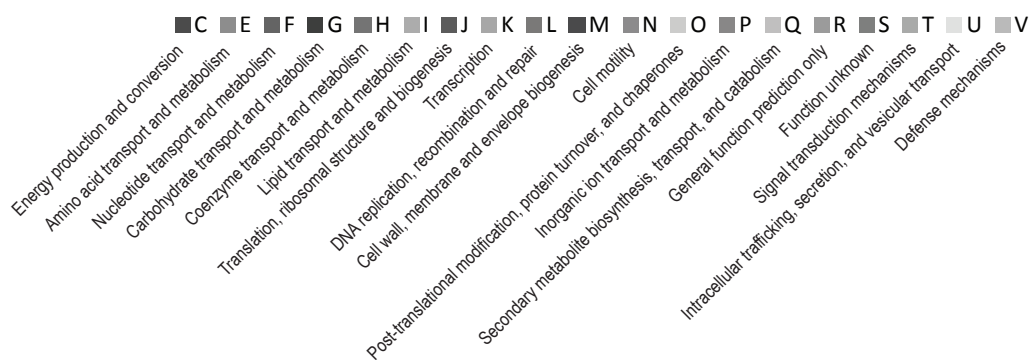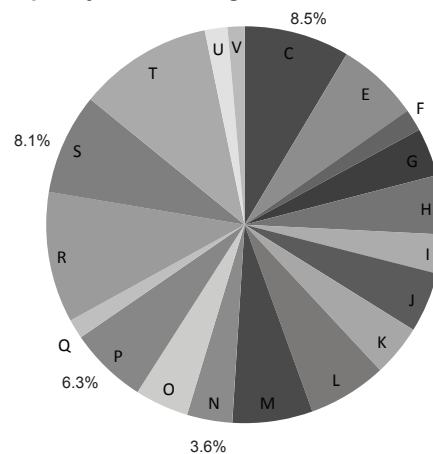| putative CtrA binding site	D51E vs D51A	D51E vs empty	D51A vs empty	gene name
	1.54	1.95	1.27	amb3052
	1.61	1.71	1.06	amb3071
	1.85	1.80	0.97	amb3081
	1.79	1.71	0.95	amb3082
	1.64	1.52	0.93	amb3103
3.57	1.79	1.78	0.99	amb3147
3.76	4.66	3.91	0.84	amb3160
	3.11	3.62	1.16	amb3165
	1.95	1.74	0.89	amb3200
	1.62	1.77	1.09	amb3221
	2.27	2.80	1.23	amb3227
	1.80	2.01	1.12	amb3229
3.64	1.82	1.89	1.04	amb3233
3.50	1.63	1.73	1.06	amb3234
	1.64	1.65	1.01	amb3254
3.56	1.80	1.72	0.96	amb3261
4.85	2.10	2.04	0.97	amb3310
	1.72	2.70	1.57	amb3333
3.63	2.25	2.63	1.17	amb3335
3.57	2.38	2.66	1.12	amb3343
	2.11	2.45	1.16	amb3352
3.83	2.06	3.23	1.56	amb3355
	1.90	2.07	1.09	amb3356
	1.66	2.17	1.31	amb3357
	2.52	3.69	1.47	amb3367
	2.45	4.18	1.70	amb3368
	2.28	3.25	1.43	amb3369
	2.33	3.27	1.40	amb3370
3.68	1.64	1.96	1.19	amb3371
	2.00	2.78	1.39	amb3372
	1.71	2.39	1.39	amb3373
	1.82	2.00	1.09	amb3375
	1.60	1.71	1.07	amb3376
	1.55	1.73	1.12	amb3377
	1.69	1.84	1.09	amb3378
3.62	1.71	1.53	0.90	amb3405
4.57	2.89	4.25	1.47	amb3430
4.18	1.60	1.58	0.99	amb3443
3.81	1.63	1.70	1.04	amb3485
	2.36	2.40	1.02	amb3495
	1.96	1.95	1.00	amb3497
	1.75	2.39	1.37	amb3541
	2.01	3.01	1.50	amb3542
	1.88	2.25	1.20	amb3553
	1.90	1.83	0.97	amb3630
	1.59	1.76	1.11	amb3638
	2.08	2.05	0.98	amb3682
	1.82	1.80	0.99	amb3685
3.70	1.54	1.56	1.01	amb3699
	1.50	1.59	1.06	amb3753
	2.25	1.93	0.86	amb3763
3.96	1.84	1.92	1.04	amb3772
4.30	1.85	2.00	1.08	amb3777
	2.32	2.18	0.94	amb3788
4.14	1.73	1.89	1.09	amb3806
	3.41	3.68	1.08	amb3825
	2.26	2.65	1.17	amb3826
	2.37	2.09	0.88	amb3827
	1.78	1.72	0.97	amb3836
	1.54	1.81	1.17	amb3855
	1.68	1.73	1.03	amb3951
	2.06	1.85	0.89	amb3954
	1.59	1.56	0.98	amb3972
3.99	1.93	2.03	1.05	amb3988
	1.78	2.02	1.14	amb3992
	1.83	1.70	0.93	amb4029
3.66	3.44	3.97	1.15	amb4043
3.64	2.23	2.53	1.13	amb4064
	1.54	1.91	1.24	amb4068
	1.61	1.98	1.23	amb4069
	4.44	5.23	1.18	amb4106
4.25	4.44	4.32	0.97	amb4122
3.61	2.31	2.21	0.96	amb4160
4.73	1.58	2.46	1.56	amb4165
	1.54	1.70	1.10	amb4168
	1.59	1.64	1.03	amb4206
	2.07	1.66	0.80	amb4301
3.63	1.62	1.71	1.06	amb4340
	1.68	1.97	1.17	amb4343
3.56	3.31	2.44	0.74	amb4351
	5.00	6.07	1.21	amb4368
	1.78	2.11	1.19	amb4375
	2.76	3.08	1.12	amb4376
3.98	1.64	1.60	0.98	amb4401
4.04	2.03	4.66	2.30	amb4411
	2.97	5.66	1.90	amb4412
	2.12	2.40	1.13	amb4445
	1.50	1.64	1.09	amb4484
	1.92	1.79	0.93	amb4493
3.58	4.02	4.02	1.00	amb4516
	1.89	2.12	1.12	amb4544
3.75	1.80	2.02	1.12	amb4557

Color scale: 9.5 9 8.5 8 7.5 7 6.5 6 5.5 5 4.5 4 3.5 3 2.5 2 1.5 1 -1.5 -2 -2.5

B

Figure 3: (A) 283 genes were up-regulated at least 1.5 fold in *ctrA* deletions expressing CtrA D51E compared to CtrA D51A and the empty vector control. These genes are depicted in genomic order and are colored according to their fold change in expression in Δ*ctrA* complemented with CtrA D51E *vs* the CtrA D51A alleles. The left-most column denotes the presence of a putative CtrA binding site, using a Z-score cutoff of 3.40. (B) Genomic context of flagellar biosynthesis genes in AMB-1. Genes are colored as in (A); slashes indicate gaps between flagellar biosynthesis genes and gene clusters. Of the 46 genes potentially involved in flagellar biosynthesis, 17 were up-regulated at least 1.5 fold in *ctrA* deletions expression CtrA D51E rather than CtrA D51A and the empty vector control; those genes are indicated by asterisks.

A

Frequency of COG categories in the microarray CtrA regulon

Frequency of COG categories in the AMB-1 genome

■C ■E ■F ■G ■H ■I ■J ■K ■L ■M ■N ☐O ■P ■Q ■R ■S ■T ☐U ☐V

Energy production and conversion
Amino acid transport and metabolism
Nucleotide transport and metabolism
Carbohydrate transport and metabolism
Coenzyme transport and metabolism
Lipid transport and metabolism
Translation, ribosomal structure and biogenesis
Transcription
DNA replication, recombination and repair
Cell wall, membrane and envelope biogenesis
Cell motility
Post-translational modification, protein turnover, and chaperones
Inorganic ion transport and metabolism
Secondary metabolite biosynthesis, transport, and catabolism
General function prediction only
Function unknown
Signal transduction mechanisms
Intracellular trafficking, secretion, and vesicular transport
Defense mechanisms

B

	COG categories	P-value	# genes in genome	# genes with CtrA motif
–	Not Assigned	0.0193	1432	34
P	Inorganic ion transport and metabolism	0.02	197	8
T	Signal transduction mechanisms	0.0608	338	10
K	Transcription	0.0736	130	5
N	Cell motility	0.5916	114	2
S	Function unknow n	0.6518	255	4
L	Replication, recombination and repair	0.6795	198	3
E	Amino acid transport and metabolism	0.7027	208	3
J	Translation, ribosomal structure and biogenesis	0.7392	152	2
M	Cell w all/membrane/envelope biogenesis	0.8705	203	2
O	Posttranslational modification, protein turnover, chaperones	0.9045	136	1
R	General function prediction only	0.9291	330	3
C	Energy production and conversion	0.9499	266	2
A	RNA processing and modification	1	0	0
B	Chromatin structure and dynamics	1	0	0
D	Cell cycle control, cell division, chromosome partitioning	1	27	0
Y	Nuclear structure	1	0	0
V	Defense mechanisms	1	43	0
Z	Cytoskeleton	1	0	0
W	Extracellular structures	1	0	0
U	Intracellular trafficking, secretion, and vesicular transport	1	57	0
G	Carbohydrate transport and metabolism	1	121	0
F	Nucleotide transport and metabolism	1	55	0
H	Coenzyme transport and metabolism	1	149	0
I	Lipid transport and metabolism	1	99	0
Q	Secondary metabolites biosynthesis, transport and catabolism	1	49	0

Figure 4: (A) Comparison of COG representation frequencies in genes positively regulated by CtrA D51E and in the entire AMB-1 genome. The CtrA regulon, as identified by microarray analysis, is enriched in functional categories C (energy production and conversion), N (cell motility), P (inorganic ion transport and metabolism), and S (hypothetical proteins). (B) Genes of unknown function and those predicted to encode proteins involved in inorganic ion transport and metabolism were enriched relative to the AMB-1 genome in upstream putative CtrA binding motifs (p-value < 0.05). Genes with predicted signal transduction and transcription functions were slightly enriched in such putative CtrA binding motifs (p-value < 0.1).
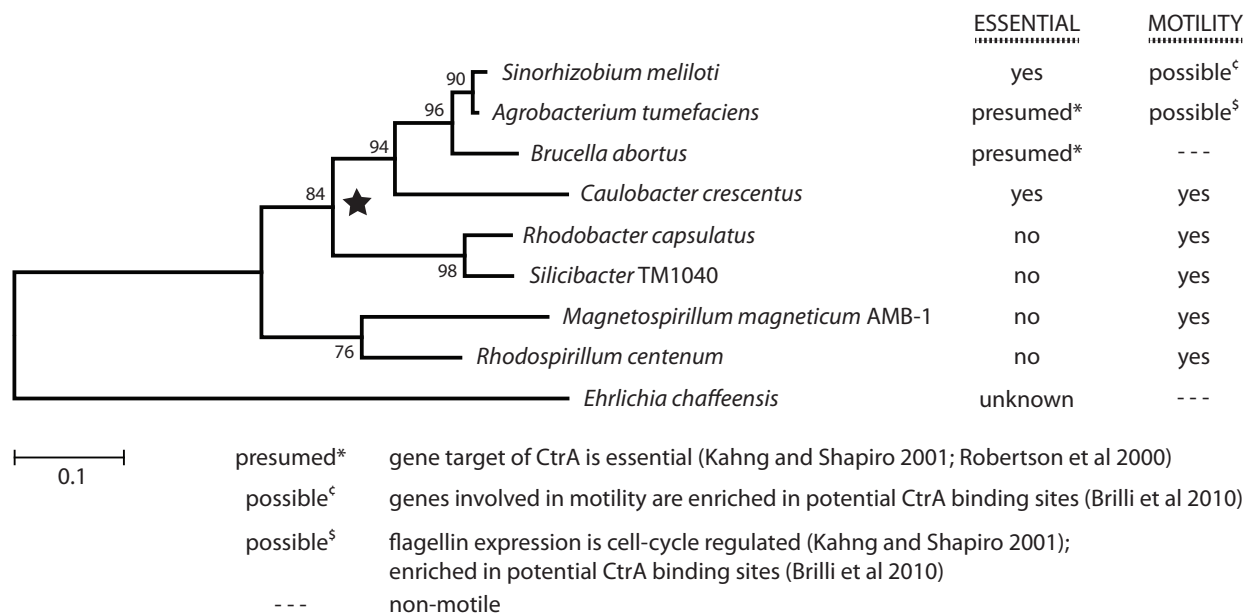
Figure 5: Phylogenetic tree depicting the evolutionary relationships among CtrA homologs from Alphaproteobacteria in which the role of CtrA has been investigated. When mapping the role(s) of CtrA onto the phylogenetic tree, a branch point (star) between organisms in which CtrA is essential or presumed to be essential, for viability and those in which CtrA is dispensable is suggested. Species which evolved from one lineage (*S. meliloti*, *A. tumefaciens*, *B. abortus*, and *C. crescentus*) have essential or presumed essential functions for CtrA. Species evolved from the alternate lineage and more ancestral divergent lineages (*R. capsulatus*, *Silicibacter*, *M. magneticum*, and *R. centenum*) lack an essential role for CtrA. In each of the above species, CtrA plays a role in the regulation of motility. Excepting the non-motile *B. abortus*, *A. tumefaciens* and *S. meliloti* encode motility genes with potential upstream CtrA binding sites (6) and further, flagellin expression in *A. tumefaciens* is cell-cycle regulated (23). CtrA regulates stress response in the intracellular pathogen *E. chaffeensis*, but its roles in viability and motility are unknown (8).
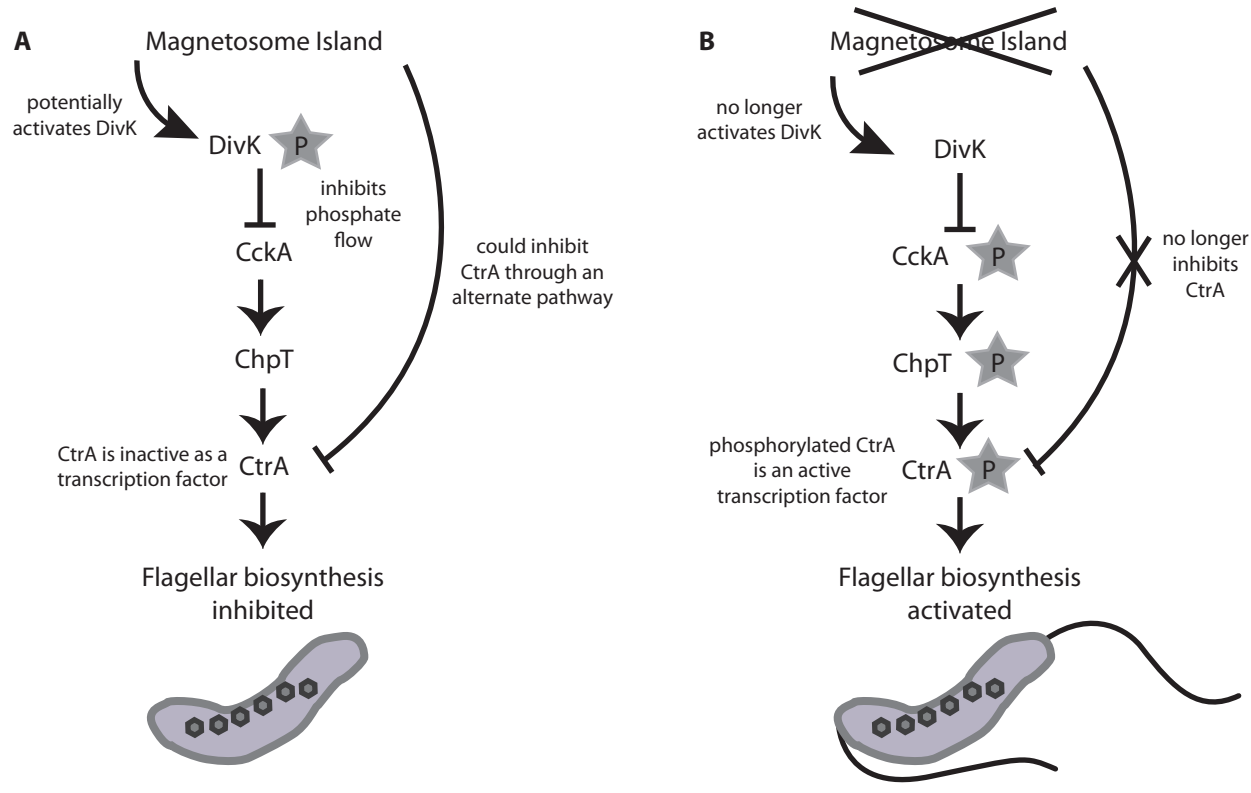
Figure 6: Model of the CtrA network and regulation of motility in AMB-1. We propose that CtrA is activated by phosphorylation through a pathway consistent with that in *C. crescentus*, whereby phosphate is transferred from CckA to CtrA via the phosphotransferase ChpT. Once it becomes phosphorylated, active CtrA promotes the transcription of flagellar biosynthesis genes. (A) In wild-type AMB-1, CtrA is deactivated by a factor or factors in the Magnetosome Island, either through its own repressor DivK or an alternative pathway. (B) In the Magnetosome Island deletion strain, repression of CtrA is lost and transcription of flagellar biosynthesis genes leads to active flagellum production and motility.
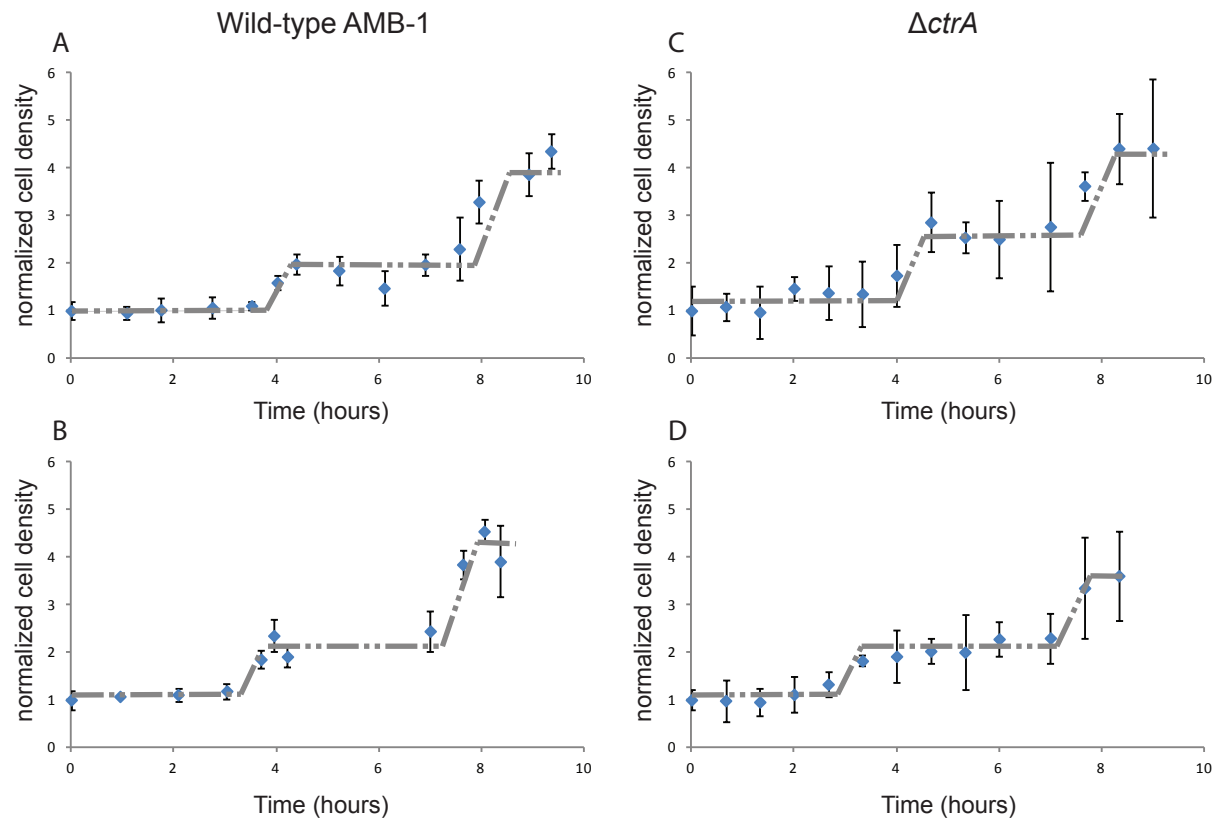
Figure S1: Additional **s**ynchronization experiments of wild-type (A, B) and Δ*ctrA* (C, D) AMB-1 via density gradient centrifugation; synchrony was assessed through visual cell counts of cells released in fresh MG medium. Error bars reflect error in cell counting from triplicate cell counts at each time point.
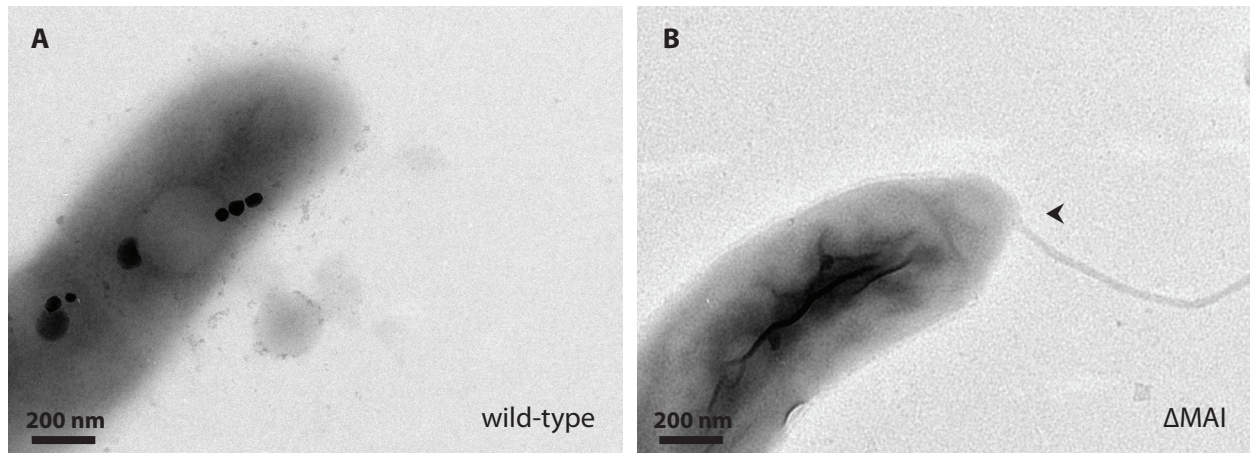
Figure S2: Transmission electron micrographs of representative wild-type (A) and Magnetosome Island deletion (B) strains, highlighting presence of flagella associated with the non-magnetic mutant (arrowhead).
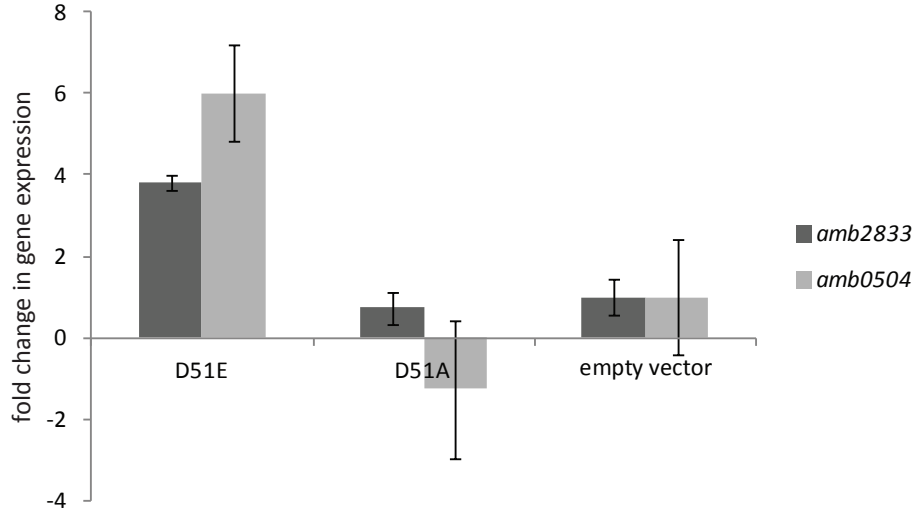
Figure S3: Microarray expression results of two genes up-regulated by CtrA D51E were confirmed by Taqman quantitative RT-PCR. *amb2833* (hypothetical protein) and *amb0504* (flagellar hook protein FlgE) targets were PCR amplified using cDNA templates reverse transcribed from RNA isolated from triplicate biological replicates of Δ*ctrA* + CtrA D51E, Δ*ctrA* + CtrA D51A, and Δ*ctrA* + empty vector control. Target amplicons were compared internally to gyrase (*amb0639*) in multiplex PCR reactions. Target to gyrase ratios in Δ*ctrA* + empty vector were normalized to 1 for both targets assayed. As compared to the empty vector control, *amb2833* and *amb0504* were up-regulated 3.81- and 6.01-fold in Δ*ctrA* + CtrA D51E, respectively. By microarray, these genes were up-regulated 9.10- and 5.65- fold, respectively, when comparing expression in Δ*ctrA* + CtrA D51E vs Δ*ctrA* + empty vector control.

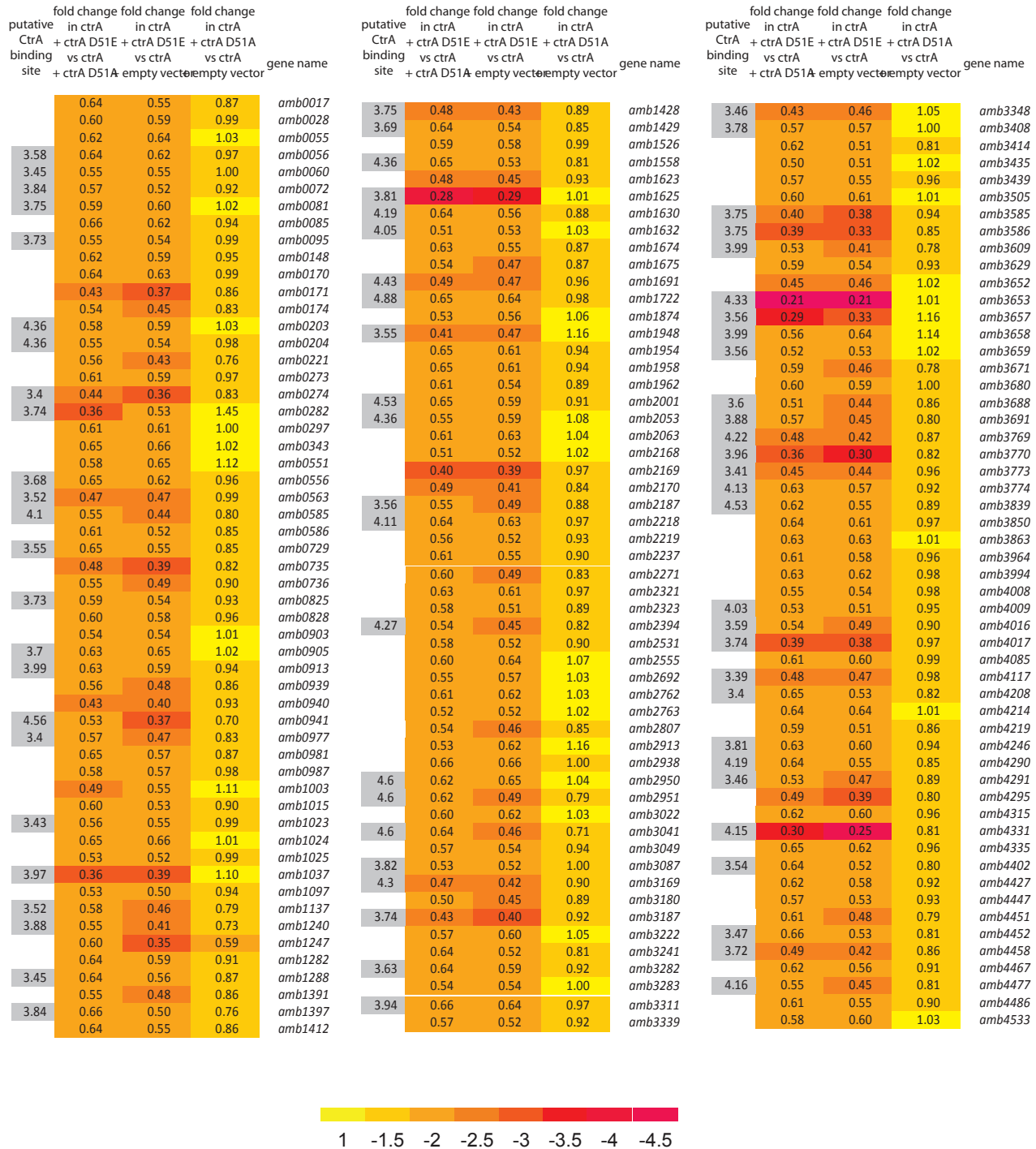| putative CtrA binding site	fold change in ctrA + ctrA D51E vs ctrA + ctrA D51A	fold change in ctrA + ctrA D51E vs ctrA empty vector	fold change in ctrA + ctrA D51A vs ctrA empty vector	gene name
	0.64	0.55	0.87	amb0017
	0.60	0.59	0.99	amb0028
	0.62	0.64	1.03	amb0055
3.58	0.64	0.62	0.97	amb0056
3.45	0.55	0.55	1.00	amb0060
3.84	0.57	0.52	0.92	amb0072
3.75	0.59	0.60	1.02	amb0081
	0.66	0.62	0.94	amb0085
3.73	0.55	0.54	0.99	amb0095
	0.62	0.59	0.95	amb0148
	0.64	0.63	0.99	amb0170
	0.43	0.37	0.86	amb0171
	0.54	0.45	0.83	amb0174
4.36	0.58	0.59	1.03	amb0203
4.36	0.55	0.54	0.98	amb0204
	0.56	0.43	0.76	amb0221
	0.61	0.59	0.97	amb0273
3.4	0.44	0.36	0.83	amb0274
3.74	0.36	0.53	1.45	amb0282
	0.61	0.61	1.00	amb0297
	0.65	0.66	1.02	amb0343
	0.58	0.65	1.12	amb0551
3.68	0.65	0.62	0.96	amb0556
3.52	0.47	0.47	0.99	amb0563
4.1	0.55	0.44	0.80	amb0585
	0.61	0.52	0.85	amb0586
3.55	0.65	0.55	0.85	amb0729
	0.48	0.39	0.82	amb0735
	0.55	0.49	0.90	amb0736
3.73	0.59	0.54	0.93	amb0825
	0.60	0.58	0.96	amb0828
	0.54	0.54	1.01	amb0903
3.7	0.63	0.65	1.02	amb0905
3.99	0.63	0.59	0.94	amb0913
	0.56	0.48	0.86	amb0939
	0.43	0.40	0.93	amb0940
4.56	0.53	0.37	0.70	amb0941
3.4	0.57	0.47	0.83	amb0977
	0.65	0.57	0.87	amb0981
	0.58	0.57	0.98	amb0987
	0.49	0.55	1.11	amb1003
	0.60	0.53	0.90	amb1015
3.43	0.56	0.55	0.99	amb1023
	0.65	0.66	1.01	amb1024
	0.53	0.52	0.99	amb1025
3.97	0.36	0.39	1.10	amb1037
	0.53	0.50	0.94	amb1097
3.52	0.58	0.46	0.79	amb1137
3.88	0.55	0.41	0.73	amb1240
	0.60	0.35	0.59	amb1247
	0.64	0.59	0.91	amb1282
3.45	0.64	0.56	0.87	amb1288
	0.55	0.48	0.86	amb1391
3.84	0.66	0.50	0.76	amb1397
	0.64	0.55	0.86	amb1412
3.75	0.48	0.43	0.89	amb1428
3.69	0.64	0.54	0.85	amb1429
	0.59	0.58	0.99	amb1526
4.36	0.65	0.53	0.81	amb1558
	0.48	0.45	0.93	amb1623
3.81	0.28	0.29	1.01	amb1625
4.19	0.64	0.56	0.88	amb1630
4.05	0.51	0.53	1.03	amb1632
	0.63	0.55	0.87	amb1674
	0.54	0.47	0.87	amb1675
4.43	0.49	0.47	0.96	amb1691
4.88	0.65	0.64	0.98	amb1722
	0.53	0.56	1.06	amb1874
3.55	0.41	0.47	1.16	amb1948
	0.65	0.61	0.94	amb1954
	0.65	0.61	0.94	amb1958
	0.61	0.54	0.89	amb1962
4.53	0.65	0.59	0.91	amb2001
4.36	0.55	0.59	1.08	amb2053
	0.61	0.63	1.04	amb2063
	0.51	0.52	1.02	amb2168
	0.40	0.39	0.97	amb2169
	0.49	0.41	0.84	amb2170
3.56	0.55	0.49	0.88	amb2187
4.11	0.64	0.63	0.97	amb2218
	0.56	0.52	0.93	amb2219
	0.61	0.55	0.90	amb2237
	0.60	0.49	0.83	amb2271
	0.63	0.61	0.97	amb2321
	0.58	0.51	0.89	amb2323
4.27	0.54	0.45	0.82	amb2394
	0.58	0.52	0.90	amb2531
	0.60	0.64	1.07	amb2555
	0.55	0.57	1.03	amb2692
	0.61	0.62	1.03	amb2762
	0.52	0.52	1.02	amb2763
	0.54	0.46	0.85	amb2807
	0.53	0.62	1.16	amb2913
	0.66	0.66	1.00	amb2938
4.6	0.62	0.65	1.04	amb2950
4.6	0.62	0.49	0.79	amb2951
	0.60	0.62	1.03	amb3022
4.6	0.64	0.46	0.71	amb3041
	0.57	0.54	0.94	amb3049
3.82	0.53	0.52	1.00	amb3087
4.3	0.47	0.42	0.90	amb3169
	0.50	0.45	0.89	amb3180
3.74	0.43	0.40	0.92	amb3187
	0.57	0.60	1.05	amb3222
	0.64	0.52	0.81	amb3241
3.63	0.64	0.59	0.92	amb3282
	0.54	0.54	1.00	amb3283
3.94	0.66	0.64	0.97	amb3311
	0.57	0.52	0.92	amb3339
3.46	0.43	0.46	1.05	amb3348
3.78	0.57	0.57	1.00	amb3408
	0.62	0.51	0.81	amb3414
	0.50	0.51	1.02	amb3435
	0.57	0.55	0.96	amb3439
	0.60	0.61	1.01	amb3505
3.75	0.40	0.38	0.94	amb3585
3.75	0.39	0.33	0.85	amb3586
3.99	0.53	0.41	0.78	amb3609
	0.59	0.54	0.93	amb3629
	0.45	0.46	1.02	amb3652
4.33	0.21	0.21	1.01	amb3653
3.56	0.29	0.33	1.16	amb3657
3.99	0.56	0.64	1.14	amb3658
3.56	0.52	0.53	1.02	amb3659
	0.59	0.46	0.78	amb3671
	0.60	0.59	1.00	amb3680
3.6	0.51	0.44	0.86	amb3688
3.88	0.57	0.45	0.80	amb3691
4.22	0.48	0.42	0.87	amb3769
3.96	0.36	0.30	0.82	amb3770
3.41	0.45	0.44	0.96	amb3773
4.13	0.63	0.57	0.92	amb3774
4.53	0.62	0.55	0.89	amb3839
	0.64	0.61	0.97	amb3850
	0.63	0.63	1.01	amb3863
	0.61	0.58	0.96	amb3964
	0.63	0.62	0.98	amb3994
	0.55	0.54	0.98	amb4008
4.03	0.53	0.51	0.95	amb4009
3.59	0.54	0.49	0.90	amb4016
3.74	0.39	0.38	0.97	amb4017
	0.61	0.60	0.99	amb4085
3.39	0.48	0.47	0.98	amb4117
3.4	0.65	0.53	0.82	amb4208
	0.64	0.64	1.01	amb4214
	0.59	0.51	0.86	amb4219
3.81	0.63	0.60	0.94	amb4246
4.19	0.64	0.55	0.85	amb4290
3.46	0.53	0.47	0.89	amb4291
	0.49	0.39	0.80	amb4295
	0.62	0.60	0.96	amb4315
4.15	0.30	0.25	0.81	amb4331
	0.65	0.62	0.96	amb4335
3.54	0.64	0.52	0.80	amb4402
	0.62	0.58	0.92	amb4427
	0.57	0.53	0.93	amb4447
	0.61	0.48	0.79	amb4451
3.47	0.66	0.53	0.81	amb4452
3.72	0.49	0.42	0.86	amb4458
	0.62	0.56	0.91	amb4467
4.16	0.55	0.45	0.81	amb4477
	0.61	0.55	0.90	amb4486
	0.58	0.60	1.03	amb4533

Scale: 1 -1.5 -2 -2.5 -3 -3.5 -4 -4.5

Figure S4: 169 genes were down-regulated at least 1.5 fold in *ctrA* deletions expressing CtrA D51E rather than CtrA D51A and the empty vector control. These genes are depicted in genomic order and are colored in accordance with their fold change in gene expression. Presence of a putative CtrA binding site is noted in the first column as done in **Figure 3A**.

Figure S5: Phylogenetic tree of members of the Alphaproteobacteria. The Maximum-Likelihood tree was generated using an alignment of eight concatenated universal proteins, with branch lengths measuring the number of substitutions per site. The tree with the highest log likelihood (-204921.1795) is shown. Numbers next to branch points indicate the percentage of replicate trees in which the associated taxa clustered together in the bootstrap test (50 replicates).
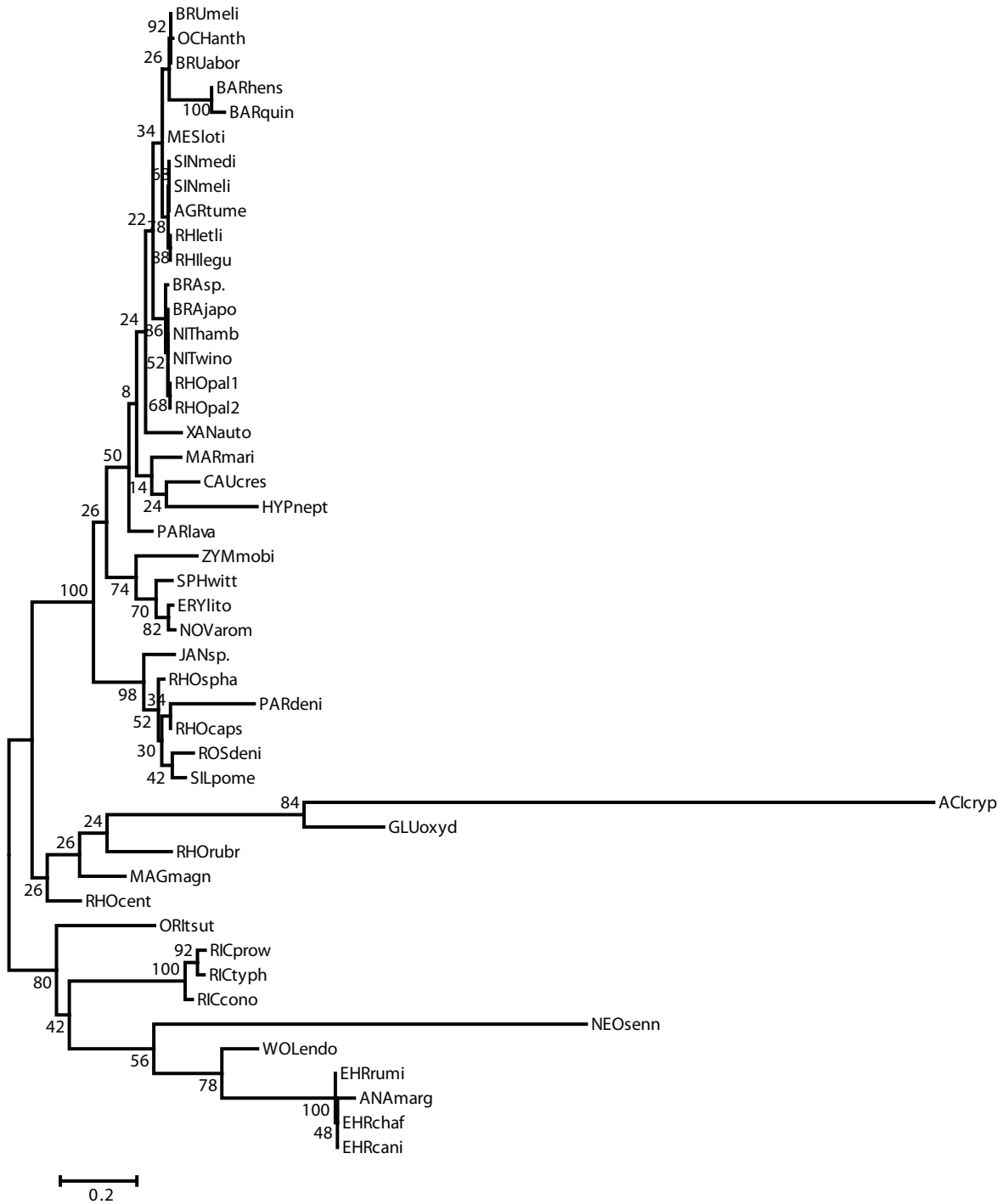
Figure S6: Expanded phylogenetic tree based on CtrA sequences in the Alphaproteobacteria. The tree was generated by the Maximum-Likelihood method, with branch lengths measuring the number of substitutions per site. The tree with the highest log likelihood (-4891.2031) is shown. Numbers next to branch points indicate the percentage of replicate trees in which the associated taxa clustered together in the bootstrap test (50 replicates).

gene name	function
amb0034	hypothetical protein
amb0035	carbamoyltransferase
amb0048	transcription antitermination protein nusG
amb0051	SAM-dependent methyltransferase
amb0125	glycosyltransferase
amb0133	CMP-2-keto-3-deoxyoctulosonic acid synthetase
amb0158	phosphatase/phosphohexomutase
amb0229	hypothetical protein
amb0345	hypothetical protein
amb0348	transcriptional regulator
amb0353	hypothetical protein
amb0354	hypothetical protein
amb0376	hypothetical protein
amb0388	hypothetical protein
amb0389	hypothetical protein
amb0390	hypothetical protein
amb0399	hypothetical protein
amb0412	hypothetical protein
amb0415	hypothetical protein
amb0424	ABC-type branched-chain amino acid transport systems
amb0426	hypothetical protein
amb0436	hypothetical protein
amb0479	hypothetical protein
amb0483	hypothetical protein
amb0485	hypothetical protein
amb0496	ATPase involved in chromosome partitioning
amb0498	flagellar biosynthesis protein FlhA
amb0500	flagellar motor switch protein
amb0502	flagellar motor switch protein G
amb0503	flagellar MS-ring protein
amb0504	flagellar hook protein FlgE
amb0505	flagellar hook capping protein
amb0506	flagellar hook-length control protein
amb0529	hypothetical protein
amb0609	hypothetical protein
amb0614	flagellar basal body protein
amb0615	flagellar basal body rod protein FlgC
amb0618	flagellar biosynthesis protein FliR
amb0641	transposase
amb0643	hypothetical protein
amb0653	hypothetical protein
amb0659	transcriptional regulator
amb0660	plasmid maintenance system antidote protein
amb0677	Acyl-CoA dehydrogenase
amb0681	Rossmann fold nucleotide-binding protein
amb0700	hypothetical protein
amb0741	hypothetical protein
amb0765	hypothetical protein
amb0779	7-cyano-7-deazaguanine reductase
amb0792	thiamine pyrophosphate-requiring enzyme
amb0797	nucleoside-diphosphate-sugar epimerase
amb0833	hypothetical protein
amb0848	response regulator
amb0853	hypothetical protein
amb0858	redox protein
amb0870	hypothetical protein
amb0899	hypothetical protein
amb0934	hypothetical protein
amb0935	hemerythrin-like protein
amb0947	hypothetical protein
amb0950	hypothetical protein
amb0970	hypothetical protein
amb0971	TPR repeat-containing protein
amb0994	methyl-accepting chemotaxis protein
amb1039	hypothetical protein
amb1063	ABC-type polysaccharide/polyol phosphate export systems
amb1084	hypothetical protein
amb1095	hypothetical protein
amb1096	magnetic particle membrane specific GTPase P16
amb1099	hypothetical protein
amb1154	hypothetical protein
amb1185	hypothetical protein
amb1186	hypothetical protein
amb1219	3-deoxy-D-arabino-heptulosonate 7-phosphate synthase
amb1285	elongation factor P
amb1302	hypothetical protein
amb1313	hypothetical protein
amb1336	Signal transduction histidine kinase
amb1338	hypothetical protein
amb1346	hypothetical protein
amb1352	hypothetical protein
amb1365	glycosyltransferase
amb1377	flavin-nucleotide-binding protein
amb1395	nitrite reductase precursor
amb1398	cytochrome c-552 precursor
amb1399	plastocyanin precursor
amb1400	uroporphyrinogen-III methylase
amb1401	cytochrome c, mono- and diheme variants
amb1405	transcriptional regulator

gene name	function
amb1450	succinoglycan biosynthesis transport protein exoP
amb1451	hypothetical protein
amb1453	hypothetical protein
amb1456	hypothetical protein
amb1461	hypothetical protein
amb1530	NTP pyrophosphohydrolase including oxidative damage repair enzyme
amb1563	hypothetical protein
amb1564	NifQ protein
amb1565	ferredoxin
amb1566	hypothetical protein
amb1567	NifX protein
amb1572	nitrogenase molybdenum-iron protein alpha and beta chains
amb1573	nitrogenase molybdenum-iron protein alpha chain
amb1574	nitrogenase reductase
amb1579	ferredoxin V
amb1580	hypothetical protein
amb1581	protein fixU-like protein
amb1582	putative nifZ protein
amb1587	hypothetical protein
amb1589	hypothetical protein
amb1614	signal transduction protein
amb1637	hypothetical protein
amb1638	hypothetical protein
amb1689	hypothetical protein
amb1694	hypothetical protein
amb1702	hypothetical protein
amb1705	hypothetical protein
amb1712	hypothetical protein
amb1713	sulfatase modifying factor 1 precursor
amb1715	hypothetical protein
amb1719	hypothetical protein
amb1728	hypothetical protein
amb1785	hypothetical protein
amb1815	hypothetical protein
amb1816	redox protein, regulator of disulfide bond formation
amb1817	NAD(FAD)-dependent dehydrogenase
amb1843	hypothetical protein
amb1887	hypothetical protein
amb1893	hypothetical protein
amb1895	hypothetical protein
amb1957	hypothetical protein
amb1960	hypothetical protein
amb1969	ammonia permease
amb2011	ABC-type sulfate transport system
amb2014	phenylacetic acid-responsive transcriptional repressor
amb2032	CBS domain-containing protein
amb2046	hypothetical protein
amb2057	site-specific DNA methylase
amb2058	hypothetical protein
amb2069	transcriptional regulator
amb2073	DNA polymerase III subunit epsilon
amb2080	transcriptional regulatory protein Ros
amb2082	DNA repair protein
amb2127	integrase
amb2159	nucleoside-diphosphate-sugar epimerase
amb2182	hypothetical protein
amb2183	hypothetical protein
amb2196	methyl-accepting chemotaxis protein
amb2200	hypothetical protein
amb2208	rhodanese-related sulfurtransferase
amb2220	hypothetical protein
amb2226	hypothetical protein
amb2236	TPR repeat-containing protein
amb2253	guanosine polyphosphate pyrophosphohydrolase/synthetase
amb2285	Zn-dependent hydrolase
amb2289	dihydrodipicolinate synthase/N-acetyl neuraminate lyase
amb2306	putative GTPase
amb2387	hypothetical protein
amb2395	hypothetical protein
amb2399	hypothetical protein
amb2400	hypothetical protein
amb2402	hypothetical protein
amb2421	hypothetical protein
amb2490	Outer membrane protein/protective antigen OMA87
amb2495	ribosome recycling factor
amb2541	peptide ABC transporter permease
amb2572	ABC-type transport system, permease component

53

genename	function
amb2583	TRAP-type mannitol/chloroaromatic compound transport system, large permease component
amb2613	NADH:ubiquinone oxidoreductase
amb2616	NADH:ubiquinone oxidoreductase, subunit RnfD
amb2617	NADH:ubiquinone oxidoreductase
amb2620	hypothetical protein
amb2633	electron transfer flavoprotein
amb2640	FOG:CheY-like receiver
amb2643	FOG:CheY-like receiver
amb2644	Signal transduction histidine kinase
amb2686	denitrification system component nirT
amb2687	nitrate reductase cytochrome c-type subunit
amb2695	phosphoribulokinase
amb2724	hypothetical protein
amb2785	NADH dehydrogenase subunit C
amb2829	response regulator
amb2833	hypothetical protein
amb2834	hypothetical protein
amb2891	Na+/H+-dicarboxylate symporters
amb2892	major facilitator superfamily permease
amb2908	hypothetical protein
amb2973	hypothetical protein
amb3020	hypothetical protein
amb3052	adenylosuccinate lyase
amb3071	hypothetical protein
amb3081	nitrous oxidase accessory protein
amb3082	hypothetical protein
amb3103	phosphatase
amb3147	preprotein translocase subunit SecE
amb3160	hypothetical protein
amb3165	flagellar motor component
amb3200	hypothetical protein
amb3221	hypothetical protein
amb3227	hypothetical protein
amb3229	electron transfer flavoprotein
amb3233	indolepyruvate oxidoreductase subunit IORA
amb3234	indolepyruvate oxidoreductase subunit beta
amb3254	hypothetical protein
amb3261	GGDEF domain-containing protein
amb3310	hypothetical protein
amb3333	hypothetical protein
amb3335	ferric reductase
amb3343	ATP phosphoribosyltransferase catalytic subunit
amb3352	hypothetical protein
amb3355	protein rdxB
amb3356	cAMP-binding protein-catabolite gene activator and regulatory subunit of cAMP-dependent protein kinase
amb3357	transporter component
amb3367	sulfite reductase, dissimilatory-type alpha subunit
amb3368	sulfite reductase, dissimilatory-type beta subunit
amb3369	intracellular sulfur oxidation protein dsrE
amb3370	hypothetical protein
amb3371	hypothetical protein
amb3372	dissimilatory sulfite reductase
amb3373	nitrate reductase gamma subunit
amb3375	putative glutamate synthase (NADPH) small subunit
amb3376	Hdr-like menaquinol oxidoreductase cytochrome c subunit
amb3377	Fe-S-cluster-containing hydrogenase components 1
amb3378	Hdr-like menaquinol oxidoreductase integral membrane subunit
amb3405	response regulator
amb3430	putative rubrerythrin
amb3443	hypothetical protein
amb3485	ABC-type transport system involved in resistance to organic solvents, auxiliary component
amb3495	flagellar basal body rod protein FlgG
amb3497	flagellar basal body-associated protein
amb3541	anaerobic dehydrogenase
amb3542	Fe-S-cluster-containing hydrogenase components 1
amb3553	permease
amb3630	putative nucleotide-binding protein
amb3638	hypothetical protein
amb3682	hypothetical protein
amb3685	hypothetical protein
amb3699	GGDEF domain-containing protein
amb3753	Zn peptidase
amb3763	transposase
amb3772	hemolysin activation/secretion protein
amb3777	hypothetical protein
amb3788	Fe-S oxidoreductase
amb3806	spore coat polysaccharide biosynthesis protein F
amb3825	chemotactic signal-response protein cheL
amb3826	hypothetical protein
amb3827	flagellar hook-associated protein
amb3836	hypothetical protein
amb3855	UDP-3-O-[3-hydroxymyristoyl] N-acetylglucosamine deacetylase
amb3951	succinate dehydrogenase, hydrophobic anchor subunit
amb3954	hypothetical protein
amb3972	homoserine O-acetyltransferase
amb3988	modification methylase CcrMI
amb3992	ATP synthase protein I
amb4029	hypothetical protein
amb4043	hypothetical protein
amb4064	16S rRNA-processing protein RimM
amb4068	isopropylmalate isomerase small subunit
amb4069	3-isopropylmalate dehydrogenase
amb4106	glutathione S-transferase
amb4122	hypothetical protein
amb4160	hypothetical protein
amb4165	nitrite reductase precursor
amb4168	3-deoxy-manno-octulosonate cytidylyltransferase
amb4206	response regulator
amb4301	response regulator
amb4340	hypothetical protein
amb4343	heat shock protein 90
amb4351	hypothetical protein
amb4368	cation transport ATPase
amb4375	hypothetical protein
amb4376	integral membrane protein
amb4401	hemerythrin-like protein
amb4411	hypothetical protein
amb4412	hypothetical protein
amb4445	1-acyl-sn-glycerol-3-phosphate acyltransferase
amb4484	hypothetical protein
amb4493	hypothetical protein
amb4516	hypothetical protein
amb4544	preprotein translocase subunit SecB
amb4557	hypothetical protein

Figure S7: Annotated genes up-regulated at least 1.5-fold by the expression of CtrA D51E in a *ctrA* deletion strain as compared to Δ*ctrA* complemented by CtrA D51A or an empty vector control.

gene name	function
amb0017	Outer membrane lipoprotein-sorting protein
amb0028	hypothetical protein
amb0055	hypothetical protein
amb0056	nucleoside-diphosphate-sugar epimerase
amb0060	ABC-type multidrug transport system
amb0072	Fe-S oxidoreductase
amb0081	SAM-dependent methyltransferase
amb0085	nucleoside-diphosphate-sugar pyrophosphorylase
amb0095	SAM-dependent methyltransferase
amb0148	hypothetical protein
amb0170	FdhA-II protein
amb0171	hypothetical protein
amb0174	benzoyl-CoA-dihydrodiol lyase
amb0203	chaperonin GroEL
amb0204	hypothetical protein
amb0221	thiamine biosynthesis protein ThiC
amb0273	Signal transduction histidine kinase
amb0274	response regulator
amb0282	hypothetical protein
amb0297	precorrin-2 methylase
amb0343	hypothetical protein
amb0551	branched-chain amino acid aminotransferase
amb0556	hypothetical protein
amb0563	pterin-4-alpha-carbinolamine dehydratase
amb0585	PAS/PAC domain-containing protein
amb0586	sensory rhodopsin II transducer
amb0729	signal transduction protein
amb0735	hypothetical protein
amb0736	hypothetical protein
amb0825	bacterioferritin subunit 1
amb0828	thioesterase
amb0903	hypothetical protein
amb0905	hypothetical protein
amb0913	hypothetical protein
amb0939	hypothetical protein
amb0940	hypothetical protein
amb0941	carbohydrate-selective porin
amb0977	sphingosine kinase and enzyme
amb0981	hypothetical protein
amb0987	hypothetical protein
amb1003	FraH protein
amb1015	cell division GTPase
amb1023	Fe2+ transport system protein A
amb1024	Fe2+ transport system protein B
amb1025	hypothetical protein
amb1037	hypothetical protein
amb1097	histone H1
amb1137	AraC-type DNA-binding domain-containing protein
amb1240	thioesterase
amb1247	hypothetical protein
amb1282	transcriptional regulator
amb1288	hypothetical protein
amb1391	putative Zn-dependent protease
amb1397	cAMP-binding protein-catabolite gene activator and regulatory subunit of cAMP-dependent protein kinase
amb1412	ABC-type amino acid transport/signal transduction systems
amb1428	superfamily II DNA/RNA helicase
amb1429	ADP-ribose pyrophosphatase
amb1526	hypothetical protein
amb1558	cAMP-binding protein-catabolite gene activator and regulatory subunit of cAMP-dependent protein kinase
amb1623	flavoprotein
amb1625	hypothetical protein
amb1630	hypothetical protein
amb1632	hypothetical protein
amb1674	ABC-type branched-chain amino acid transport systems
amb1675	hypothetical protein
amb1691	hypothetical protein
amb1722	hypothetical protein
amb1874	Outer membrane protein
amb1948	hypothetical protein
amb1954	hypothetical protein
amb1958	hypothetical protein
amb1962	chemotaxis signal transduction protein
amb2001	Type V secretory pathway, adhesin AidA
amb2053	hypothetical protein
amb2063	hypothetical protein
amb2168	cytochrome C oxidase assembly protein
amb2169	Heme/copper-type cytochrome/quinol oxidase
amb2170	Heme/copper-type cytochrome/quinol oxidase
amb2187	hypothetical protein
amb2218	Thiol-disulfide isomerase and thioredoxins
amb2219	hypothetical protein
amb2237	hypothetical protein
amb2271	HTH-type transcriptional regulator budR
amb2321	dihydrolipoamide dehydrogenase
amb2323	oligoketide cyclase/lipid transport protein
amb2394	hypothetical protein
amb2531	hypothetical protein

gene name	function
amb2555	hypothetical protein
amb2692	ferredoxin
amb2762	dethiobiotin synthetase
amb2763	adenosylmethionine-8-amino-7-oxononanoate aminotransferase
amb2807	RNA polymerase factor sigma-32
amb2913	hypothetical protein
amb2938	FOG: CheY-like receiver
amb2950	molybdopterin-binding protein
amb2951	ABC-type molybdate transport system, periplasmic component
amb3022	hypothetical protein
amb3041	hypothetical protein
amb3049	hypothetical protein
amb3087	hypothetical protein
amb3169	site-specific recombinase
amb3180	transcriptional regulator
amb3187	RNA polymerase factor sigma-32
amb3222	ABC-type transport system involved in resistance to organic solvents, auxiliary component
amb3241	histone H1
amb3282	response regulator
amb3283	cold shock protein
amb3311	hypothetical protein
amb3339	translation initiation factor 1
amb3348	hypothetical protein
amb3408	Outer membrane protein and related peptido-glycan-associated lipoprotein
amb3414	transcriptional regulator
amb3435	hypothetical protein
amb3439	response regulator
amb3505	hypothetical protein
amb3585	transcriptional regulator
amb3586	Acyl-CoA dehydrogenase
amb3609	hypothetical protein
amb3629	hypothetical protein
amb3652	hypothetical protein
amb3653	hypothetical protein
amb3657	hypothetical protein
amb3658	hypothetical protein
amb3659	hypothetical protein
amb3671	hypothetical protein
amb3680	pyruvate-formate lyase-activating enzyme
amb3688	integrase
amb3691	cAMP-binding protein-catabolite gene activator and regulatory subunit of cAMP-dependent protein kinase
amb3769	hypothetical protein
amb3770	hypothetical protein
amb3773	heme utilization/adhesion protein
amb3774	flagellar motor component
amb3839	protein mraZ
amb3850	UDP-N-acetylenolpyruvoylglucosamine reductase
amb3863	hypothetical protein
amb3964	transcriptional regulator
amb3994	ATP synthase C chain
amb4008	methyl-accepting chemotaxis protein
amb4009	PAS/PAC domain-containing protein
amb4016	hypothetical protein
amb4017	multimeric flavodoxin WrbA
amb4085	hypothetical protein
amb4117	polynucleotide phosphorylase/polyadenylase
amb4208	hypothetical protein
amb4214	lysophospholipase
amb4219	hypothetical protein
amb4246	transcriptional regulator
amb4290	ATPase involved in DNA replication
amb4291	hypothetical protein
amb4295	hypothetical protein
amb4315	xylanase/chitin deacetylase
amb4331	hypothetical protein
amb4335	cobalt transport protein CbiM
amb4402	hypothetical protein
amb4427	cobaltochelatase subunit CobN
amb4447	ribosome-associated heat shock protein implicated in the recycling of the 50S subunit
amb4451	UDP-glucose pyrophosphorylase
amb4452	nuclease precursor
amb4458	redox protein, regulator of disulfide bond formation
amb4467	apolipoprotein N-acyltransferase
amb4477	major facilitator superfamily permease
amb4486	inorganic pyrophosphatase
amb4533	glutamine amidotransferase

Figure S8 legend on opposite page

Figure S8: Annotated genes down-regulated at least 1.5-fold by the expression of CtrA D51E in a *ctrA* deletion strain as compared to Δ*ctrA* complemented by CtrA D51A or an empty vector control.

CHAPTER THREE

Investigation of the Regulation of Motility by the Magnetosome Island and Environmental Conditions in *Magnetospirillum magneticum* AMB-1

Shannon E Greene

Plant and Microbial Biology
University of California, Berkeley
Berkeley, CA 94720

INTRODUCTION

Magnetotactic bacteria, although visually defined by their internal chains of magnetic minerals, are classically identified from environmental samples by their ability to not only align with but move along magnetic fields. This characteristic behavior was observed as early as the 1950s by the Italian graduate student Salvatore Bellini. He posited that these cells were able to synthesize magnetic materials themselves, and that iron compounds comprise the biomagnetic minerals (3). Remarkably, many of his predictions have proved prescient including that "the manufacturing of the hypothesized internal compass of the Magnetosensitive Bacteria is a biological operation perfectly organized and controlled in every aspect and at each step" (2). Recent genetic studies of magnetotactic bacteria (MTB) suggest stepwise formation of magnetosome, with each step from magnetosome membrane formation to chain organization to biomineralization under genetic control (11, 14).

In addition to the predictions made about the cell biology underlying these magnetic organisms, Bellini also developed experiments to test microbial responses to magnetic fields (2). His early MTB isolation techniques have been modified in subsequent decades but primarily rely on motility in conjunction with magnetic field alignment. To obtain pure cultures of MTB, current methods, such as the race-track assay, separate actively swimming MTB away from their similarly motile, but non-magnetic, cohort (19).

At its core, magnetotaxis encompasses any movement in response to magnetic fields. Bacterial responses to these conditions are varied, including polar movement in which motility is directed towards a preferred magnetic pole, and axial movement in which general alignment with the magnetic field lines is achieved but motion occurs equally in both polarities (6, 10). Magnetotaxis combined with the general MTB necessity for microaerobic or anaerobic environments proves a powerful localizing force for these cells. Opposing oxygen gradients can be used to trap MTB in the oxic-anoxic transition zone (OATZ); MTB guided by a magnetic field assemble at this boundary more quickly than their non-magnetically-guided counterparts (18).

The most prevalent hypothesis explaining the evolution of magnetotaxis holds that alignment with geomagnetic field lines facilitates the search for low oxygen environments in the aquatic habitats where MTB are found. In the Northern hemisphere, for example, North-seeking MTB are particularly prevalent and could follow the downward inclination of geomagnetic North towards the OATZ near the sediment-water interface. In support of this idea, MTB are primarily found at high latitudes, although equatorial species have been described (5, 7). Magnetotaxis chasing oxygen gradients leads to an overall phenotype of magnetoaerotaxis.

While several studies have characterized the physical aspects of magnetoaerotaxis, the molecular mechanisms behind the behavior and its regulation are unknown. In traditional chemotaxis systems, the chemical attractant or repellent is detected by receptors often localized in discrete polar clusters or arrays (1, 4). When the methyl-accepting chemotaxis receptors are activated, signaling cascades result in altering flagella rotation from a counterclockwise to a clockwise fashion (16). Reversing flagellar rotation results in tumbling behavior that directs the cell in a new direction. Theoretically, magnetoaerotaxis could be regulated in a similar manner. Oxygen

sensors could activate or repress flagellar rotation which, directed by linear magnetic fields, would result in a simplified, one-dimensional search for the optimal oxygen concentration in the water column.

Intriguingly, MTB and particularly the magnetospirilla, are known to encode several dozen of these methyl-accepting chemotaxis proteins and homologs of many other chemotaxis components (8, 12). Putative chemotaxis regulators are encoded in the Magnetosome Island (MAI) of *Magnetospirillum magneticum* AMB-1, a genomic region whose core is highly conserved among MTB, and is essential for magnetosome formation (17). This suggests direct communication between magnetotactic machinery and the magnetosome chain.

In Chapter Two, I presented evidence linking a non-chemotactic regulatory network to motility in AMB-1. The response regulator CtrA is essential for swimming behavior in AMB-1 and its phosphorylation is critical for this process. Evidence suggests that CtrA is responsible for motility at the level of flagellar biosynthesis. Δ*ctrA* mutants are non-motile and produce no flagella while a *ctrA* deletion complemented with an allele mimicking the phosphorylated, active version of the regulator leads to increased swimming and up-regulation of several flagellar biosynthesis gene clusters. Epistasis results suggest that CtrA is downstream of motility regulation from the MAI. The loss of the entire MAI renders AMB-1 cells hyper motile and because this strain produces no magnetosomes, cells are unable to respond to magnetic fields. A Δ*ctrA*ΔMAI strain is completely non-motile, hinting that factors encoded by the MAI negatively regulate motility and that CtrA is downstream.

To determine the role of the MAI in the regulation of motility in AMB-1 and to probe swimming behavior in magnetotactic bacteria more broadly, I sought to identify mutants within the MAI that would phenocopy the loss of the entire MAI. After following some promising leads, reexamination of an initial mutant led to an investigative dead end. Further, no environmental conditions consistently altered the motility behavior of wild-type AMB-1. These results indicate that swimming in AMB-1 is governed by potentially redundant factors or multiple levels of control. Teasing apart the genetic control of magnetoaerotaxis, while scientifically rewarding, became outside the scope of this thesis work.

MATERIALS AND METHODS

Growth conditions *Magnetospirillum magneticum* strain AMB-1 was grown in Magnetospirillum Growth media (MG) under microaerobic conditions, as previously described in Chapter Two. AMB-1 was grown in conical tubes or glass bottles filled with MG medium and incubated at 30°C in a microaerobic chamber in which the oxygen concentration was kept below 10%. These media conditions shall be referred to subsequently in the text as MG_1.

To determine the role of environmental factors in eliciting novel swimming behaviors in wild-type AMB-1, the amended Magnetospirillum Growth media 2 (MG_2) was used. MG_2 differed from MG_1 with (1) half the thiosulfate; (2) 1/100 volume ferric malate at 6mM $FeCl_3$ and 9mM malate, adjusted to pH 7.0 before filtering; and (3) $FeSO_4$ no longer omitted from Wolfe's mineral solution. MG_2 media was additionally prepared in sealed 200mL bottles, which were flushed with 2% O_2/N_2 after autoclaving.

Strain construction and complementation All clonings were performed in *Escherichia coli* DH5αλpir grown in LB media. The antibiotics kanamycin and chloramphenicol were used at 50μg/mL, and 25 μg/mL, respectively. The initial deletion of R6 of the Magnetosome Island in *M. magneticum AMB-1* was previously described (14). Briefly, regions (approximately 1000bp) upstream and downstream of R6 were PCR amplified such that they would overlap with a 21-bp linker containing a SwaI restriction site. A fusion PCR fragment was generated and cloned into the SpeI restriction site of pAK0, a suicide plasmid carrying a kanamycin resistance cassette and the *sacB* gene. The CAT cassette conferring resistance to chloramphenicol was cloned into the internal SwaI linker site to yield the pAK234 vector for deleting R6 (**Table 2**). The plasmid was transferred to AMB-1 using conjugation via *E. coli* WM3064, and the transconjugants were selected for on MG plates containing kanamycin. Transconjugants were grown in liquid MG media and deletion mutants selected for on MG plates containing 2% sucrose and 40μg/mL chloramphenicol. The sucrose and chloramphenicol resistant colonies were screened for the desired deletion and the absence of the kanamycin resistance cassette and *sacB* gene by PCR (14). The resulting ΔR6 strain (AK39) shall subsequently be referred to as $\Delta R6_{DO}$ (**Table 1**)

In later experiments, it was determined that pAK234 had acquired two point mutations. The correctly sequenced R6 deletion scar was PCR amplified from $\Delta R6_{DO}$ genomic DNA and cloned into pAK31 using Spe1 restriction sites. This vector (pAK653) was transferred to AMB-1 as described above to yield $\Delta R6_{SG}$ (AK118).

The $\Delta R6_{DO}$ strain was complemented by expressing 6 of the Region 6 genes from the *tac* promoter. The genes *amb0980*, *amb0982*, *amb0983*, and *amb0993* were PCR amplified and cloned into the expression vector pAK22 (9) using the EcoRI and SpeI restriction sites downstream of the *tac* promoter. The unannotated ORFs R6-1 and R6-2 (as designated in Chapter Two) were similarly PCR amplified and cloned into the pAK253 plasmid for integrating genes at the intergenic locus near *amb0397* (14), expressing downstream genes from the tac promoter, using either the Spe1 and Not1 restriction sites, or just the Spe1 restriction site, respectively. The plasmids were introduced into $\Delta R6_{DO}$ AMB-1 by conjugation, and were selected for using 10 μg/mL kanamycin in liquid MG media, and 15μg/mL kanamycin on solid media.

All primers are listed in **Table S1**.

RESULTS

A dissection of the Magnetosome Island suggests Region 6 as a regulator of motility It was previously discussed in Chapter Two that the spontaneous loss of the entire Magnetosome Island creates cells not only incapable of any aspect of magnetosome formation, but also motile such that 100% of the cells are swimming. These cells, in accordance with their behavior, are consistently flagellated while flagella are rarely observed attached to wild-type AMB-1. A comprehensive dissection of the Magnetosome Island by Murat *et al* (14) yielded a sub-deletion strain which also exhibited motility, although not to the extent of that of the loss of the entire Magnetosome Island. A deletion of Region 6 ($\Delta R6_{DO}$) exhibited 60-70% motile cells, which

sharply contrasted with the scant swimming behavior of wild-type AMB-1 (less that 1% motile cells) (13).

Because no other regional deletions within the MAI resulted in an increased swimming percentage, R6 was hypothesized to encode a putative negative regulator of motility. This hypothesis was supported by the predicted regulatory functions of several genes within R6 (**Table 3**). In particular, R6 encodes two putative CheY-like receivers (R6-1 and *amb0980*), two putative transcriptional regulators (*amb0982* and *amb0993*), a response regulator (*amb0983*) and large PAS domain-containing histidine kinase (R6-2) (**Fig 1**).

To determine whether any one of these genes with potential regulatory functions encodes a negative regulator of motility in AMB-1, I attempted to complement the $\Delta R6_{DO}$ swimming phenotype by exogenously expressing the six candidate genes from the *tac* promoter either from a plasmid or integrated on the chromosome at an intergenic locus. Transformation of each of the six target genes failed to reduce the motility phenotype of the $R6_{DO}$ mutant strain. Ultimately, these results are inconclusive, because expression of the target genes was not verified either by reverse transcription PCR or Western blot.

Further analysis of the R6 mutant rules out its involvement in the regulation of motility
During the construction of the various R6 complementation vectors, I sought to confirm the swimming phenotype initially observed in the characterization of $\Delta R6_{DO}$. In my hands, this strain, revived from frozen stock, was 60-70% motile, consistent with previous observations. Because R6 of the MAI is too large to complement with a single expression vector, and because attempts to complement its deletion with large sub-sections was proving technically difficult, I instead sought to verify that the swimming phenotype was indeed due to the loss of R6 and not to a secondarily acquired mutation.

Following the previously published protocol for the generation of the $\Delta R6_{DO}$ strain, I transformed the R6 deletion vector (pAK234) into wild-type AMB-1 via conjugation using *E. coli* WM3064. Potential integrants were selected for on solid MG media containing 7µg/mL kanamycin and were passaged in liquid MG media devoid of antibiotic selection. After one and two days of growth in the microaerobic chamber, cells were plated on solid MG media containing sucrose and chloramphenicol to select for recombination between the R6 flanking regions to yield a replacement of this region with the CAT chloramphenicol resistance cassette.

Two potential $\Delta R6$ strains were isolated in this manner, and I was able to amplify a PCR product indicative of the loss of R6, and additionally was unable to amplify the *sacB* gene, indicating that the suicide vector had recombined from the genome. Surprisingly, these two strains contained only 10% motile cells, a significant reduction in the percentage of swimming cells relative to the previously characterized strain. I verified the loss of R6 by PCR against an internal gene, *amb0982*.

A possible explanation for the reduced motility phenotypes was that the population contained mutants which had undergone an additional homologous recombination event; the MAI of AMB-1 contains direct repeats of the genes *mamQ*, *mamR*, and *mamB* in R5 and R9. Spontaneous recombination events between these direct repeats had been observed previously in the

laboratory, and occurred more frequently during attempts to excise portions of the MAI between the repetitive sequences (14). The resulting strain, noted as SID25, is non-motile, and because SID25 encompasses in the complete deletion of R6 in addition to *mamSTUV* of R5, R7, R8, and the first three genes of R9 (*amb1002*, *amb1003*, and *amb1004*), a positive regulator of motility must exist within this SID25 region in addition to the putative negative regulator in R6. If the populations isolated in the attempt to regenerate an R6 deletion contained SID25 deletions, the reduced motility phenotypes could be explained. Unfortunately, a PCR to amplify the SID25 deletion scar was negative, despite robust positive controls.

The remaining explanation of the observed motility differences between $\Delta R6_{DO}$ and the putative $\Delta R6$ strains I obtained was that one or the other harbored a secondary mutation. Sequencing of the upstream and downstream flanking regions of R6 in $\Delta R6_{DO}$ and both of my potential $\Delta R6$ strains revealed the presence of two point mutations present in both of my $\Delta R6$ strains but not $\Delta R6_{DO}$. Both point mutations were identified in the downstream region flanking R6, in a section of the MAI previously identified as intergenic between *amb0993* and R7-1. In this region, a small, previously unidentified ORF was found. The first point mutation in the potential ORF was silent, while the second altered the stop codon to a tryptophan, effectively doubling the predicted coding region. The small ORF is homolgous to the N-terminal portions of two transcriptional regulators in AMB-1: *amb2081* and *amb2180*, which are 90% identical to each other. The sequencing results suggested that the second mutation observed in my $\Delta R6$ strains could be responsible for lowering the percentage of motile cells.

Sequencing of the vector used to generate my $\Delta R6$ strains revealed the presence of both mutations, and so instead I cloned the correctly sequenced R6 deletion scar from $\Delta R6_{DO}$ into the pAK31 backbone. After successfully obtaining pAK653, I transformed wild-type AMB-1 and obtained six potential deletions of R6 as verified by the PCR tests described above. A range of motility phenotypes were observed, but none were consistent with that of the original $\Delta R6_{DO}$ mutant. In initial 10mL cultures, four of the six potential $\Delta R6$ strains exhibited only 5-10% motile cells, while two contained 40-50% motile cells. Upon subsequent passaging however, each strain behaved identically to wild-type with only 1% motile cells, and this phenotype persisted after several days of growth. Sequencing of the deletion scars of these mutants revealed wild-type downstream flanking regions.

Additional screening of other $\Delta R6$ candidates also failed to yield swimming cultures. The parental strain used to generate the $\Delta R6$ mutants still retains the ability to produce flagella, for some putative deletion progeny were instead determined to be hyper-motile Magnetosome Island deletion strains.

These experiments suggest that the original $\Delta R6_{DO}$ strain carries a secondary mutation which renders the cells motile relative to wild-type, and that the phenotype observed is not solely due to the loss of R6.

Environmental effects on motility in AMB-1 Upon its isolation, *Magnetospirillum magneticum* AMB-1 was described as being 95% non-motile under all phases of growth (13). This phenotype has been consistently observed in this laboratory for over a decade. It has become clear, however, that strains of AMB-1 exist in other laboratories with alternate motility phenotypes.

Indeed, AMB-1 is actively studied for its properties of photo- and magnetotaxis in two separate laboratories. Upon conferring with members of one such scientific group, it was discovered that the AMB-1 growth media is amended slightly differently.

I obtained a motile culture of AMB-1 courtesy of Jean-Baptise Rioux and Nicolas Ginet, and proceeded to inquire whether the differing chemical compositions of the two media (MG_1 and MG_2) could account for the conflicting swimming attributes of the strains. Representative isolates of the two strains, referred to hereafter as B and FR for their laboratories of origin (Berkeley and France), were passaged in triplicate in both MG_1 and MG_2 (**Fig 2**). Cells were washed twice in the new media before being inoculated at 1/100 in 10mL cultures. After reaching mid-exponential phase in one day of growth, neither the B nor FR strains acquired the motility phenotypes of the other in novel media. The B strain acquired a maximal motility of 25% after three days of growth in MG_2, while the same strain washed and transferred into its native media MG_1 never progressed beyond 5% motility. These results suggested that MG_2 could perhaps increase the number of swimming cells relative to MG_1 media, but passaging of a Day 2 B culture from MG_2 into MG_2 again (denoted as Day 2-1) yielded only 5% motile cells, when its parental culture had begun at 15%.

Further, growth of the FR strain in MG_1 media failed to reduce this strain's swimming phenotype, as would have been expected if differing media conditions resulted in alternative swimming phenotypes.

DISCUSSION

Through genetic manipulations and motility experiments, I sought to investigate additional regulatory mechanisms controlling swimming behavior in AMB-1. Previous work had shown that flagella biosynthesis is under the genetic control of the CtrA regulatory network, but the signals leading to CtrA activation or repression were unknown. The hyper-motile swimming behavior of the Magnetosome Island deletion strain is highly suggestive of negative regulation of motility from a gene or subset of genes within that genomic region. Initial characterization of a deletion of Region 6 of the MAI ($\Delta R6_{DO}$) revealed up to 80% motility in this strain, which pointed to R6 as harboring the potential motility regulatory factor. However, expression of candidate signaling genes or transcription factors from R6 failed to complement the swimming phenotype, and multiple attempts to regenerate the swimming phenotype of $\Delta R6_{DO}$ in novel isolates of the strain were also unsuccessful.

These results led to the suspicion that $\Delta R6_{DO}$ might have acquired an additional mutation to render this isolate particularly motile. As this mutation could be harbored at any genomic locus, whole genome sequencing would be necessary to identify the causal mutational event.

It is similarly likely that the hyper-motile swimming exhibited by the MAI deletion strain is indirectly caused by the loss of the MAI, and not because of the loss of a gene or cluster of genes within that genomic region. Potentially, the loss of the MAI stimulates stress leading to a compensatory mutation which additionally induces uncontrolled swimming behavior. This hypothesis helps to explain the perplexing result that no large regional deletion within the MAI consistently causes a swimming phenotype reminiscent of the loss of the entire MAI. One could

imagine that because the ability to swim is so intricately linked to the defining behavior of MTB – magnetoaerotaxis – motility is highly regulated. It is also possible that multiple levels of motility regulation, both positive and negative, are encoded by the MAI and this redundancy has prevented the identification of motility control factors thus far.

The role of environmental factors in the regulation of motility in AMB-1 also remains undetermined. It has been casually observed that cell cultures well into stationary phase develop motility over time, although no consistent timeline for the arrival of swimming has ever been noted. The swimming behavior of weeks-old cultures could be due to isolated ΔMAI strains arising in the population and subsequently propagating, or it could be due to unknown growth conditions progressing stochastically among independent cultures.

While I initially hypothesized that differences in growth conditions contributed to motility differences between the B and FR strains of AMB-1, these differences are now thought to have arisen via differences in passaging of cell cultures over many years. After the initial AMB-1 strain was isolated and characterized by Matsunaga *et al* in 1991 (13), its progeny have been distributed to various laboratories around the globe. As the FR strain was maintained, efforts to enrich for the most magnetotactic individuals via racetrack assays likely selected for not only the most magnetic cells for study, but also the most motile. Such enrichments were never performed for the B strain, and we can hypothesize that the motility differences between the B and FR strains are genetic in nature, either reflecting specific mutations that confer motility or phase variation.

Thus far, the only clue to mechanism of magnetoaerotaxis in *M. magneticum* AMB-1 is the potential interaction between the putative methyl-accepting chemotaxis (MCP) protein Amb0994 and the MamK filaments aligning the magnetosome chain. As external magnetic fields exert force on the magnetosome chain, and consequently, torque on MamK filaments, this stress could be transferred to polar Amb0994 clusters to activate the downstream signaling cascade with ultimate outputs in flagellar rotation (15). This model of mechanical signal transduction, however, is reliant on the active production of flagella by the bacterium. Although we known that flagellar biosynthesis is activated by the CtrA pathway, the upstream signaling remains mysterious. Uncovering and manipulating those signals will facilitate the development of a genetically tractable system with which to probe in detail the mechanisms of magnetoaerotaxis in a magnetotactic bacterium.

REFERENCES

1. **Alley, M. M. R., J. J. R. Maddock, and L. L. Shapiro.** 1992. Polar localization of a bacterial chemoreceptor. Genes Dev. **6:**825-836.
2. **Bellini, S.** 2009. Further studies on "magnetosensitive bacteria". Chinese J. Ocean. Limno. **27:**6-12.
3. **Bellini, S.** 2009. On a unique behavior of freshwater bacteria. Chinese J. Ocean. Limno. **27:**3-5.
4. **Briegel, A., M. Beeby, M. Thanbichler, and G. J. Jensen.** 2011. Activated chemoreceptor arrays remain intact and hexagonally packed. Mol. Microbiol. **82:**748-757.

5.   **De Araujo, F. F. T., F. A. Germano, M. A. Goncalves, and R. B. Frankel.** 1990. Magnetic polarity fractions in magnetotactic bacterial populations near the geomagnetic equator. Biophys. J. **58:**549-555.

6.   **Frankel, R. B., D. A. Bazylinski, and D. Schüler.** 1998. Biomineralization of magnetic iron minerals in bacteria. Supramol. Sci. **5:**383-390.

7.   **Frankel, R. B., R. P. Blakemore, F. F. T. De Araujo, D. M. S. Esquivel, and J. Danon.** 1981. Magnetotactic Bacteria at the Geomagnetic Equator. Science **212:**1269-1270.

8.   **French, C. E., J. M. L. Bell, and F. B. Ward.** 2008. Diversity and distribution of hemerythrin-like proteins in prokaryotes. FEMS Microbiol. Letters **279:**131-145.

9.   **Komeili, A., Z. Li, D. K. Newman, and G. J. Jensen.** 2006. Magnetosomes are cell membrane invaginations organized by the actin-like protein MamK. Science **311:**242.

10.   **Lefevre, C. T., T. Song, J.-P. Yonnet, and L.-F. Wu.** 2009. Characterization of Bacterial Magnetotactic Behaviors by Using a Magnetospectrophotometry Assay. Appl. Environ. Microbiol. **75:**3835-3841.

11.   **Lohbe, A., S. Ullrich, E. Katzmann, S. Borg, G. Wanner, M. Richter, B. Voigt, T. Schweder, and D. Schuler.** 2011. Functional Analysis of the Magnetosome Island in *Magnetospirillum gryphiswaldense*: The *mamAB* Operon Is Sufficient for Magnetite Biomineralization. PLoS ONE **6:**e25561.

12.   **Matsunaga, T., Y. Okamura, Y. Fukuda, A. T. Wahyudi, Y. Murase, and H. Takeyama.** 2005. Complete genome sequence of the facultative anaerobic magnetotactic bacterium Magnetospirillum sp. strain AMB-1. DNA Res **12:**157-166.

13.   **Matsunaga, T., T. Sakaguchi, and F. Tadokoro.** 1991. Magnetite formation by a magnetic bacterium capable of growing aerobically. Appl. Environ. Microbiol. **35:**651-655.

14.   **Murat, D., A. Quinlan, H. Vali, and A. Komeili.** 2010. Comprehensive genetic dissection of the magnetosome gene island reveals the step-wise assembly of a prokaryotic organelle. Proc. Natl Acad. Sci. USA **107:**5593–5598.

15.   **Philippe, N., and L.-F. Wu.** 2010. An MCP-like protein interacts with the MamK cytoskeleton and is involved in magnetotaxis in *Magnetospirillum magneticum* AMB-1. J. Mol. Biol. **400:**309-322.

16.   **Porter, S. L., G. H. Wadhams, and J. P. Armitage.** 2009. Signal processing in complex chemotaxis pathways. Nat Rev Micro **9:**153-165.

17.   **Richter, M., M. Kube, D. A. Bazylinski, T. Lombardot, F. O. Glockner, R. Reinhardt, and D. Schüler.** 2007. Comparative Genome Analysis of Four Magnetotactic Bacteria Reveals a Complex Set of Group-Specific Genes Implicated in Magnetosome Biomineralization and Function. J. Bacteriol. **189:**4899-4910.

18.   **Smith, M. J., P. E. Sheehan, L. L. Perry, K. O Connor, L. N. Csonka, B. M. Applegate, and L. J. Whitman.** 2006. Quantifying the magnetic advantage in magnetotaxis. Biophys. J. **91:**1098-1107.

19.   **Wolfe, R. S., R. K. Thauer, and N. Pfennig.** 1987. A "capillary racetrack" method for isolation of magnetotactic bacteria. FEMS Microbiol. Lett. **45:**31-35.

Table 1: Strains of AMB-1 used in this work

Strain number	Name and Description	Source
AK30	AMB-1 wild-type	12
AK31	ΔMAI spontaneous magnetosome island deletion	13
AK39	$\Delta R6_{DO}$	13
AK118	$\Delta R6_{SG}$	this work

Table 2: Plasmids generated in this work

Plasmid name	Plasmid of origin	Experiment	Antibiotic
pAK653	pAK234-derived	re-generation of R6 deletion	kan, chlor
pAK651	pAK253-derived	complementation of ΔR6 with R6-1	kan
pAK643	pAK22-derived	complementation of ΔR6 with *amb0980*	kan
pAK645	pAK22-derived	complementation of ΔR6 with *amb0982*	kan
pAK649	pAK22-derived	complementation of ΔR6 with *amb0983*	kan
pAK641	pAK253-derived	complementation of ΔR6 with R6-2	kan
pAK647	pAK22-derived	complementation of ΔR6 with *amb0993*	kan

Table 3: Genes encoded by R6 of the Magnetosome Island

Gene name	Genomic start site	Genomic termination site	Predicted function
amb0979	1039930	1039265	response regulator
amb0980	1040888	1042117	CheY-like receiver
amb0981	1042284	1042637	sulfate permease
amb0982	1043157	1042747	transcriptional regulator
amb0983	1043388	1044641	CheY-like receiver
amb0984	1045256	1044690	hypothetical
amb0985	1045926	1045411	hemerythrin-like receiver
amb0986	1046142	1045951	hypothetical
amb0987	1046224	1046571	hypothetical
amb0988	1046800	1047027	hypothetical
amb0989	1047351	1047554	hypothetical
amb0990	1049080	1048895	PAS domain
amb0991	1049581	1049237	homology to PAS sensor histidine kinase
amb0992	1049755	1050087	nucleiod DNA-binding protein
amb0993	1050077	1050490	transcriptional regulator
R6-1	1040560	1039265	CheY-like receiver
R6-2	1047290	1049650	histidine kinase with PAS domain

Table S1: Primers used to generate deletion and complementation vectors

Name	Sequence	Experiment	In Plasmid
6a.1 *	ggACTAGTtcgcctatttggttgagg	re-generation of ΔR6	pAK653
6d *	ggACTAGTcttcaaggctgacgatgttgg	re-generation of ΔR6	pAK653
LD6 CheY spe1 F	gggACTAGTatgttgactctaccatca	complementation of ΔR6	pAK651
LD6 CheY not1 R	gGGCGGCCGCCtacgctgttggcgattggtt	complementation of ΔR6	pAK651
amb0980 ecoR1 F	GAATTCatgaagccatttgctgcctgt	complementation of ΔR6	pAK643
amb0980 spe1 R	ACTAGTtcagcggcccgcagg	complementation of ΔR6	pAK643
amb0982 ecoR1 F	GAATTCatcggcacggaaaaggggg	complementation of ΔR6	pAK645
amb0982 spe1 R	ACTAGTctaaagcagccgccggac	complementation of ΔR6	pAK645
amb0983 ecoR1 F	gggGAATTCatgtcattgaatacctcc	complementation of ΔR6	pAK649
amb0983 spe1 R	ACTAGTtcaagccttctccccccc	complementation of ΔR6	pAK649
LD6 HK spe1 F	ACTAGTatgacctccgctgcacaacca	complementation of ΔR6	pAK641
LD6 HK spe1 R	ACTAGTctataccggcaccgtgaaccg	complementation of ΔR6	pAK641
amb0993 ecoR1 F	GAATTCatggccgatgacatcaaggct	complementation of ΔR6	pAK647
amb0993 spe1 R	ACTAGTtcaggtggctgatttgggctt	complementation of ΔR6	pAK647

* previously published by Murat *et al* (2010)
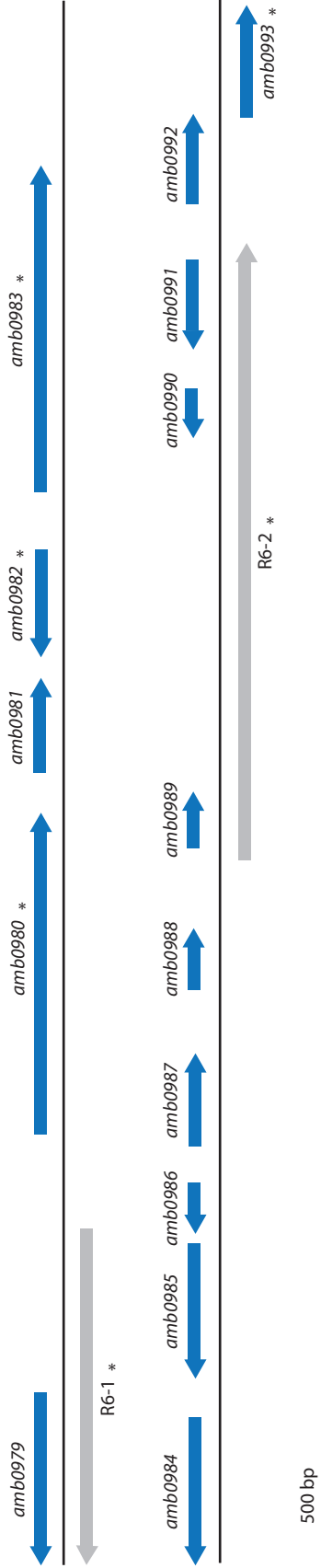
Figure 1: Genomic context of annotated and unannotated ORFs in Region 6 of the MAI. Unannotated ORFs (R6-1 and R6-2) are depicted in grey. Genes with putative regulatory functions are denoted with an asterisk. Scale bar represents 500 bp.
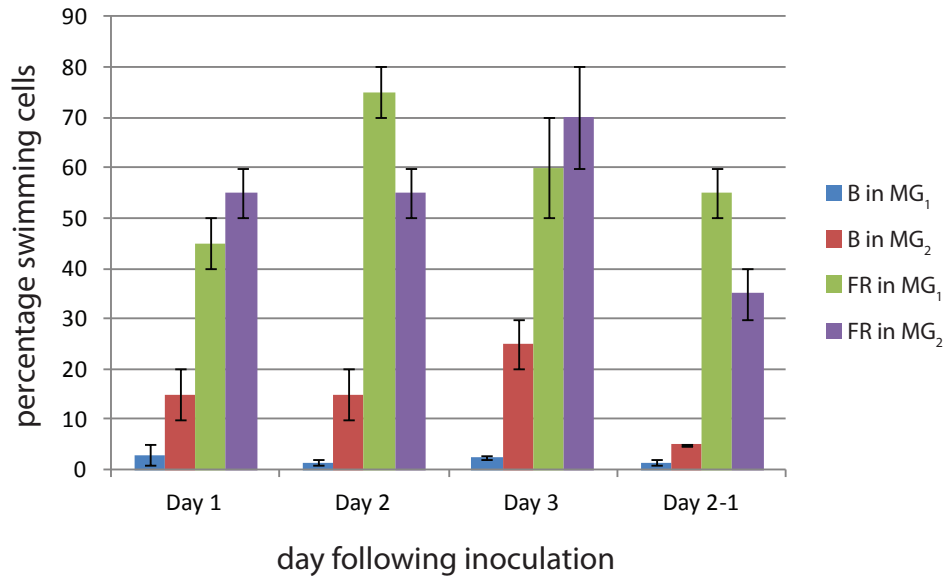
Figure 2: Percentages of swimming cells when passaged in either MG_1 or MG_2 media. Cultures of Berkeley (B) or French (FR) strains of wild-type AMB-1 were transferred to either MG_1 or MG_2 media in triplicate and the percentage of motile cells were observed over time. After two days of growth, cells were passaged a second time and observed after one day of growth (Day 2-1).

CHAPTER FOUR

Characterization of Global Gene Expression Across the Cell Cycle of *Magnetospirillum magneticum* AMB-1

Shannon E Greene

Plant and Microbial Biology
University of California, Berkeley
Berkeley, CA 94720

INTRODUCTION

All living organisms must reproduce. For sexually-reproducing organisms, reproduction involves generation of gametes, species-specific fusion of those gametes, and subsequent survival and growth of the zygote to perpetuate the circle of life. For bacteria, reproduction is quite often simply the binary fission of a single cell into two identical daughter cells, but this process, while facile in theory, is heralded by the complexity of coordinated enzymatic activity, gene expression, and regulatory signaling. Often, prokaryotic cell division is accompanied by reorganization of the cytoskeletal proteins which give the cell its shape (36). Microtubule-like filaments coalesce in a central ring pinching the daughter cells apart (7). Between each division event, bacterial chromosomes are duplicated and segregated to future daughter cells, processes which are tightly regulated to ensure that both progeny receive a full complement of genetic information.

In *Escherichia coli* grown in rich media replete with sugars and macro- and micronutrients, DNA replication is initiated multiple times per division cycle (10). Checkpoint mechanisms exist to ensure that termination of each genome replication occurs faithfully prior to septum formation and daughter cell segregation (1). Similar mechanisms to prevent bisection of the chromosome upon cell separation exist in other bacteria as well (37).

Genome replication in *Caulobacter crescentus*, however, occurs once and only once per cell cycle. Control of DNA replication initiation is achieved through a balance of repressor proteins which physically block binding sites for the replication initiation machinery, stimulate the inactivation of initiation proteins, and gene expression control of these factors (4, 9, 27). In *C. crescentus*, other events are also regulated such that they occur at specific points in the cell cycle. Prior to DNA replication, a single polar flagellum is shed, whose synthesis must be reinitiated at the opposite cellular pole during G2 (3, 19). Similarly, pili are synthesized coincidently with polar flagella in G2 (30) while *C. crescentus* cells only generate a stalk and holdfast complex following the polar flagellum ejection (29).

A key feature of *C. crescentus* in the study of its cell cycle is the relative simplicity with which cell cultures can be synchronized. *C. crescentus* cell divisions yield daughter cells which are morphologically distinct from one another and are capable of being separated via density gradients. Predivisional cells harvested from such a gradient and released in fresh media will progress synchronously throughout the cell cycle, enabling the examination of changes in morphology, gene and protein expression, and protein localization (8). 553 genes, representing 19% of the *C. crescentus* genome, exhibit variable expression levels throughout the cell cycle (21). Proteomic analysis of synchronized *C. crescentus* cultures further established that 91 proteins identifiable by mass spectrometry were differentially expressed during the cell cycle; expression of half of those proteins showed patterns identical to those observed in gene expression studies (13). Cell cycle-regulated genes include cell division factors, DNA methyltransferases, polar morphogenesis genes, as well as genes involved in cell metabolism (20).

Gene expression changes across the cell cycle are not, however, unique to *C. crescentus*. Indeed, in *E. coli*, cells synchronized via either phosphate starvation or sucrose gradient segregation

show cell cycle regulation of the *nrd* operon, encoding ribonucleotide reductase (32). Maximal *nrd* expression corresponds with the initiation of DNA replication (32). Further, *ftsZ* transcription is cell cycle controlled in both *E. coli* and *C. crescentus* (12, 16).

Because of the unique life-cycle of the asymmetrically dividing *C. crescentus*, it has become a model organism for the study of the bacterial cell cycle. However, despite the complexity of the *C. crescentus* cell cycle, investigations of its pathways fail to yield insight into developmental events in other organisms. Several bacterial species are known to form intracellular organelles and studies seeking to ascertain bacterial organelle biogenesis, maintenance, and distribution during the cell cycle are in their infancy (11, 25, 35). Magnetotactic bacteria present an intriguing case study for the investigation of organelle formation during the cell cycle as these organisms depend upon continued synthesis of new magnetosomes, membrane-bounded compartments in which individual magnetic minerals are synthesized, to maintain chains of the organelles in each daughter cell post-division.

While progress has been made to understand the molecular mechanisms underlying magnetosome formation, including the identification of genes involved in magnetosome membrane biogenesis, crystal size and morphology, and chain organization, little is known about the regulation of these genes (17). Further, the activities of the translated gene products during the cell cycle are unknown. Recent evidence suggests against a model in which a burst of magnetic mineral synthesis occurs just prior to cell division (31), but the timing of magnetosome membrane formation and placement of new magnetosomes within the existing chain are unknown.

To investigate magnetosome formation during the cell cycle, and to delineate global cell cycle events in a previously uncharacterized lineage of the Alphaproteobacteria, I synchronized populations of *Magnetospirillum magneticum* AMB-1 and analyzed genome-wide gene expression patterns throughout the cell cycle. While the techniques developed to address individual components of these experiments were sound, difficulties arose in assembling those components into a functional and repeatable means of assessing gene expression in a synchronized population of AMB-1 cells. I conclude with suggestions for further inquiry into this topic.

MATERIALS AND METHODS

Growth conditions *Magnetospirillum magneticum* strain AMB-1 was grown in Magnetospirillum Growth media (MG) under microaerobic conditions, as previously described in Chapter Two. AMB-1 was grown in conical tubes or glass bottles filled with MG medium and incubated at 30°C in a microaerobic chamber in which the oxygen concentration was kept below 10%.

Synchronization of AMB-1 4-time point synchrony: 4 x 50mL cultures of AMB-1 were grown overnight to mid-exponential phase. The entire 100mL was then used to inoculate 4L MG media in glass bottles incubated in the microaerobic chamber until mid-exponential phase (OD$_{400}$ ~0.7-0.9) was reached. Four continuous Percoll gradients were established in 15mL conical tubes by centrifuging 10mL 50% Percoll/MG solution (100% Percoll represents 90% Percoll diluted by

10% 10x MG salts) at 10,000xg for 30 minutes. The 4L of AMB-1 cells were harvested by pelleting at 8000xg for 10 minutes, pooling the pellets in 1.5mL eppendorfs. Cells were further concentrated by centrifugation at 16,000xg for 2 minutes. All pellets were resuspended together in 1mL and evenly loaded (333µL each) on the top of 3 of the gradients. The 4th gradient was used as a balance with density marker beads (Amersham) to monitor gradient formation.

Gradients were centrifuged in a swing rotor at 800xg for 20 minutes. The top 500µL containing few cells were removed from each gradient, and the next 200µL fractions were pooled. 125µL from the total 600 µL synchronized population was used to inoculate each of 4 x 50mL MG cultures which were grown in the microaerobic chamber. To verify synchronization of each culture, 100µL were removed every 40 minutes for cell counts using a haematocytometer.

In the 4-time point synchronization experiments, individual 50mL cultures of AMB-1 were removed from the microaerobic growth chamber and filtered for RNA extraction at the following times post-inoculation: 2.0, 3.5, 4.5, and 6.0 hours.

9-time point synchrony: 2 x50mL cultures of AMB-1 were grown overnight to mid-exponential phase. Sufficient cell culture was inoculated in 400mL MG for overnight incubation in the microaerobic chamber until mid-exponential phase again. This culture was used to inoculate 9L of MG media. Eight continuous Percoll gradients were established as described above. The 9L of AMB-1 cells were harvested by pelleting as described above. The pellets were pooled in 1.5mL eppendorfs and further concentrated by centrifugation. All pellets were resuspended in 1mL MG and evenly loaded (120 µL each) on the top of 7 of the gradients. The 8th gradient was used a balance as described above.

In the 9-time point synchronization experiments, individual 50mL cultures of AMB-1 were removed from the microaerobic growth chamber and filtered for RNA extraction at the following times post-inoculation: 2.0, 2.5, 3.0, 3.5, 4.0, 4.5, 5.0, 5.5, and 6.0 hours.

RNA extraction and cDNA synthesis At each time point during the synchrony, one 50mL culture of synchronized AMB-1 cells was vacuum-filtered using a side-arm flask apparatus onto sterile Whatman Nucleopore Track-Etch Membrane filters. Filters were removed with sterilized forceps and deposited in sterile microcentrifuge tubes, which were immediately plunge frozen in liquid nitrogen and stored thereafter at -80°C. RNA was extracted directly off of the filters by applying 1mL Trizol reagent to each microcentrifuge tube. Samples were mixed by vortexing and left to incubate for five minutes. Supernatants were then transferred to 2mL Heavy Phase Lock tubes, to which 200µL chloroform were added and mixed. Phase Lock tubes were spun at 4°C at 12,000xg for 15 minutes, after which the supernatants were decanted into fresh microcentrifuge tubes. 500µL isopropanol were added, and the tubes were tilted gently for 10 minutes at room temperature before a second spin at 4°C of 12,000xg for 15 minutes. The supernatant was removed and the pellet washed with 1mL cold 75% ethanol and vortexed. Tubes were spun at 4°C at 7500xg for 5 minutes and the supernatants again removed. Pellets were air-dried for 10 minutes, then resuspended in 100µL RNase-free water.

RNA quantity and quality were assessed using a NanoDrop (Thermo Scientific). Samples were treated with DNaseI (Invitrogen) and purified using the Qiagen RNeasy kit. 1µg RNA was

reverse transcribed using the Invitrogen SuperScript RT III kit as directed. Resulting cDNA was treated with RNaseA (NEB) and RNaseH (Invitrogen) to remove residual RNA, and was purified using the Qiagen PCR Clean up-kit, and eluted in 10% EB. cDNA quantity and quality was assessed using a NanoDrop.

Microarray sample preparation and array design 0.5µg cDNA was fluorescently-labeled with Cy3 using the Nimblegen One Color DNA Labeling kit as directed. Labeling reactions were incubated at 37°C overnight in the dark. Labeling reactions were stopped as directed, and samples were resuspended in 25µL nuclease-free water. 2µg Cy3-labeled cDNA was dried in a SpeedVac at 30°C in the dark. Microarray sample hybridization and scanning were conducted at the Fred Hutchinson Cancer Research Center, Seattle WA.

Our microarray consists of full coverage of the AMB-1 genome (GenBank Accession NC_007626), and is described in further detail in Chapter Two.

Microarray data analysis Scanned microarray images were processed using ArrayScan software (Nimblegen). .pair files were generated for all arrays in the dataset, which were then normalized together using quantile normalization as described (2); gene calls were generated using the Robust Multichip Average (RMA) algorithm (14, 15). Gene expression changes between strains were considered significant if an average change across three biological replicates was greater than 1.5-fold above or below the average of three biological replicates of the comparison samples.

Expression of MamA during the cell cycle A 50mL culture of AMB-1 was grown overnight to mid-exponential phase and used to inoculate 200mL MG media at a 1:25 dilution of cells. Two continuous Percoll gradients were established in 15mL conical tubes by centrifuging 10mL 50% Percoll/MG solution (100% Percoll represents 90% Percoll diluted by 10% 10x MG salts) at 10,000xg for 30 minutes. The 200mL of mid-exponential phase AMB-1 cells were harvested by pelleting at 8000xg for 10 minutes, pooling the pellets in a 1.5mL eppendorf. Cells were further concentrated by centrifugation at 16,000xg for 2 minutes. The pellet was resuspended in 100µL and loaded on the top of one of the gradients. The 2nd gradient was used as a balance with density marker beads (Amersham) to monitor gradient formation.

Gradients were centrifuged in a swing rotor at 800xg for 20 minutes. The top 500µL containing few cells were removed from the gradient and the next 200µL fractions was used to inoculate a 15mL MG culture which was grown in the microaerobic chamber. To verify synchronization of each culture, 100µL were removed every 40 minutes for cell counts using a haematocytometer.

After 3.5 hrs, every 45-50 minutes, 1mL of the synchronous culture was removed to ascertain MamA protein levels. 10µL cells were removed and amended with 4µL sample buffer and 6µL dH$_2$O. The remaining 990µL cells were pelleted and resuspended in 20µL sample buffer. All samples were stored at -80°C.

Both samples (frozen 10µL and resuspended pellets) were boiled and 10µL loaded onto a 12% SDS-PAGE gel. Western blotting was performed using standard techniques. Following protein

transfer, the nitrocellulose membrane was blotted with 1/5000 αMamA, generously obtained from Y. Fukumori.

RESULTS

Synchronization of *Magnetospirillum* via density gradient centrifugation A previous protocol to develop synchronous cultures of *Magnetospirillum magneticum* sp AMB-1 relied on passaging the cells through repeated cold and warming treatments (28, 39). This method was successful in generating AMB-1 cultures which doubled in population every four hours. Using this technique, the authors were able establish that although iron uptake occurs at a steady rate throughout the cell cycle, a magnetosome-related gene *magA* potentially changed in its expression throughout the cell cycle (28, 39). In order to examine global gene expression patterns in AMB-1 more closely, I sought to develop a synchronization protocol that would minimize any artifacts of repeated and lengthy cold treatments on cell physiology and, more particularly, on gene expression.

Density gradient centrifugation has been widely used for decades to separate bacterial cells of varying sizes, morphologies, as well as life stages: for example to isolate sporulating cells from their parents (33). This technique can therefore be used to synchronize populations of cells, as cells in different stages of the cell cycle will segregate according to size, shape and/or density (6, 24). The silica colloid Percoll is commonly used for its iso-osmotic properties and is non-toxic to cells. Synchronization of cells using self-formed Percoll density gradients was an attractive option, as it could be diluted with concentrated MG salts to achieve equal osmolarity with traditional MG media, and would therefore expose the cells to as little growth disruption as possible.

Percoll percentages were varied until I achieved sufficient separation of cell types in the gradient. Positions of cell morphologies were marked by density marker beads in control gradients (**Fig 1A**); AMB-1 cells primarily segregated between the blue, pink, and orange density marker beads. Therefore, a 50% Percoll solution was chosen to provide optimal separation between these density regions. Cells applied to a pre-formed 50% Percoll density gradient were observed under the microscope at 250µL intervals. Consistently, the top 500µL fraction contained very few cells and mostly debris particles. Below this initial layer, cell density increased noticeably and the cells were primarily quite small. Deeper into the gradient, cells doubled in size and were observed in the process of division with septa forming at midcell. Up to 50% dividing cells could be observed in a combined 500µL fraction.

In initial synchrony experiments, the top 750µL was withdrawn and discarded, and cells from the following 250µL used to inoculate a 10mL MG culture. A second, control 10mL culture was inoculated with exponential phase AMB-1 cells such that both cultures would begin with the same cell density. Both cultures were monitored for population growth over eight hours by visual cell counts every 40 minutes. However, in these experiments, cell cycle synchronization was not achieved, most likely due to mixing of gradient layers during the removal of the upper layer and subsequent inoculation of the MG culture (**Fig 1C**). Mixing would ensure that cells of varying cell cycle stages would be introduced into the same culture, disrupting synchronous growth.

Ultimately, it was determined that extremely careful removal of the upper 500µL fraction followed by the additionally careful inoculation of the next 200µL into fresh MG media would consistently yield synchronized wild-type AMB-1 cultures (**Fig 1B and D**).

Magnetosome protein levels potentially vary during the cell cycle Once a protocol to generate synchronized populations of AMB-1 was established, I sought to examine the expression of MamA, a magnetosome-associated protein involved in magnetosome activation (18). MamA is proposed to form a self-associating aggregate coating the surface of the magnetosome chain, interacting with magnetosome membrane proteins to support biomineralization (38, 40).

I was first concerned that the meager cell densities obtained in the synchronous cultures would not yield protein concentrations sufficient to be detected by MamA antibodies. Thus, I grew wild-type AMB-1 to late-exponential phase and diluted the culture to a range of cell densities to ascertain the efficacy of the MamA antibody. At each cell density, 1mL of cells was pelleted and resuspended in 20µL sample buffer. Using a 1/5000 MamA antibody dilution and a 1 minute exposure, MamA was detectable even at 1.2×10^6 cells (**Fig 2A**). This figure corresponded perfectly with cell densities achieved in the synchronous cultures, which typically ranged between 10^6 to 10^7 cells/mL in 10 mL cultures.

To investigate the variability of MamA levels during the cell cycle, AMB-1 cells were grown to mid-exponential phase and synchronized as described previously. Synchronous growth was verified by microscopic cell counts approximately every 45 minutes (**Fig 2B and C**). After the culture was verified to have divided synchronously once, 1mL cells were removed approximately every 45-50 minutes for MamA protein analysis. Protein levels were below detection in the 10µL cells immediately resuspended in sample buffer and stored, while MamA was detectable from the cell pellet fractions obtained from the residual 990µL cells.

In both experiments, MamA levels appear to drop during cell division. This event is more significant in **Fig 2C**, while a drop in expression is still observed in **Fig 2B**. However, at the low cell densities achieved in the synchronized AMB-1 populations, Coomassie staining to verify consistent loading controls across all samples in the experiments was too faint to detect. Antibodies for alternative house-keeping genes were unavailable.

Gene expression during the cell cycle of AMB-1 Thus far, only the expression of *magA* had been examined in synchronous populations of AMB-1. Fluorescent *in situ* hybridization suggested that expression of this putative magnetosome gene was repressed just before and after cell division (39). As MagA has been proposed to function in iron transport in magnetosome formation (23), this finding suggests that iron uptake and coincidentally biomineralization, might halt around cell division. To gain greater insight into magnetosome formation in the context of the cell cycle, large populations of exponential phase cells were synchronized and at four or nine time points during the cell cycle, cells were isolated for global gene expression analysis via microarray.

To obtain sufficient cell, and thus RNA, material for microarray studies, the well-developed synchronization protocol first needed to be scaled. This proved challenging, although ultimately

synchronization of 4L AMB-1 cultures was achieved. A delicate balance between sufficient cell material and synchrony sensitivity needed to be struck. Passing too many cells through a single density gradient resulted in insufficient separation between cell sizes and thus asynchronous cultures. Alternatively, too few cells yielded inadequate RNA for microarray analysis. Ultimately, multiple density gradients were generated, and subsets of the large cell cultures were concentrated and segregated on them. The fractions containing the smallest cells were pooled and used to inoculate a single synchronous MG culture. Concerned that removing 50mL of cells from a 200mL culture at each of the four time points would alter the atmosphere of the entire culture, we elected to divide the 200mL synchronous culture into four independent 50mL conical tubes, each of which would serve as an end point. Synchronous growth in each of the four tubes was monitored as best as possible, although time limitations prevented counting cells in every tube at each measurement. Therefore, tubes were rotated and counted as often as possible. The time necessary to count 3-4 cultures was averaged along with the cell counts observed and were plotted to generate growth curves in each experiment (**Fig 3**).

When gene expression was examined in four time points throughout the cell cycle, a 50mL culture was filtered at 2-, 3.5-, 4.5-, and 6-hours post-inoculation. The aim was to capture the cell division event in between the 3.5- and 4.5-hour time points. This experiment was performed in triplicate. Later, in an attempt to refine the sensitivity of detecting gene expression changes in the context of the AMB-1 cell cycle, a nine time point synchrony was performed. This experiment called for 9L of exponential phase cells. The same time points from the 4L synchrony were repeated, and this time, cells from additional 50 mL cultures were isolated at 30 minute intervals (**Fig 3**).

Global gene expression patterns were first ascertained by pooling data from the triplicate four-time point synchronization experiments. Gene expression values across the cell cycle were normalized to their expression at the first time point, 2 hours post-inoculation. Targets were determined to be cell cycle-regulated if their expression increased or decreased more the 1.5-fold between any two time points across all triplicates. Further, the expression of those targets at the first and last time points should be within 1.5-fold of each other, as these two time points should ideally capture identical gene expression profiles being separated by the 4 hour division cycle.

Imposing these criteria, 56 genes were determined to be cell cycle-regulated in AMB-1 (**Fig 4**). Twenty-five of these increased at least 1.5-fold just before cell division, after which point their expression resumed a level of expression consistent with that the initial time point. Another four genes maintained their pre-divisional gene expression increased past the division point before dropping back to mid-cell cycle levels of the first time point. Four more genes only increased in expression just following cell division before returning to pre-divisional levels.

Similarly, nine genes decreased in expression at least 1.5-fold prior to and following cell division. An additional three genes exhibited a similar pattern except that their expression levels never rejoined that of the first time point. Perhaps the general decrease in expression over time for these genes was subject to increasing cell mass in the cultures, rather than progression through the cell cycle. A final 11 genes maintained their starting expression values prior to cell division, and then dropped subsequently.

The majority of the genes identified as being cell cycle-regulated encode proteins with no homology to other known protein families. Intriguingly, 12 of the 56 genes encode factors with potential functions in signal transduction. Other strongly represented gene categories are metabolism and energy production and DNA replication. Eight magnetosome genes exhibited substantial gene expression changes throughout the cell cycle. Among this set is *mamL*, which encodes a protein essential for magnetosome membrane formation.

A final experiment was conducted to examine more closely the changes in gene expression during the AMB-1 cell cycle. In this experiment, I used nine time points spanning cell division, four of which should have overlapped with those time points from the 4L synchronies described in detail above (**Fig 3**). However, a truly synchronous population was extremely difficult to achieve. Although visual inspection of the various cell cultures under the microscope showed evidence of a synchronously-dividing group of cells, the cell counts did not reflect the visual observations.

DISCUSSION

A major point of interest in the study of magnetotactic bacteria is the relationship between magnetosome formation and the cell cycle. While significant progress has been made in the discovery of novel biomineralization proteins, magnetosome chain organization and dynamics, and the identification of factors essential for magnetosome membrane formation, the coordination of these processes in the context of the cell cycle remains unclear. Already, connecting threads between these systems are emerging, such as the multiple roles of the protease MamE in both crystal formation and protein sorting (22, 26), with further links to MamB's involvement in magnetosome membrane biogenesis (34). In the cell cycles of organisms from bacteria to humans, check points exist to ensure the proper sequence of events is met. Quite possibly similar mechanisms exist in bacterial organelle biogenesis, where the initiation of one stage is dependent upon a cue from a prior one. MamB seems a likely candidate for linking magnetosome membrane formation to the establishment of a mature compartment in which a fledgling crystal can be nucleated. The potential stabilization of MamB by MamM possibly ensures that properly folded transporters are positioned to facilitate the flux of iron and other components in and out of the magnetosome (34). Proteolytic activity of MamE could then prime additional magnetosome membrane proteins to begin crystal nucleation, a process further facilitated (or regulated) by the heme-binding capability of MamE itself (26). Once the biomineralization proteins are recruited to and activated at the magnetosome, size and shape control can be exerted on the growing crystal. As these events occur, the cell itself is growing and preparing for cell division. Magnetosome membrane proteins interacting with MamK filaments may stimulate MamK ATPase activity to hasten filament disassembly at the midcell in preparation for septum formation and cell division (5).

Global gene expression analysis throughout the AMB-1 cell cycle was proposed to address many of these questions. Potentially, changes in magnetosome gene expression in the context of the cell cycle would shed light on the timing of various steps of magnetosome formation, and could additionally provide a means to probe the regulation of various magnetosome genes.

Unfortunately, gene expression studies were hampered by significant technical difficulties. First, the amount of RNA necessary for robust microarray studies required drastic scaling up of the synchronization protocol. Scaling up the protocol, however, posed many challenges, such as the need to balance a tightly-regulated synchrony with abundant cell material. While synchronous populations of AMB-1 could be generated from initial 4L cultures, the method failed as often as it succeeded. In addition, every synchrony proceeds slightly differently. The timing between cell divisions is consistently located between 3.5 to 4 hours apart, but the placement of the first division event relative to the inoculation of the synchronous culture varies. In some instances, cells divide at 3 hours post-inoculation, while in others the division is displaced by 30-60 minutes. When the ability to successfully generate a synchronized population of AMB-1 is already tenuous, the added uncertainty of the timing of the first cell division event renders individual experiments rather impossible to compare to one another.

One possible solution to this dilemma would be to begin sampling RNA from synchronized populations only after one division event has been observed. However, the observation of an entire cell division cycle would require following that culture through two full division events. It is apparent that AMB-1 populations do remain relatively well synchronized through two divisions, but that errors in cell counting increase significantly over time. Therefore, the most ideal solution would be to determine what factor induces a synchronous culture to divide at 3 hours or 4 hours post-inoculation such that one could always be sure that sampling time points are consistent across experiments.

To approach the methodology from another angle, it might be possible to design the experiment such that less initial RNA is necessary. This could be achieved by using an RNA amplification protocol. Thus, the robust, smaller scale synchrony could be generated and allowed to progress as before while still managing to supply enough genetic material for microarray analysis.

In addition to the experimental faults enumerated above, it has also been brought to attention that the preparation of RNA samples for microarray analysis was not ideal. After extensive analysis of various AMB-1 strains, it was determined that the entire pool of contaminating genomic DNA was not being removed from the RNA samples. While some gene expression changes were still able to be detected despite the dampening effect of the genomic DNA on gene expression signals, it is highly likely that there are more potential cell cycle-regulated genes than identified thus far.

While the technical challenges facing these experiments are many, it remains possible that the gene expression changes observed in these preliminary experiments are still valid. Even despite variability in the exact timing of the three 4-time point synchronies, there were still elements of consistency among them. Notably, the expression changes observed were not striking, but these features could have been dampened by the presence of genomic DNA in the isolate RNA samples. The potential down-regulation of *mamL* prior to and following the cell division event is particularly exciting, since perhaps the continued expression of membrane-shaping forces would be detrimental to and interfere with septum formation.

Continued exploration of this field, while technically challenging, may prove a fertile ground of insight into both magnetosome formation during the cell cycle and also discoveries about the

progression of the cell cycle in an organism where suspected and conserved regulatory pathways are known to be dispensable.

REFERENCES

1. **Autret, S., A. Levine, I. B. Holland, and S. J. Seror.** 1997. Cell cycle checkpoints in bacteria. Biochimie **79:**549-554.
2. **Bolstad, B. M., R. A. Irizarry, M. Astrand, and T. P. Speed.** 2003. A comparison of normalization methods for high density oligonucleotide array data based on variance and bias. Bioinformatics **19:**185-193.
3. **Champer, R., R. Bryan, S. L. Gomes, M. Purucker, and L. Shapiro.** 1985. Temporal and Spatial Control of Flagellar and Chemotaxis Gene Expression during Caulobacter Cell Differentiation. Cold Spring Harbor Symposia on Quantitative Biology **50:**831-840.
4. **Collier, J., S. R. Murray, and L. Shapiro.** 2006. DnaA couples DNA replication and the expression of two cell cycle master regulators. EMBO J. **25:**346-356.
5. **Draper, O., M. E. Byrne, Z. Li, S. Keyhani, J. C. Barrozo, G. Jensen, and A. Komeili.** 2011. MamK, a bacterial actin, forms dynamic filaments in vivo that are regulated by the acidic proteins MamJ and LimJ. Mol. Microbiol. **82:**342-354.
6. **Dwek, R. D., L. H. Kobrin, N. Grossman, and E. Z. Ron.** 1980. Synchronization of cell division in microorganisms by percoll gradients. J. Bacteriol. **144:**17-21.
7. **Erickson, H. P., D. E. Anderson, and M. Osawa.** 2010. FtsZ in Bacterial Cytokinesis: Cytoskeleton and Force Generator All in One. Microbiol. Mol. Biol. Rev. **74:**504-528.
8. **Evinger, M., and N. Agabian.** 1977. Envelope-associated nucleoid from *Caulobacter crescentus* stalked and swarmer cells. J. Bacteriol. **132:**294-301.
9. **Fernandez-Fernandez, C., D. Gonzalez, and J. Collier.** 2011. Regulation of the Activity of the Dual-Function DnaA Protein in *Caulobacter crescentus*. PLoS ONE **6:**e26028.
10. **Fritsch, A., and A. Worcel.** 1971. Symmetric multifork chromosome replication in fast-growing *Escherichia coli*. J Mol Biol **59:**207-211.
11. **Galán, B., N. Dinjaski, B. Maestro, L. I. de Eugenio, I. F. Escapa, J. M. Sanz, J. L. García, and M. A. Prieto.** 2011. Nucleoid-associated PhaF phasin drives intracellular location and segregation of polyhydroxyalkanoate granules in *Pseudomonas putida* KT2442. Mol. Microbiol. **79:**402-418.
12. **Garrido, T., M. Sanchez, P. Palacios, M. Aldea, and M. Vicente.** 1993. Transcription of ftsZ oscillates during the cell cycle of *Escherichia coli*. EMBO J. **12:**3957-3965.
13. **Grunenfelder, B., G. Rummel, J. Vohradsky, D. Roder, H. Langen, and U. Jenal.** 2001. Proteomic analysis of the bacterial cell cycle. Proc. Natl Acad. Sci. USA **98:**4681-4686.
14. **Irizarry, R. A., B. M. Bolstad, F. Collin, L. M. Cope, B. Hobbs, and T. P. Speed.** 2003. Summaries of Affymetrix GeneChip probe level data. Nucleic Acids Res **31:**e15.
15. **Irizarry, R. A., B. Hobbs, F. Collin, Y. D. Beazer-Barclay, K. J. Antonellis, U. Scherf, and T. P. Speed.** 2003. Exploration, normalization, and summaries of high density oligonucleotide array probe level data. Biostatistics **4:**249-264.
16. **Kelly, A. J., M. J. Sackett, N. Din, E. Quardokus, and Y. V. Brun.** 1998. Cell cycle-dependent transcriptional and proteolytic regulation of FtsZ in Caulobacter. Genes Dev. **12:**880-893.

17. **Komeili, A.** 2011. Molecular mechanisms of compartmentalization and biomineralization in magnetotactic bacteria. FEMS Microbiol. Rev. **36:**232-255.

18. **Komeili, A., H. Vali, T. J. Beveridge, and D. K. Newman.** 2004. Magnetosome vesicles are present before magnetite formation, and MamA is required for their activation. Proc. Natl Acad. Sci. USA **101:**3839-3844.

19. **Lagenaur, C., and N. Agabian.** 1978. Caulobacter flagellar organelle: synthesis, compartmentation, and assembly. J. Bacteriol. **135:**1062-1069.

20. **Laub, M. T., S. L. Chen, L. Shapiro, and H. H. McAdams.** 2002. Genes directly controlled by CtrA, a master regulator of the Caulobacter cell cycle. Proc. Natl Acad. Sci. USA **99:**4632-4637.

21. **Laub, M. T., H. H. McAdams, T. Feldblyum, C. M. Fraser, and L. Shapiro.** 2000. Global analysis of the genetic network controlling a bacterial cell cycle. Science **290:**2144-2148.

22. **Murat, D., A. Quinlan, H. Vali, and A. Komeili.** 2010. Comprehensive genetic dissection of the magnetosome gene island reveals the step-wise assembly of a prokaryotic organelle. Proc. Natl Acad. Sci. USA **107:**5593–5598.

23. **Nakamura, C., T. Kikuchi, J. G. Burgess, and T. Matsunaga.** 1995. Iron-Regulated Expression and Membrane Localization of the MagA Protein in Magnetospirillum sp. Strain AMB-1. J Biochem **118:**23-27.

24. **Pertoft, H.** 2000. Fractionation of cells and subcellular particles with Percoll. J. Biochem. Biophys. Methods **44:**1-30.

25. **Pfeiffer, D., A. Wahl, and D. Jendrossek.** 2011. Identification of a multifunctional protein, PhaM, that determines number, surface to volume ratio, subcellular localization and distribution to daughter cells of poly(3-hydroxybutyrate), PHB, granules in *Ralstonia eutropha* H16. Mol. Microbiol. **82:**936-951.

26. **Quinlan, A., D. Murat, H. Vali, and A. Komeili.** 2011. The HtrA/DegP family protease MamE is a bifunctional protein with roles in magnetosome protein localization and magnetite biomineralization. Mol. Microbiol. **80:**1075-1087.

27. **Quon, K. C., B. Yang, I. J. Domian, L. Shapiro, and G. T. Marczynski.** 1998. Negative control of bacterial DNA replication by a cell cycle regulatory protein that binds at the chromosome origin. Proc. Natl Acad. Sci. USA **95:**120-125.

28. **Sato, R., T. Miyagi, S. Kamiya, T. Sakaguchi, R. Thornhill, and T. Matsunaga.** 1995. Synchronous culture of *Magnetospirillum* sp. AMB-1 by repeated cold treatment. FEMS Microbiol. Lett. **128:**15-19.

29. **Shapiro, L.** 1976. Differentiation in the *Caulobacter* cell cycle. Annu. Rev. Microbiol. **30:**377-407.

30. **Skerker, J. M., and L. Shapiro.** 2000. Identification and cell cycle control of a novel pilus system in Caulobacter crescentus. EMBO J **19:**3223-3234.

31. **Staniland, S. S., C. Moisescu, and L. G. Benning.** 2010. Cell division in magnetotactic bacteria splits magnetosome chain in half. J. Basic Microbiol. **50:**392-396.

32. **Sun, L., and J. A. Fuchs.** 1992. *Escherichia coli* ribonucleotide reductase expression is cell cycle regulated. Mol. Biol. Cell **3:**1095-105.

33. **Tamir, H., and C. Gilvarg.** 1966. Density gradient centrifugation for the separation of sporulating forms of bacteria. J. Biol. Chem **241:**1085-1090.

34. **Uebe, R., K. Junge, V. Henn, G. Poxleitner, E. Katzmann, J. M. Plitzko, R. Zarivach, T. Kasama, G. Wanner, M. Pósfai, L. Böttger, B. Matzanke, and D.**

Schüler. 2011. The cation diffusion facilitator proteins MamB and MamM of *Magnetospirillum gryphiswaldense* have distinct and complex functions, and are involved in magnetite biomineralization and magnetosome membrane assembly. Mol. Microbiol. **82:**818-835.

35.   **Van Niftrik, L., W. J. C. Geerts, E. G. Van Donselaar, B. M. Humbel, R. I. Webb, H. R. Harhangi, H. J. M. O. d. Camp, J. A. Fuerst, A. J. Verkleij, M. S. M. Jetten, and M. Strous.** 2009. Cell division ring, a new cell division protein and vertical inheritance of a bacterial organelle in anammox planctomycetes. Mol. Microbiol. **73:**1009-1019.

36.   **Vats, P., J. Yu, and L. Rothfield.** 2009. The dynamic nature of the bacterial cytoskeleton. Cell and Mol. Life Sci. **66:**3353-3362.

37.   **Wu, L. J., and J. Errington.** 2011. Nucleoid occlusion and bacterial cell division. Nat Rev Micro **10:**8-12.

38.   **Yamamoto, D., A. Taoka, T. Uchihashi, H. Sasaki, H. Watanabe, T. Ando, and Y. Fukumori.** 2010. Visualization and structural analysis of the bacterial magnetic organelle magnetosome using atomic force microscopy. Proc. Natl Acad. Sci. USA **107:**9382-9387.

39.   **Yang, C.-D., H. Takeyama, T. Tanaka, A. Hasegawa, and T. Matsunaga.** 2001. Synthesis of bacterial magnetic particles during cell cycle of *Magnetospirillum magneticum* AMB-1. Appl. Biochem. Biotechnol. **91:**155-160.

40.   **Zeytuni, N., E. Ozyamak, K. Ben-Harush, G. Davidov, M. Levin, Y. Gat, T. Moyal, A. Brik, A. Komeili, and R. Zarivach.** 2011. Self-recognition mechanism of MamA, a magnetosome-associated TPR-containing protein, promotes complex assembly. Proc. Natl Acad. Sci. USA **108:**E480-E487.
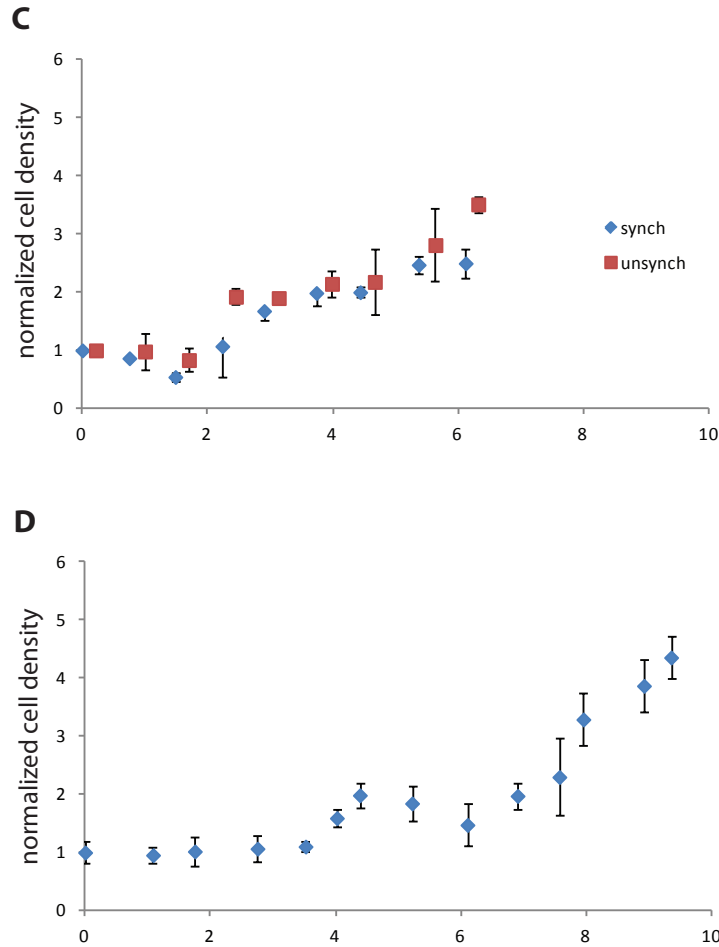
C

D
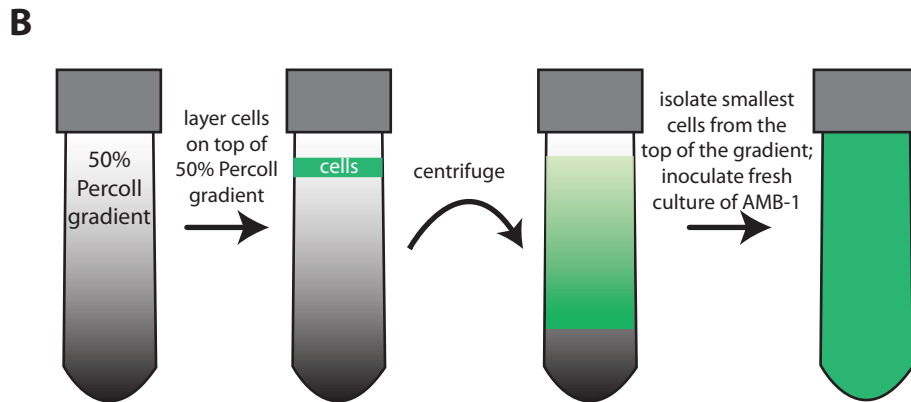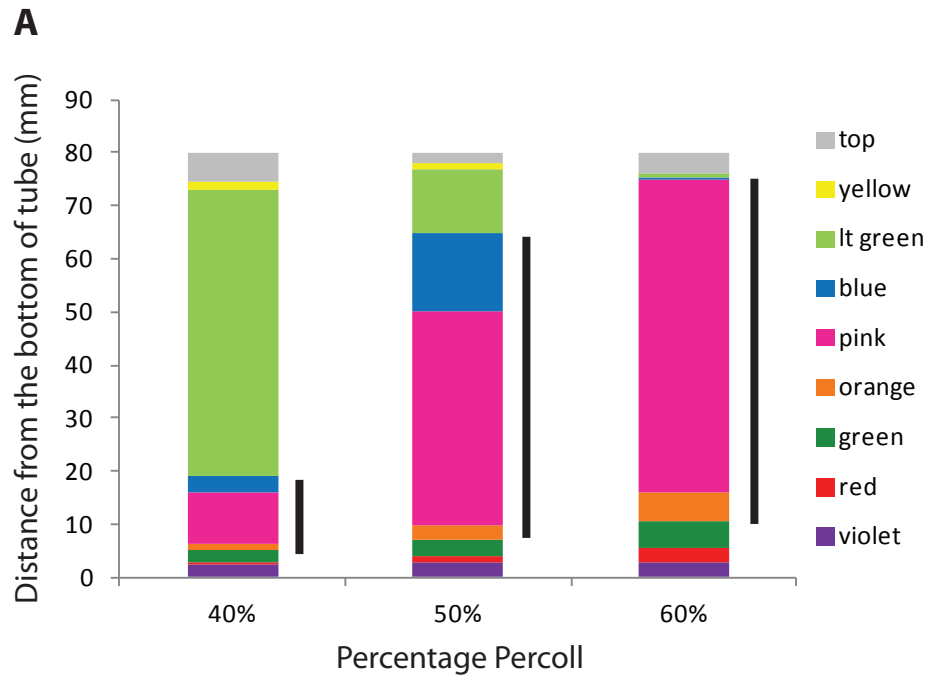
Figure 1: Development of a robust synchronization protocol for *M. magneticum* AMB-1 (A) Segregation of density marker beads in Percoll density gradients formed by centrifugation. Black bars denote the spread of AMB-1 cells relative to the density marker beads. 50% Percoll gradients provided the most separation of the smallest cells in the blue region. (B) Synchronously dividing cultures of AMB-1 are achieved through density gradient centrifugation. 50% Percoll gradients are pre-formed, and concentrated AMB-1 cells are loaded on top of the gradient. Centrifugation in a swing-bucket rotor allows the cells to settle to different densities in the gradient according to cell size. AMB-1 from the uppermost layer, corresponding to the smallest, newly divided cells, are used to inoculate MG growth media. Synchronization of the resulting culture is monitored by visual cell counts every 40 minutes. (C) Example of unsuccessful synchronization attempt, in which both the "synchronized" and "unsynchronized" control cultures behaved identically, and their populations increased steadily throughout the growth period. (D) Properly synchronized wild-type AMB-1 maintains a consistent population size for 4 hours, then doubles. This population holds steady for a second 4 hour growth period, and doubles again.
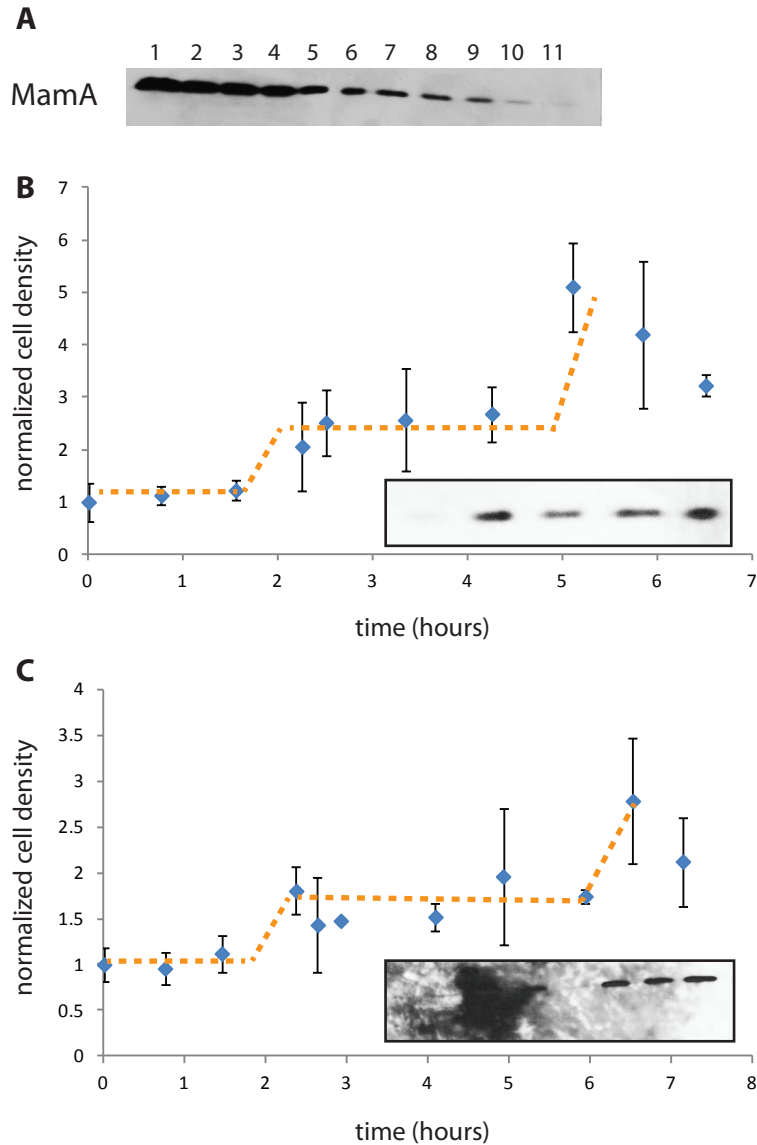
Figure 2: MamA levels potentially vary during the cell cycle in AMB-1 (A) Detection of MamA protein at varying cell densities. Lane 1: 6 x 10^7cells, Lane 2: 4.8 x 10^7cells, Lane 3: 3.6 x 10^7cells, Lane 4: 2.4 x 10^6, Lane 5: 1.2 x 10^7cells, Lane 6: 6.0 x 10^6 cells, Lane 7: 4.8 x 10^6cells, Lane 8: 3.6 x 10^6cells, Lane 9: 2.4 x 10^6cells, Lane 10: 1.2 x 10^6cells, Lane 11: 0.6 x 10^6 cells. (B) Synchronization of wild-type AMB-1. Dividing and very small cells were observed around 2 hrs post-inoculation and again at 5.5 hrs post-inoculation. MamA protein levels for the final 5 cell count time points are shown in the inset. (C) Second synchronization of wild-type AMB-1. Dividing and very small cells were observed around 2.5 hrs post-inoculation and again at 6 hrs post-inoculation. MamA protein levels for 8 cell cycle time points are shown in the inset.
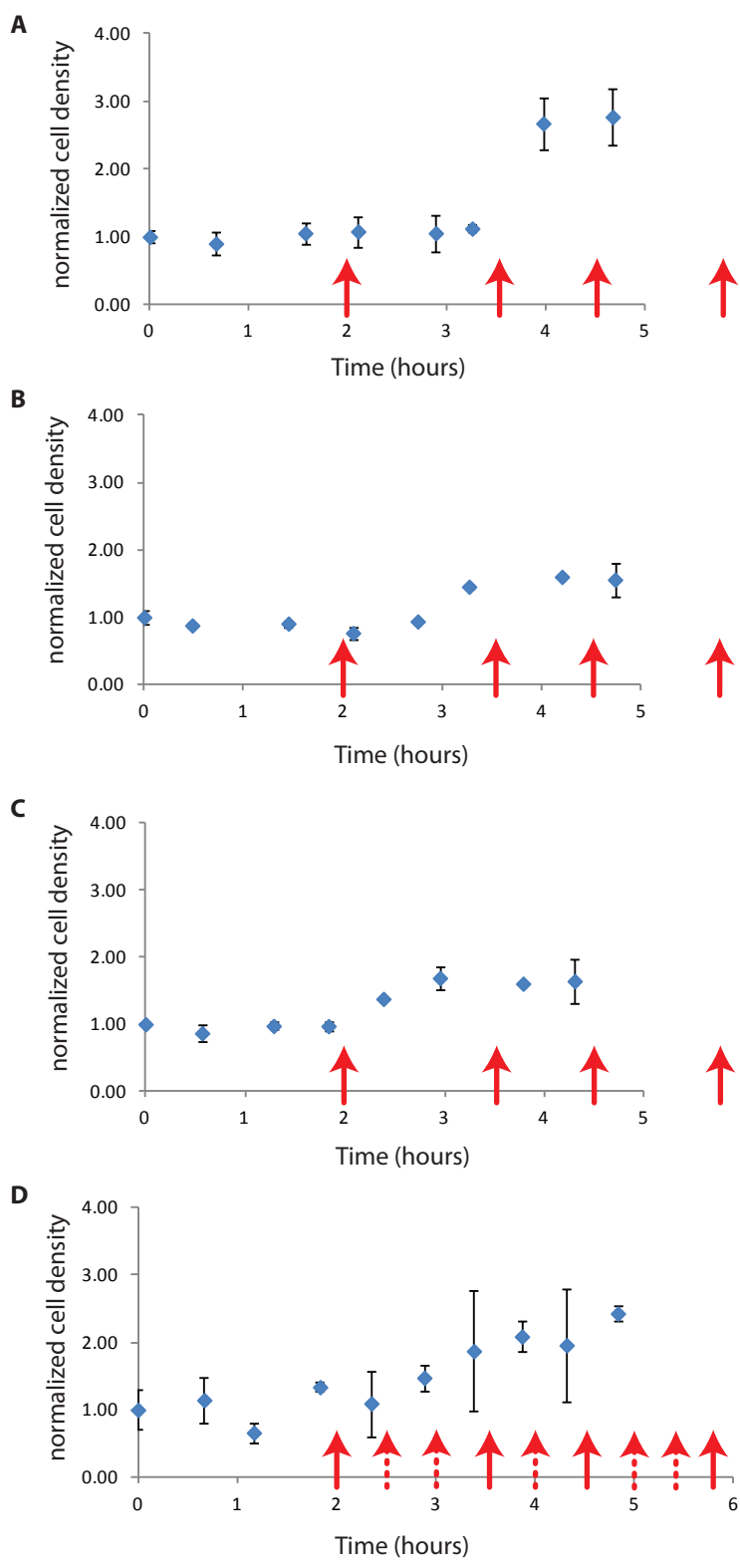
Figure 3: 4L (A, B, C) and 9L (D) of AMB-1 were synchronized to achieve sufficient cell quantities in the resulting synchronous cultures for microarray analysis of global gene expression during the cell cycle. The 4L synchronies were suitable to collect cells at 4 time points throughout the cell cycle, denoted by red arrows, at 2, 3.5, 4.5, and 6 hours post-inoculation. The 9L synchrony was suitable to college cells at 9 time points throughout the cell cycle. Time points matching those from the 4L synchrony are shown as solid arrows, while the unique time points (every 0.5 hrs) are shown as dashed arrows.

A

Gene	2 Hours	3.5 Hours	4.5 Hours	6 Hours
amb1628	1	2.039407	0.745502	0.920188
amb1785	1	2.020809	1.287376	0.926502
amb4368	1	1.96319	1.201539	1.011245
amb3698	1	1.903582	1.229226	1.111211
amb0399	1	1.777993	1.038379	1.057543
amb2908	1	1.725782	0.999711	0.831584
amb2079	1	1.719831	0.940935	1.229709
amb2400	1	1.716357	1.140843	0.747019
amb0934	1	1.715921	1.07792	0.879283
amb2678	1	1.704364	1.402921	0.969839
amb4032	1	1.699115	1.259281	0.848831
amb4122	1	1.681909	1.400249	0.977747
amb0935	1	1.675626	0.921666	0.933421
amb0643	1	1.662745	1.27711	1.050784
amb2039	1	1.638319	0.936326	1.034117
amb3335	1	1.627491	0.98273	1.053033
amb1195	1	1.626758	1.169669	1.047089
amb1893	1	1.622179	1.170385	0.86815
amb0464	1	1.619371	1.208765	1.0028
amb0947	1	1.600216	0.994815	0.915956
amb0961	1	1.599791	1.172889	1.484661
amb2073	1	1.585568	0.792381	0.711244
amb3770	1	1.57071	0.82381	1.144248
amb2186	1	1.537284	0.81495	0.942022
amb0398	1	1.52061	1.367904	0.92554
amb0681	1	1.511468	1.702652	0.940707
amb0615	1	1.822834	1.693041	1.212807
amb1302	1	2.269226	1.634425	1.039748
amb4307	1	1.597796	1.633783	0.957725
amb1995	1	1.058717	1.719314	1.048238
amb0640	1	1.215388	1.572453	0.907928
amb3907	1	1.252896	1.572235	1.2464
amb4106	1	1.233636	1.542175	1.000532

B

Gene	2 Hours	3.5 Hours	4.5 Hours	6 Hours
amb0842	1	0.547216	0.84043	0.656128
amb4257	1	0.552948	0.788418	0.671263
amb0546	1	0.485884	0.808881	0.488151
amb0843	1	0.579622	0.640454	0.744013
amb2947	1	0.63141	0.635721	1.09954
amb3211	1	0.599023	0.594872	0.820505
amb0966	1	0.56554	0.551029	0.752197
amb3992	1	0.550984	0.552125	0.806297
amb2657	1	0.539334	0.614933	0.89994
amb4403	1	0.52487	0.595318	0.79132
amb0352	1	0.505856	0.578484	0.778472
amb1545	1	0.447228	0.603259	0.826832
amb0659	1	1.463612	0.713013	0.937333
amb2074	1	1.28589	0.703595	0.804697
amb0917	1	1.202942	0.634907	0.931235
amb2014	1	0.916041	0.666942	0.855951
amb0985	1	0.866437	0.564697	0.957769
amb3647	1	0.859776	0.576749	0.999192
amb2303	1	0.809012	0.550247	0.761826
amb0351	1	0.803201	0.635318	0.797321
amb2060	1	0.793783	0.522716	0.809208
amb3693	1	0.744116	0.663668	0.915512
amb0957	1	0.70696	0.640624	1.120415

C

D

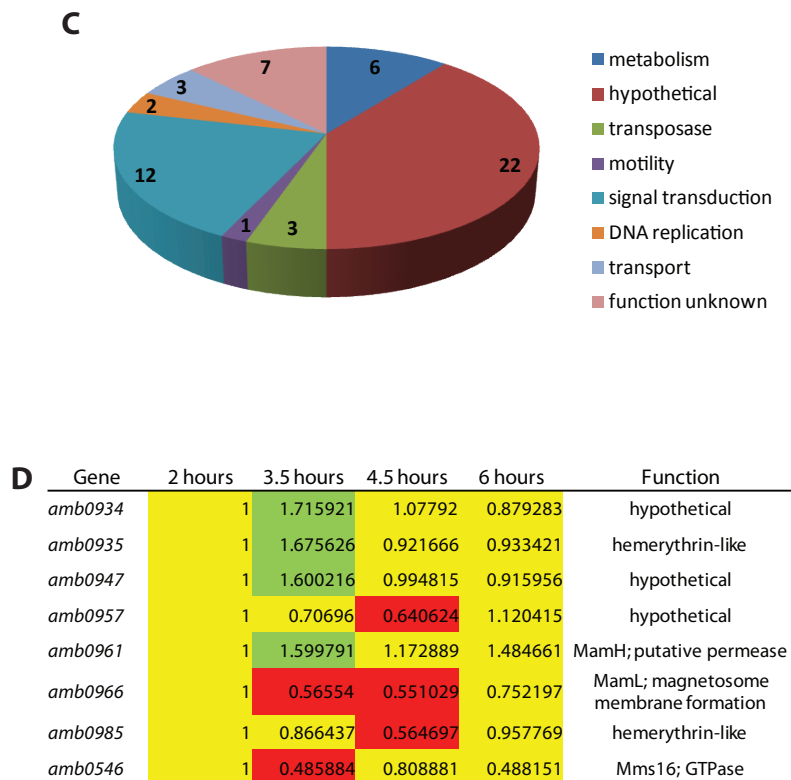| Gene	2 hours	3.5 hours	4.5 hours	6 hours	Function
amb0934	1	1.715921	1.07792	0.879283	hypothetical
amb0935	1	1.675626	0.921666	0.933421	hemerythrin-like
amb0947	1	1.600216	0.994815	0.915956	hypothetical
amb0957	1	0.70696	0.640624	1.120415	hypothetical
amb0961	1	1.599791	1.172889	1.484661	MamH; putative permease
amb0966	1	0.56554	0.551029	0.752197	MamL; magnetosome membrane formation
amb0985	1	0.866437	0.564697	0.957769	hemerythrin-like
amb0546	1	0.485884	0.808881	0.488151	Mms16; GTPase

Figure 4: Potential cell cycle-regulated genes in AMB-1 (A) Genes whose expression increases at least 1.5-fold relative to expression values at the 2-hour time point (representing the midpoint of the cell cycle) either prior to or following cell division. (B) Genes whose expression decreases at least 1.5-fold relative to expression values at the 2-hour time point either prior to or following cell division. (C) Functional categorization of cell cycle-regulated genes in AMB-1. (D) Magnetosome Island genes whose expression is suggested to be cell cycle-regulated. Gene expression values are reported as relative to values at the 2-hour time point (also normalized to 1). Expression values labeled in green are up-regulated while those with orange to red hues are down-regulated.

CHAPTER FIVE

Conclusions

While the presence of membrane-bounded organelles has been hailed as the defining feature of eukaryotic organisms, it has become clear that prokaryotic cells can be similarly compartmentalized. In recent years, the magnetosome of magnetotactic bacteria has emerged as a model system for the study of organelle biogenesis in bacteria. Magnetotactic bacteria are a diverse group of microorganisms which biomineralize chains of magnetic minerals within their cells, allowing the bacteria to align with the geomagnetic field and locate microaerobic environments more efficiently in a process termed magnetoaerotaxis. Biochemical and genetic analyses of magnetotactic species, such as the alpha-Proteobacterium *Magnetospirillum magneticum* AMB-1, have identified a number of proteins that participate in magnetite biomineralization, magnetosome "activation" and magnetosome alignment (2). However, the coordination of these events across the organism's cell division cycle remains unexplored.

Already, efforts in a few model systems, including the proteinaceous carbon-fixation microcompartment called the carboxysome and the magnetosome of magnetotactic bacteria, have yielded significant insight into the construction of these specialized features and have hinted at mechanisms by which organelles are segregated to daughter cells upon cell division (1, 3). As more genes participating in the process of magnetosome formation are discovered and characterized, we may begin to construct not only physical pathways of organelle development, but regulatory ones as well. Magnetosome formation is already dependent upon oxygen and iron concentrations in the environment, and potentially could be responsive to other environmental or internally-generated cues. Temporal regulation of magnetosome gene expression throughout the cell cycle could prime the bacterium for specific stages of magnetosome formation in concert with other cell cycle events.

This work suggests that ultimately cell cycle progression in *Magnetospirillum magneticum* AMB-1 is beyond the sphere of influence of the CtrA regulatory network, despite the essential roles played by this network in other Alphaproteobacteria where it is conserved. How, then, AMB-1 proceeds through the cell cycle is unknown and further investigation in AMB-1 may yield significant insight into the more broad study of the bacterial cell cycle and organelle formation in its context.

Although CtrA was not found to be a master regulator of the AMB-1 cell cycle, its role as a transcriptional regulator of flagellar biosynthesis genes is conserved in this organism. Comparisons of CtrA functions across the Alphaproteobacteria led to the proposal that motility is a deeply ancestral trait in this group and that early on CtrA acquired a regulatory function in motility.   Then, during the branching event which led to the emergence of *Caulobacter crescentus*, *Brucella abortus*, *Sinorhizobium meliloti* and *Agrobacterium tumefaciens*, CtrA became essential for cell cycle progression.

CtrA's role as a terminal regulator of flagellar biosynthesis is supported by motility phenotypes, gene expression data, and the presence of putative CtrA binding sites upstream of key flagellar biosynthesis genes. However, motility is also controlled in AMB-1 through the Magnetosome

Island, which is a genomic island conserved among magnetotactic bacteria and essential for magnetosome formation. The loss of the entire Magnetosome Island renders AMB-1 cells incapable of producing magnetosomes, and the cells additionally become hyper-motile. This phenotype suggests that a negative regulator of motility is encoded by the Magnetosome Island. Efforts to discern the identity of the Magnetosome Island motility regulatory factor were unsuccessful, and it is possible that no such factor actually exists. Potentially the loss of the Magnetosome Island triggers a compensatory mutation elsewhere in the genome that leads to the observed hyper motility phenotype.

In cumulative, we have learned that the cell cycle of AMB-1 is governed by different principles than its well-studied phylogenetic relative *C. crescentus* and that the CtrA regulatory network, which plays such a prominent role in *C. crescentus*, is still active in AMB-1 yet controls a distinct regulon. Further, comprehensive analysis of CtrA and its regulon suggest that activity of CtrA is dependent upon phosphorylation state and that when activated, CtrA is capable of activating or repressing the transcription of genes including flagellar biosynthesis clusters. Motility in AMB-1 is thus ultimately controlled through the CtrA regulatory network, while the signals upstream of this pathway remain unknown. Establishing connections between the magnetosome of magnetotactic bacteria and the regulation of motility in these organisms will have intriguing implications for the mechanisms of magnetoaerotaxis.

Magnetosome formation in the context of the AMB-1 cell cycle is also mysterious. Preliminary studies to investigate the timing of magnetosome gene expression during the cell cycle are promising in their methodologies and will provide a platform for future discoveries in the field. Any insights gained into the formation of bacterial compartments during the cell cycle, as well as links between compartmentalization and other cellular activities such as motility will prove interesting and intriguing.

REFERENCES

1. **Katzmann, E., F. D. Müller, C. Lang, M. Messerer, M. Winklhofer, J. M. Plitzko, and D. Schüler.** 2011. Magnetosome chains are recruited to cellular division sites and split by asymmetric septation. Mol. Microbiol. **82:**1316-1329.
2. **Komeili, A.** 2011. Molecular mechanisms of compartmentalization and biomineralization in magnetotactic bacteria. FEMS Microbiol. Rev. **36:**232-255.
3. **Savage, D. F., B. Afonso, A. H. Chen, and P. A. Silver.** 2010. Spatially Ordered Dynamics of the Bacterial Carbon Fixation Machinery. Science **327:**1258-1261.